NTNU – Trondheim
Norwegian University of
Science and Technology

One-pot Conversion of Biomass to Ethylene Glycol, Propylene Glycol and other Polyols over Carbon Supported Tungsten Catalysts

Cecilie Bjørgen

I declare that this is an independent work according to the exam regulations of the Norwegian University of Science and Technology (NTNU).

Preface

This Master Thesis is the result of work done following a Specialisation project called "Direct catalysis of lignocellulosic material into polyols using a CNT supported tungsten catalyst" at the Group of Catalysis, Department of Chemical Engineering, NTNU in the fall of 2012. The work was conducted at the Laboratory of Catalysts and New Materials for Aerospace at Dalian Institute of Chemical Physics (DICP), Chinese Academy of Sciences, in Dalian, China.

I want to express sincere gratitude to my supervisor at DICP, Professor Aiqin Wang, for her guidance and support during my work there. In addition, I want to thank my supervisor at NTNU, Professor De Chen, for his assistance and guidance with the progress of my work.

I also want to thank my colleges at DICP for supplying necessary training and assistance in the laboratory throughout my stay. Finally I want to express my appreciation to Ingvild Skeie Liland, my fellow NTNU student who shared this experience with me.

Abstract

Tungsten carbide and nickel promoted tungsten oxide catalysts supported on CNTs and AC were prepared for the catalytic conversion of cellulose towards polyols, particularly EG. Incipient wetness impregnation was used for the synthesis of tungsten oxide and tungsten carbide catalysts with AC as support, while the Pechini method was used with both supports. It was found that the choice of a suitable loading method was influenced by the physical structure of the carbon support. AC, being a microporous material, was best coated by incipient wetness impregnation, whereas the mesoporous structure of CNTs allowed the larger metal complexes formed by the Pechini method to enter the pores, giving better dispersion of metal particles. The catalysts were characterised by BET, TGA, ICP, Chemisorption, S(T)EM, XRD and Raman. Both TGA and ICP analysis showed that the CNT support might contain trace metals, such as nickel from the CNT synthesis. This nickel content is most likely the reason for better EG yields with CNT based catalysts, and is also the reason for generally better yields by the nickel promoted tungsten oxide catalysts. The conversion tests were performed in a stainless-steel autoclave at a hydrogen pressure of 60 bar (increased to 130 bar during heating) and 245 °C. Among the catalysts tested, a CNT supported tungsten carbide catalysts, 20WCx/CNT, had the best catalytic activity, giving a total yield of 85 % and the second highest EG yield of 53.8 %. This is an exceptionally good result considering no promotion of nickel had intentionally been made. The highest EG yield (63.8 %) was obtained with an AC supported, nickel promoted tungsten oxide catalyst made by the Pechini method, 2Ni20WO3/AC-p. Reusability tests showed that the EG yield is significantly reduced in the second run and this problem must be overcome if these catalysts are to be an option in the conversion of cellulose. ICP results showed that leaching occurred during the reusability tests, both of tungsten and nickel. The CNT based carbide catalyst displayed a lower nickel leaching in first run compared to the tungsten oxide catalyst, which might have contributed to the slightly superior performance in the second run.

Table of contents

List of figures

List of tables

List of pictures

List of equations

1. Introduction

Two important issues are causing increasing concern for humanity; energy and the environment [1]. Supplying enough energy for the steadily increasing population will become one of the main challenges of the future. Energy is already an issue, especially with regard to transportation fuels. Increasing demand and depleting resources is already presentation its effect on the financial trade [2]. It is well known that the fossil fuel supply will one day run out, and with most of the transportation fuels today being based on petroleum derived fossil resources, an alternative must be found for the future.

The fuel issue is closely related to the environmental concern as the focus has long been on the environmental impact and greenhouse effect of fossil fuels [2]. The demand for cleaner burning fuels and lower emissions are making us look for alternatives to petroleum fuels. Many scientists are working towards producing energy and chemicals in a sustainable and environmentally friendly way [1]. One of the potential alternatives is biomass. Biomass is a raw material resource whose components can be utilized in much the same way as fossil resources. Conversion of biomass into desired products has been considered one of the most important alternatives because of its renewable and carbon-neutral properties [1]. For several years, biomass has been explored as feedstock for transportation fuels. Both biodiesel produced from vegetable oils and ethanol from corn and sugar industry have been successfully implemented into the existing supply of transportation fuels [3,4]. However, the processes are demanding and less economical than the present day petroleum production [4].

Contrary to the positive environmental aspect of biomass utilization is the "food or fuel" dilemma arising when considering biomass production. Growing biomass for the sole purpose of fuel production will compete with land areas and crops for food production [5]. Two of the important components in biomass are cellulose and starch. Starch is one of the main components in corn, rice, potato etc., and is a polymer of D-glucose with α-1,4-glycosidic bonds which is soluble in water [6]. Seeing as starch is primarily used as a source of food, it should not be used to produce fuels and chemicals. Solving this problem is done by using second generation biomass feedstock. Non-edible lignocellulosic biomass, such as wood and wood residues, agricultural waste and non-wood energy crops, is a renewable and abundant supply of biomass feedstock with an estimated worldwide production of 170×10^9 t/year (in 2006) [7].

Lignocellulose is a fibrous material consisting of cellulose, hemicellulose and lignin as the main components [2]. Contrary to starch, cellulose cannot be digested by humans [8] and is therefore a great biomass alternative. In addition, cellulose is the most abundant component of biomass, accounting for 30–60 wt% of dried plants [1]. A variety of products are possible from the conversion of cellulose. With regard to the atom economy rule, transforming cellulose into oxygenates such as polyols, is more efficient than producing fuels [7]. The relatively high O/C ratio in cellulose mean excess oxygen must be removed to compare to the much lower O/C ratio of fuels. This removal is normally achieved at the expense of C or H, giving a poor atom economy [7]. As a feedstock for the production of polyols, cellulose is ideal considering the abundance of hydroxyl groups in its structure [9]. However, the intra- and intermolecular hydrogen bonding in its structure present a challenge with regard to efficient depolymerisation. Furthermore, the thermal instabilities of cellulose derived sugars make control of product selectivity difficult [7].

Both cellulose and hemicellulose, being C_5 and C_6 sugar polymers, make up the carbohydrate fraction of the lignocellulose [2]. The long chains of sugar molecules twist together in the cell walls of plants. Cellulose is made up of only one type of molecule, D-glucose, a C_6 sugar [6]. The molecules are linked together by β-1,4-glycosidic bonds, creating a linear polymer with a polymerisation degree up to 10 000 [7]. Due to the strong glycosidic bonds, cellulose has a robust, crystalline structure which protects with from attack by most solvents [9]. The crystalline structure therefore makes it difficult to hydrolyse [10] and catalytic conversion under mild conditions is a challenge [9].
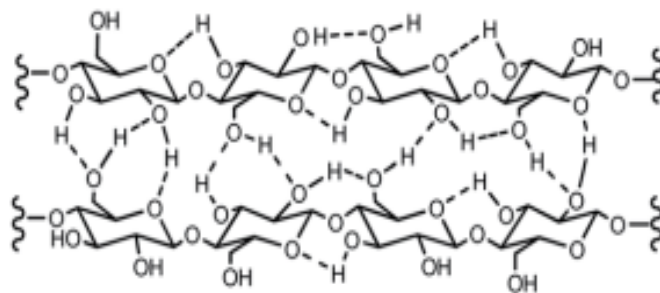
Figure 1: Schematic structure of cellulose (Adapted from [2]).

Conversion of cellulose is normally done in two steps; overcoming its insolubility by hydrolysing it into water-soluble saccharides such as oligomers and glucose, and hydrogenation and/or hydrogenolysis of these compounds into sugar alcohols and other chemicals [5]. Hydrolysis has generally involved acids or enzymes and is normally a challenge either with regard to the environment or from an efficiency point of view [11]. The use of mineral acids is not a desirable process as it encounters common problems associated with the use of liquid acids, such as corrosion and acid recovery or disposal [12]. Supercritical water can also depolymerise cellulose to a substantial degree, but require harsh operating conditions [7].

Developing a green and efficient process for cellulose conversion has been of interest for a long time. Processes such as fermentation with enzymes to produce ethanol, thermo-pyrolysis to bio-oils and syn-gas, and hydrolysis with dilute acids in ionic liquids to yield oligomers, glucose and HMF, are some of the attempts made [1]. However, the conversion of cellulose into fuels or chemical should ideally be done in a single-step catalytic process [10] as it proves an environmentally friendly process with milder reactions [7]. The main challenge with this process has long been the focus of research; finding a suitable catalyst capable of promoting several types of reactions including hydrolysis, hydrogenolysis, and hydrogenation [10].

The one-pot catalytic transformation is one of the most attractive routes of cellulose utilisation [8]. As an effective and green approach, the process uses a solid catalyst to convert cellulose into useful organic compounds in an aqueous solution [1]. Sugar alcohols, a possible product of cellulose conversion, can be used as chemicals in their own right or as new starting materials for the production of fuels [8]. However, a more profitable product is polyols, such as ethylene glycol, EG, propylene glycol, 1,2-PG, glycerol, xylitol, sorbitol, and mannitol. These products can be used as chemical directly or as precursors in the synthesis of fuels and value-added compounds [13], such as monomers in the plastic industry, functional additives in the food industry, and intermediates in the pharmaceutical industry [7]. EG especially, is of great importance with a consumption exceeding 20 million tons per year (2011) for the

synthesis of polyesters and antifreezes [9]. The chemical is currently produced from petroleum derived ethylene via multiple steps of cracking, epoxidation, and hydration [7].

The one-pot conversion of cellulose now exists, however not yet in industrial scale. Cellulose is only one of the three main components in lignocellulose, and from an industrial point of view, using raw lignocellulose as feedstock is preferred [2]. Investigation has therefore been made into the conversion of the other two lignocellulosic components; hemicellulose and lignin. Hemicellulose, the other carbohydrate fraction, is an amorphous polymer of both C_5 and C_6 sugars. Having shorter, branched chains of a number of different sugar molecules, such as xylose, mannose and glucose, hemicellulose is fairly easy to break down to monomeric sugars. The difficulty lies in the conversion of lignin. Lignin is an amorphous 3D polymer of three main units; p-coumaryl, coniferyl and sinapyl alcohols [2]. The polymer embeds in and binds to the cellulose and hemicellulose [6]. Containing more C–C bonds and providing the lignocellulose with structural rigidity, lignin helps protect against transformation [2].
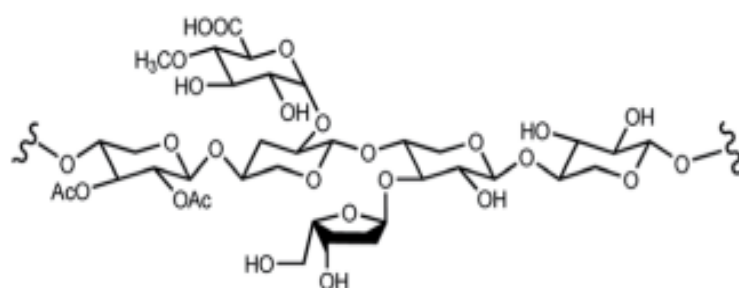
Figure 2: Schematic structure of hemicellulose (Adapted from [2]).

Figure 3: Schematic structure of lignin indicating the three main units (Adapted from [2]).

Even though lignocellulose has physiochemical, structural and compositional features making it resistant to chemical transformation [2], processes exist for the conversion of all three components. Thermal routes have the advantage of converting all the lignocellulosic fractions, however, high temperatures makes controlling the chemical structure challenging. More recently, studies have reported promising results in the one-pot catalytic transformation of lignocellulosic biomass to polyols. In this process, catalyst choice is of great importance and this master thesis, being further work to previous study by the author [14], involves the development and characterisation of possible catalysts for this process.

2. Literature review

2.1. Direct conversion of cellulose – one-pot catalytic transformation

The one-pot catalytic transformation of cellulose was first demonstrated by Fukuoka et al. [6]. In this study supported Pt and Ru catalyst were used to convert cellulose into sugar alcohols such as sorbitol and mannitol. The conversion was conducted using cellulose to represent the biomass component. Water was used as the reaction media and the reaction took place under hydrogen pressure [6].

The reaction scheme proposed by Fukuoka et al. involved the hydrolysis of cellulose to glucose and the reduction of glucose to sugar alcohols (see Figure 4). It was found that heterogeneous catalysis with a Pt/Al_2O_3 catalyst gave a 31 % yield of sugar alcohols (25% sorbitol and 6% mannitol) [6]. By studying the activity and selectivity towards certain polyols it was found that both the choice of metal and support material is of great influence to the process. The higher yields of sugar alcohols were obtained with Pt and Ru based catalyst, still, Pd, Ir and Ni catalysts also displayed a certain activity for the conversion of cellulose. Among the support materials tested, γ-Al_2O_3, HUSY(40), SiO_2–Al_2O_3 and HUSY(20) proved to give the highest yields [6]. These results indicated that solid acidity was effective for the catalytic reaction, but the activity did not correspond well with the apparent strength of the acid.
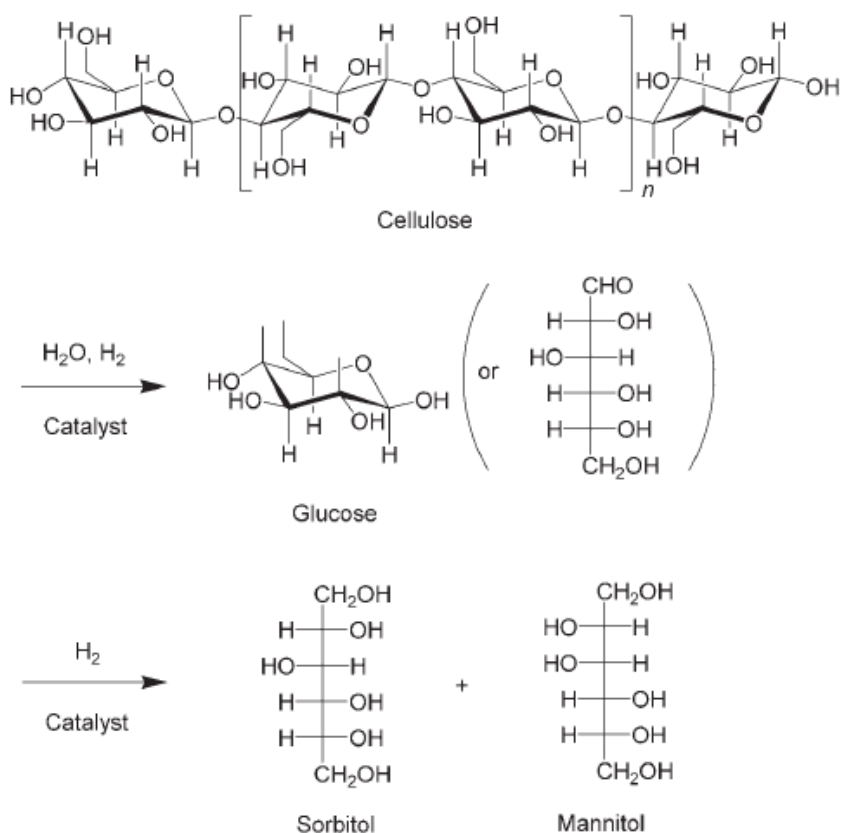
Figure 4: Catalytic conversion of cellulose into sugar alcohols [6].

Based on this one-pot transformation process several other studies were conducted on the conversion of cellulose. Among them, Luo et al. [12] further studied this reaction. Changing the support of their catalyst to carbon, making a Ru/C catalyst and elevating the reaction temperature, they successfully increased the cellulose conversion and the yield of sugar alcohols. In the high temperature water, H^+-ions are reversibly formed, which are capable of catalysing the hydrolysis reaction even in the absence of a catalyst [5]. The subsequent hydrogenation reaction is catalysed by the ruthenium catalyst [12]. Figure 5 shows the modified reaction scheme including the H^+-ions and Ru/C catalyst.
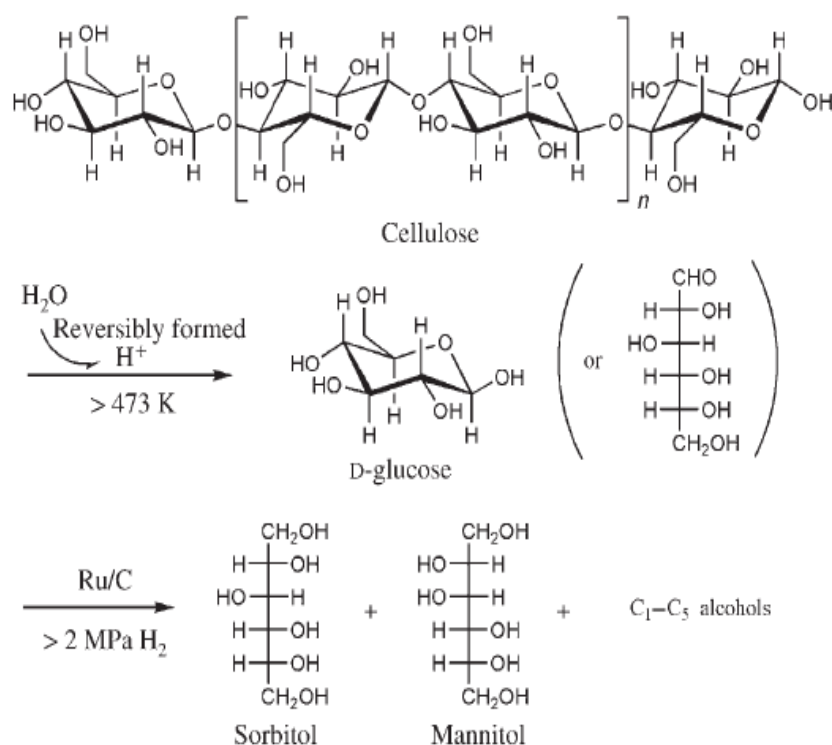
Figure 5: Catalytic cellulose conversion into polyols [12].

A disadvantage to the process in these studies is the use of precious metal catalysts. Precious metals are expensive and would be too costly with regards to conversion of large amounts of cellulose. As a solution to this problem Ji et al. [8] investigated the use metal carbides as catalysts for the cellulose conversion. The carbides of Groups 4–6 metals are similar to those of Platinum-group metals with regard to catalytic performance in reactions involving hydrogen [8]. With this in mind it was found that tungsten carbide work in similar ways as Platinum-group metal catalysts.

Fukuoka et al. displayed a successful conversion of cellulose into sugar alcohols, which can be used as chemicals in their own right or as base chemicals for the production of fuels [8]. However, the study done by Ji et al. reports an effective conversion of cellulose into polyols by the use of a carbon supported tungsten carbide catalyst. Even more, the study show that when the catalyst is promoted with a small amount of nickel, the yield of polyols increases. The Ni-W_2C/AC catalyst show remarkable selectivity towards ethylene glycol, EG, when compared to the previously developed catalysts [8].

Further to their study on the use of metal carbides as a replacement for noble metals in the conversion of cellulose, Ji et al. conducted a second study on the optimisation of EG yield by varying H_2 pressure, reaction temperature and reaction time. With regard to reaction pressure,

the highest EG yield was obtained at 6 MPa. The yield increased when the pressure increased from 5 MPa, but remained almost unchanged when further increased to 7 MPa [10]. Reaction time and temperature was found to affect both the product distribution as well as the product yield. The maximum value of the EG yield was found at a temperature of 518 K [10]. Both temperatures below and above this value gave lower EG yields. Cellulose conversion on the other hand, was hardly affected by the reaction temperature at all, suggesting that the formation of EG is not a thermally stable process, with EG undergoing further decomposition into smaller molecules at a higher reaction temperature [10]. With regard to reaction time, the study reports that the EG yield was initially greatest after 0.5 hours. Prolonging the reaction time first leads to an unusual decline in the yield at 1 hour, however, after this valley the yield continue increasing [10]. The 1,2-PG yield proved to increase rapidly with the reaction time and optimising the reaction conditions can lead to high yields in both EG and 1,2-PG.

In addition to optimisation by reaction conditions, features with the catalyst itself were investigated for the optimal conversion process. The active phases of the catalysts proved to have an effect on the cellulose conversion. The study reported that product selectivity was remarkably different when comparing the active components; Pt, Ni and carbides, on the AC support. Both Pt/AC and Ni/AC exhibited a moderate conversion of cellulose and a low yield of EG, while the AC supported tungsten carbide catalysts led to a nearly complete conversion of cellulose [10]. In addition, a difference could be noted between the different tungsten based catalysts. The study showed, that the catalyst with a single active phase, W_2C, was slightly more active and selective towards EG than the catalyst with two active phases, WC and W_2C [10].

As mentioned previously, the support material used in the catalyst greatly affects the cellulose conversion. Ji et al. reports that the support itself exerts a great influence on the product distribution [10]. For the carbide catalysts it was shown that carbon supports performed better than the alumina supported catalysts. In addition, the different carbon supports yielded different catalyst performance [10]. Three types of carbon were considered; activated carbon (AC), carbon black (CB) and activated carbon fibres (ACF). It was shown that the AC produced the highest EG yield, while the ACF exhibited a very low yield of EG.

Following the development of the nickel promoted tungsten carbide catalysts, scientists from the same institute conducted a study to investigate if any other catalysts are effective for the conversion of cellulose into EG and what cause the synergetic effect observed between Ni and W in the conversion process. Zheng et al. tested several monometallic M(8, 9, 10) catalysts such as Ni/AC, Pd/AC, Pt/AC, Ru/AC and Ir/AC, and found that these catalysts could not degrade cellulose completely in the way that W/AC could [1]. With the aim of transforming cellulose into EG or other desired polyols they develop a series of bimetallic catalysts based on tungsten, including Ni–W, Pd–W, Pt–W, Ru–W, and Ir–W, using different supports [1]. It was found that the cellulose conversions were significantly higher for the bimetallic catalysts than for the monometallic catalysts. In addition, significantly higher EG yields were obtained and it was observed that the product selectivity could be tuned by changing the weight ratio of W to M(8, 9, 10). With complete cellulose conversion, the highest EG yield was obtained with the Ni–W/SBA-15 catalyst.

An issue concerning the process addressed by Xiao et al., is the low starting concentration of cellulose in solution (about 1–3 wt%) used in previous studies. This is an issue as it leads to increased energy and water consumption. Previous work reports that cellulose is transformed into polyols in the presence of hydrogen over various noble metals [6,12] or transition

bimetallic carbide catalysts [1]. Even more, nickel nano-particles supported on a variety of supports such as Al_2O_3, Kieselguhr, TiO_2, SiO_2, AC, ZnO, ZrO_2, MgO, and carbon nanofibres (CNFs), have been used for the hydrogenolysis of cellulose to polyols [5]. Based on these facts, Xiao et al. performed direct hydrogenolysis of highly concentrated cellulose in liquid phase over a CuCr catalyst [5].

The study proved that the CuCr catalyst showed excellent performance and good resistance to coking [5]. Complete conversion of cellulose was obtained with 1,2-Propanediol, 1,2-PD, as the main product. Significant increase in the EG yield was obtained by addition of $Ca(OH)_2$ as a co-catalyst. The effect of cellulose concentration on conversion was reported with total conversion up to a concentration of 15 wt% [5]. A trend could be seen in the 1,2-PD yield, as well as for the total yield. Initially the yields would increase with increasing cellulose concentration, but after a maximum value, the yields would decrease. This occurs as the amount of water soluble saccharides becomes so large that they cover the active sites and supress the desorption of products. At lower cellulose concentrations, the catalysts have enough active sites for hydrogenolysis.

Previous studies performed by Ji et al. [8] and [10] proved that tungsten carbide catalysts promoted by a small amount of Ni gave higher EG yields. Tungsten carbides are particularly efficient for the selective formation of EG, and Ni is a well-known active catalyst for glucose hydrogenation [10]. Bimetallic catalysts of Ni-WxC can therefore further enhance the EG yield. In their study Ji et al. reported an increase in the EG yield from 29.0 % to 61.0 % by addition of 2 % Ni [8]. Similarly, Li et al. [2] uses a nickel promoted tungsten carbide catalyst for higher yields in their study. In addition, it was found that the sum of the EG yields of W_2C/AC and Ni/AC catalysts were lower than that of the bimetallic catalysts [8]. This result indicates a synergetic effect between Ni and W_2C in the reaction.

Similarly to Ji et al. [8,10], Zheng et al. observed a remarkable synergy between tungsten and metals of group 8, 9 and 10 [1]. In their study Ni-W catalysts were prepared and tested using different supports to make sure that this effect did not originate from the influence of a particular support. By mixing Ni/AC and W/AC catalysts mechanically and testing for cellulose conversion, it was noted that the synergistic effect between Ni and W did not necessarily require intimate contact between the two metallic components [1]. In order to understand the modification effect of Ni, Ji et al. performed surface science studies of EG on WC and Ni-WC [10]. It was found that the bonding configuration of EG on WC was significantly modified by the presence of Ni. The results clearly indicated that the presence of Ni on tungsten carbides reduces the activity toward the decomposition of ethylene glycol. The enhanced EG yields are therefore partially due to weaker bonding between EG and Ni-promoted tungsten carbides [10].

As the synergetic effect was investigated, Zheng et al. [1] demonstrated the separate functions of the catalyst components. It was found that W is the key component for the C-C cracking reactions, and thereby the degradation of cellulose, while the Ni is responsible for the hydrogenation reactions of unsaturated intermediates. By changing the weight ratio of Ni to W, the reactions can thereby be tuned to determine the final product and give a desired selectivity towards EG.

In addition to the synergetic effect between Ni and W, the active phases in the catalyst might be of great influence to the process. XRD can be used to determine the active phases in catalysts and Ji et al. showed that the carbothermal hydrogen reduction, CHR, temperature

influences the tungsten phases [10]. According to literature [15], the formation of W_2C by CHR involved the progressive reduction of WO_3 to W and then to W_2C, which can be represented by the following overall reaction:

$$WO_x + C^* + H_2 \rightarrow W_2C + CO + H_2 \hspace{2cm} \text{Equation 1}$$
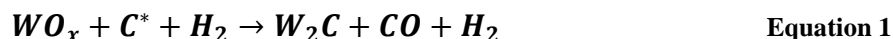
A higher CHR temperature promoted further carburisation of W_2C to form WC. In previous work [16] they had found that the metastable W_2C has an intrinsically higher activity than the thermally stable WC. In addition, higher CHR temperature could lead to sintering of WC particles and thereby a decrease in active sites. It was also shown that the present of Ni during CHR can facilitate the reduction of WOx by promoting the dissociation of H_2, resulting in the formation of W_2C at a lower temperature. Presence of Ni also led to sintering of W_2C particles which could be due to presence of Ni accelerating the methanation of the carbon support [10]. With methanation of the carbon support the Ni and W content of the catalyst would increase.

2.2. Direct conversion of lignocellulose

Previous studies have been conducted with microcellulose as the biomass representative. However, from an industrial point of view, large-scale production of biomass based products will be much more profitable with raw lignocellulose as the feedstock. The challenge of using lignocellulose as feedstock lies in degrading all three main components at the same time. By the use of their previously developed Ni-W_2C/AC catalyst [8] Li et al. demonstrated a one-pot catalytic conversion of raw woody biomass, converting the three major components in one step [2]. In this process the carbohydrate fraction, cellulose and hemicellulose, could be cracked into diols, while lignin was cracked into monomeric phenols.

In their previous work, an EG yield of 61 % was reported for a pure cellulose feed [8]. Interestingly Li et al. reports high EG yields, up to 51.4 %, for a raw biomass (birch wood) feed. These results are fairly good considering the wood had not undergone any pretreatment prior to conversion. In the reaction, cellulose is converted to EG as seen in Figure 6. This is done by hydrolysis and subsequent cracking (such as retro-aldol condensation) over tungsten sites to form C_2 molecules [2]. These molecules are then further hydrogenated, forming EG as the desired product.

This study also revealed a link between the hemicellulose content and the 1,2-PG yield. In the previous study with cellulose as feedstock the 1,2-PG yield reached 7.6 %, while the reaction with birch wood produced a 1,2-PG yield of 14.2 %. As birch wood contains 19.3 wt% hemicellulose Li et al. hypothesized that hemicellulose is the reason for the increased 1,2-PG yield [2]. In the reaction hemicellulose undergoes hydrolysis to xylose, which is then cracked (retro-aldol condensation pathway) into glycolaldehyde (C_2 intermediate) and glyceraldehyde (C_3 intermediate). Glycolaldehyde is further hydrogenated into EG, while glyceraldehyde goes through a series of steps, including dehydration and hydrogenation, resulting in 1,2-PG.
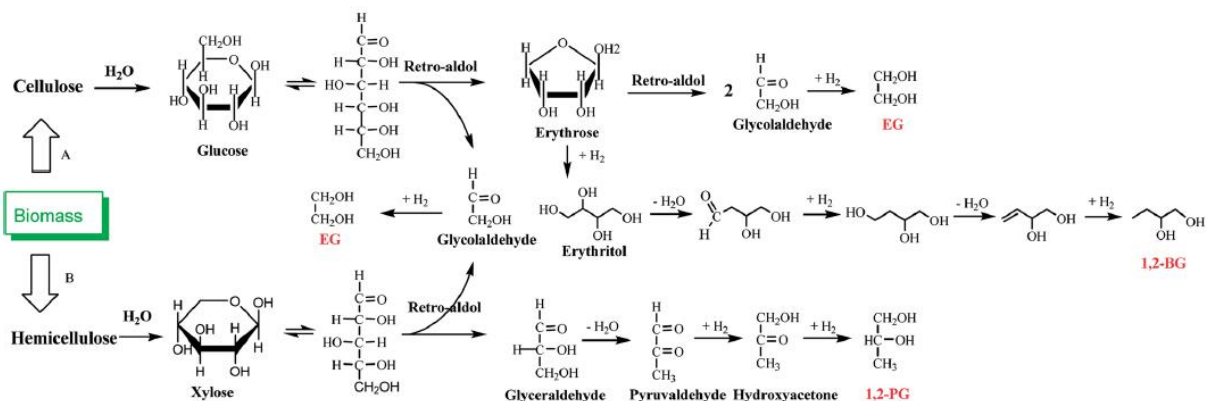
Figure 6: Possible reaction pathways from cellulose (A) and hemicellulose (B) to diols [2].

With regard to lignin it was noted that a monophenol yield of 36.9 % was obtained in the reaction with birch wood [2]. The four main monomers produced were guaiacylpropanol, syringylpropanol, guaiacylpropane and syringylpropane (see Figure 7). In order to affect the lignin degradation, Li et al. performed the reaction in a small-molecule alcohol to increase the activity of the catalyst. It was found that methanol increased the mono-phenol yield to 42.2 %, while using EG as the solvent further increased it to 46.5 % [2]. The yield improvement is most likely due to the increased solubility of the birch lignin, as well as increasing the hydrogen solubility, facilitating the hydrogenolysis of phenolic ether linkages. The reaction results indicate that the Ni-W_2C/AC catalyst is active for the degradation of lignin, and suggests that the synergistic effect between Ni and W_2C can also be found in lignin conversion.
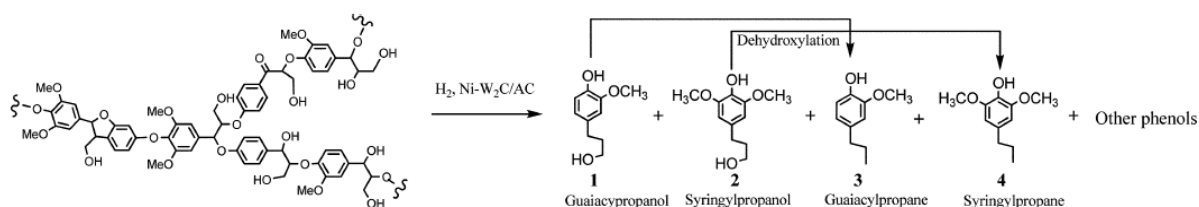
Figure 7: Ni-W_2C/AC catalysed degradation of lignin component into phenols [2].

Li et al. proved that the Ni-W_2C/AC catalyst could be used in the conversion of birch wood and applied the same procedure to several other wood sawdust (poplar, pine, basswood, ashtree, beech, xylosma, and yate) to investigate the general used of the catalyst on lignocellulosic materials [2]. It was found that the conversion efficiency and product distribution was significantly affected by the source of lignocellulose. The lignin content of the wood is one of the key factors inhibiting the production of diols. Woods with lignin contents below 20 % gave EG yields of approximately 50 % and a total diols yield of over 70 %, while a lignin content of approximately 25 % gave yields of 35 % and 60 % respectfully [2]. The poorest yields were obtained with lignin contents higher than 30 %. Although the diol yields vary with lignin content, it was found that EG and 1,2-PG are the main products no matter what type of wood was used as a source. However, the distribution and total yield of monophenols vary with the different wood sources due to the different lignin structures.

9

2.3.   Reaction mechanism

A major advantage with the direct conversion of lignocellulose to polyols is avoiding many of the disadvantages found in other methods, such as pretreatment requirement and harsh operating conditions. The processes also allow for high selectivity towards certain polyols such as EG and 1,2-PG. However, the catalytic conversion of cellulose to polyols is a complex process involving hydrolysis of cellulose to glucose, and hydrogenation and/or hydrogenolysis of glucose to the desired products.

A possible reaction scheme proposed by Ji et al. involves hydrolysis of cellulose to glucose, followed by hydrogenation to hexitol (sorbitol and mannitol) and hydrogenolysis to low molecular polyols, such as EG and 1,2-PG [10]. In addition, further degradation of polyols to gas products such as CO, CO_2, H_2 and alkanes might occur. Figure 8 shows the possible reaction scheme proposed by Ji et a. [10]. In their scheme they propose that EG and other low molecular weight polyols are products of the hydrogenolysis of glucose, whereas hydrogenation of glucose gives sugar alcohols.
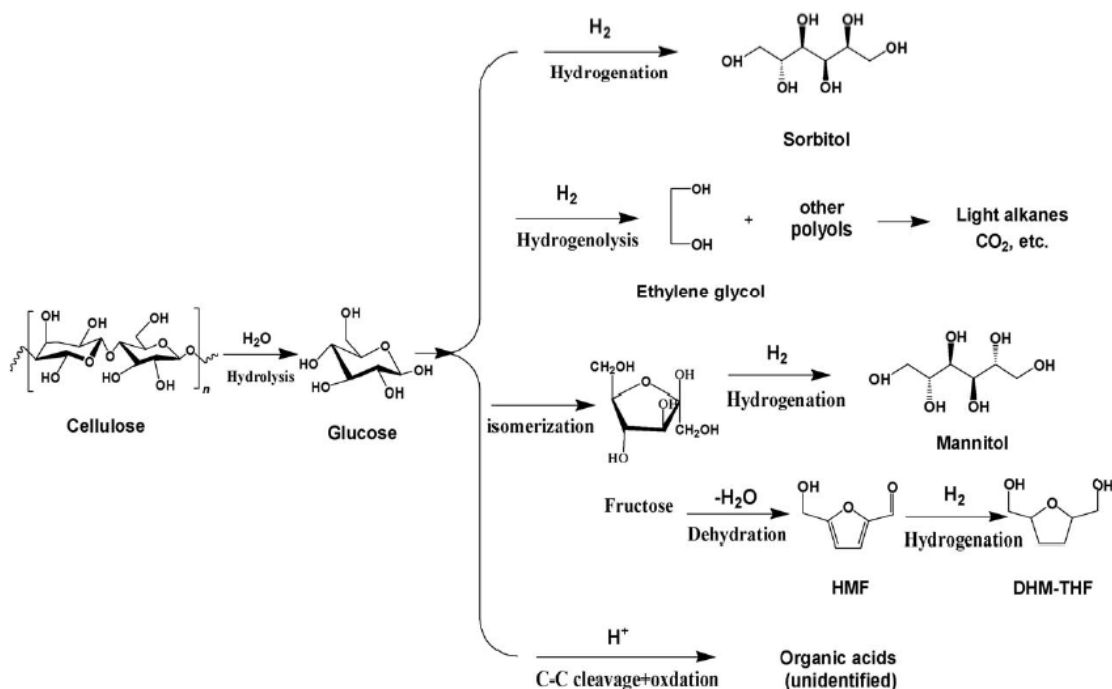
Figure 8: Possible reactions for the conversion of cellulose [10].

Xiao et al. also proposed a reaction scheme for the conversion of cellulose using their CuCr catalyst, as well as a nickel promoted tungsten catalyst [5]. In this pathway cellulose is hydrolysed into water-soluble saccharides, including both oligomers and glucose [5]. These compounds are subsequently converted by hydrogenation and/or hydrogenolysis to various polyols (see Figure 9).
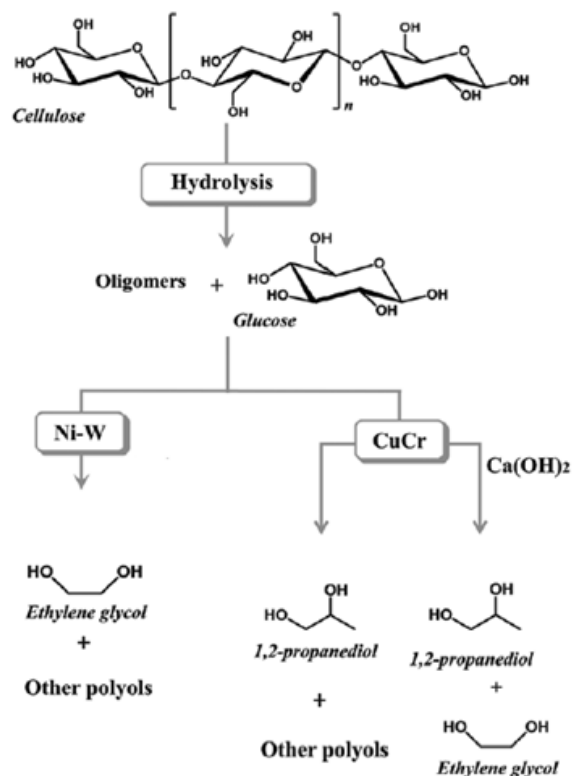
Figure 9: Catalytic conversion of cellulose into polyols (Adapted from [5]).

In their study into transition metal-tungsten bimetallic catalysts, Zheng et al. proposed a reaction scheme including the same three reaction types: hydrolysis, cracking and hydrogenation [1]. The cracking reactions were assumed to take place over tungsten sites, while the hydrogenation reaction were to take place on active sites by Ni and noble metals. It was found that the Ni/W ratio would greatly affect the product distribution. Too many hydrogenation sites would promote the hydrogenation reactions and dominate over cracking reactions, leading to increased hexitols and erythritol yields instead of EG. If the number of hydrogenation sites was very low, only a small amount of polyols would be formed [1].

In a study conducted by Liu et al., tungsten trioxide, WO_3, was used as an alternative tungsten source and in combination with a Ru/C catalyst used in cellulose conversion [17]. The study showed that the WO_3 crystallite effectively accelerates the hydrolysis of cellulose to sugar intermediates and the selective cleavage in the C-C bonds in these sugars. The combination of activated carbon as a support and the presence of WO_3 gave a significant high yield of propylene glycol. A reason for this might be the surface basicity of the carbon support accelerating the isomerisation of glucose to fructose (see Figure 10).

11
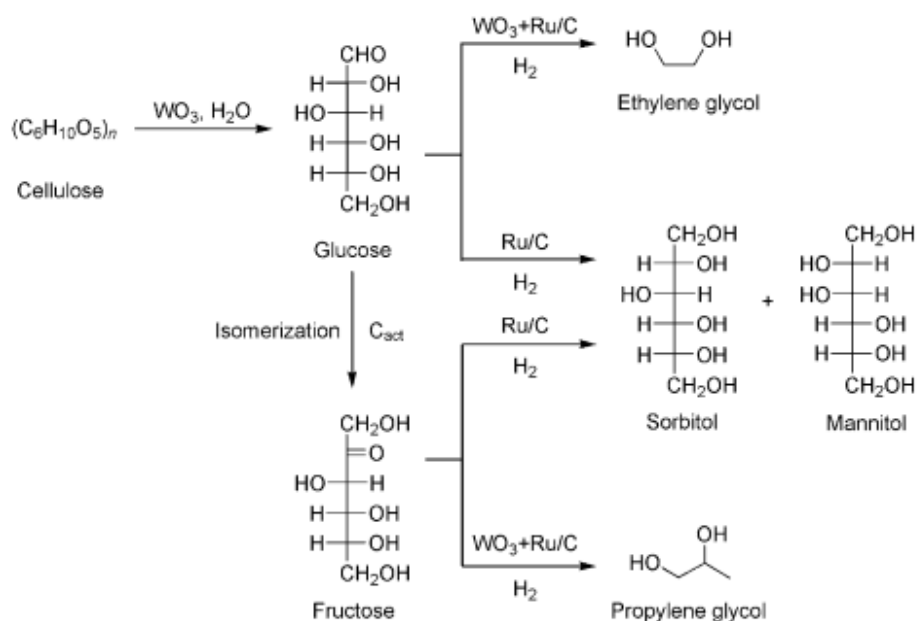
Figure 10: Catalytic conversion of cellulose into polyols (Adapted from [17]).

Tungsten compounds, both alone and in combination with hydrogenation catalysts, have been proven as active and selective for the hydrolytic hydrogenolysis of cellulose to EG. It is now known that the tungsten species catalyse the C-C bond cleavage of cellulose, as well as promoting hydrolysis. With this background Liu et al. examined the phase change of different tungsten species before and after reaction [17]. The results indicated that WO_3 always dominated the surface independently of the initial tungsten species. Based on these results it was suggested that the actual active sites for C-C bond cleavage is WO_3.

Considering that the characterisation by Liu et al. [17] was performed ex-situ, Wang et al. examined the tungsten oxide recovered immediately after the reaction and found typical XRD patterns for tungsten bronze (H_xWO_3) instead of WO_3 [7]. Tungsten bronze is not stable in atmospheric conditions and gradually transforms into WO_3, suggesting that tungsten species are transformed to H_xWO_3 by H_2 during reaction. In addition, taking leaching into account as an important factor to the reaction mechanism, it was found that low concentrations of 20-200 ppm dissolved H_xWO_3 was observed after reaction regardless of the tungsten species used [7]. They also found that the tungsten bronze, in combination with a hydrogenation catalyst (Ni, Ru etc.), was catalytically active for cellulose conversion into EG.

With the above mentioned results, Wang et al. concluded that the dissolved H_xWO_3 is the real active species for the C-C bond cleavage, with the reaction taking place through a homogeneous catalysis pathway. The H_xWO_3 was partially dissolved in hot water, while upon cooling and exposure to air it is transformed to insoluble tungsten acid and precipitate from the solution. Based on this temperature dependant phase-transfer behaviour they developed a highly active, selective and reusable tungsten acid and Ru/C catalyst.

Wang et al. also investigated the reaction mechanism of the one-pot conversion of cellulose to EG based on multifunctional tungsten-based catalysts [7]. Similarly to previous studies, it was found that implementation of a transition metal in the catalyst greatly increased the EG yield. In addition the unsaturated by-products decreased, making the carbon balance approach 95 %. Further evaluation into the function of transition metals like Ni, Ru, Pt, Pd and Rh showed that these metals only act as a promoter. Transition metals themselves have excellent

hydrogenation activities, but are not effective for the C-C bond cleavage and gives very low EG yields. If the hydrogenation capability of the tungsten carbide is insufficient, the transition metal acts as a promoter, giving remarkable results. If the hydrogenation activity of the tungsten carbide is high enough, the promotional effect will become less prominent. The study showed that Ni and Ru was found to behave the best and are most cost effective, with maximum EG yields obtained at Ni/W = 1 and Ru/W = 0.1. In addition, the tungsten carbide is kept from oxidation by spill-over of dissociated H by the presence of a transition metal [7].

With regard to the reaction pathway, Wang et al. found results suggesting that the H_xWO_3-catalysed C-C cleavage follows the retro-aldol pathway [7]. The C-C bond cleavage of sugars or cellooligosaccharides in supercritical water follows the retro-aldol condensation pathway. In reactions with only tungsten species under typical reaction conditions (518 K, 6 MPa H_2, and 30 min), glycolaldehyde was found to be the main product from cellulose conversion with a yield 4-6 times those obtained without a catalyst. Glycolaldehyde is the precursor to EG, and its presence indicates the retro-aldol pathway for the cleavage of C-C bonds [7].

Figure 11 shows the reaction pathway as proposed by Wang et al. [7]. The mechanism involves a cascade reaction in 3 steps [7]: Initially, hydrolysis of cellulose to water-soluble oligosaccharides and glucose is catalysed by H^+, both from hot water and dissolved H_xWO_3 (R_1). The glucose and cellooligosaccharides then instantaneously undergo C-C bond cleavage catalysed by a tungsten catalyst. The key intermediate glycolaldehyde is formed via the retro-aldol pathway with homogeneous catalysis of dissolved H_xWO_3 from the tungsten species (R_2). Finally, the end product is produced by hydrogenation of glycolaldehyde with a transition metal catalyst (Ru or Ni) (R_3).

Figure 11: Reaction pathway scheme for cellulose conversion to EG over tungsten based catalysts (Adapted from [7]). *The red part represents the overall reaction, the black part represents the three consecutive reactions towards EG, and the blue part represents the temperature controlled phase transfer behaviour of tungsten acid.*

In addition to the main reaction steps, metastable intermediate sugars and glycolaldehyde causes side reactions to occur. Limiting these reactions can be done by keeping the concentration of these intermediate sugars and glycolaldehyde at very low values. This means that the rated of the three consecutive reactions should satisfy the relationship: $R_1 < R_2 < R_3$ [7]. A kinetic study of the conversion of cellobiose, which is much easier to hydrolyse, showed that higher reaction temperatures guarantee $R_1 < R_2$ due to difference in activation energies [7].

EG is often the preferred product of cellulose conversion; however propylene glycol is a desirable by-product. An increase in the propylene glycol yield can be observed when the cellulose is converted to fructose instead of glucose. Liu et al. reported on higher 1,2-PG

13

yields due to isomerisation of glucose to fructose [17]. Similarly, Wang et al. reported on a comparative study which showed that glucose produced primarily EG, while fructose produced 1,2-PG under catalysis of Ni-W_2C [7]. It was found that the different positions of the C=O bond in the two sugar isomers resulted in different products during reaction.

As previously mentioned, Li et al. used their nickel-promoted tungsten catalyst, Ni-W_2C/AC for the simultaneous conversion of all three major components in lignocellulose; cellulose, hemicellulose and lignin [2]. In their proposed reaction pathway cellulose is converted to EG by hydrolysis, cracking and hydrogenation, while hemicellulose undergoes hydrolysis and cracking, before the two different intermediates (glycolaldehyde and glyceraldehyde) undergoes further steps resulting in EG and 1,2-PG (see Figure 6, Section 2.2.). Lignin is degraded into four main monomers as shown in Figure 7 .

2.4. Catalyst stability and reusability

Not only the product distribution and yields are important to the biomass conversion process. Lignin degradation has proven to be effective in the one-pot catalytic conversion of lignocellulose. Another major challenge to this process is catalyst stability. The ability for recycling is always important for metal catalysed liquid-phase reactions [10]. Ji et al. reports on the nickel promoted tungsten carbide catalyst with a slight decrease in the EG yield in the second run, while it remained nearly constant in the third run. It was concluded that leaching of metals was negligible and should not be considered as a major reason for the yield loss during recycling. XRD was also performed and it was found that the active W_2C phase on the after-run catalyst had been slightly oxidised. This oxidation might contribute to the loss of EG during recycling [10].

Li et al. tested the recycling ability of their Ni-W_2C/AC catalyst which showed good reusability for the conversion of the carbohydrate fraction [2]. After four runs, the EG and other diols yields were only slightly decreased. However, the total phenols yield dropped considerably in the fourth run after having been stable in the first three runs. In order to try and explain the drop in activity after four runs, XRD measurements on the recovered catalysts were done. Similarly to Ji et al. [10], it was found that the W_2C phase had been partially oxidised during reaction [2]. In this case, some leaching of Ni and W was also noticed and could, in combination with the oxidised surface, lead to the loss in activity. Furthermore, tar formed after the third and fourth run mixed with the catalyst and cause aggregation [2].

Scientists from the same institute that developed the Ni-W_2C/AC catalyst have also reported on a new 3D mesoporous carbon replicated from commercial silica as support or the tungsten carbide catalyst [11]. Dispersion and accessibility of active sites significantly affect the activity and selectivity of a catalyst. Activated carbon, being a microporous material, often gives rise to low dispersion and poor accessibility. Zhang et al. reports that the new support provides a significantly improved catalytic performance of tungsten carbide by facilitating the transport of reactant and product molecules in addition to the dispersion of tungsten carbide [11].

Similarly to Liu et al. [17] it was found that the WC_x phase had been partially oxidised on the recovered catalysts [11]. As a solution to this problem, regeneration in H_2 flow was performed after the fourth run. The results showed that the EG yield was partly recovered and the loss of selectivity could be attributed to the surface oxidation of the tungsten carbide. On the other

hand, the activated carbon supported catalyst used by Li et al. [2] had a much higher EG yield loss after four repeated runs than the mesoporous carbon supported catalyst. In addition, leaching was found to be one of the main reasons for the reduced performance in the fourth run with the WC_x/AC catalyst, while in the case of the WC_x/MC it was concluded that W leaching was not the main reason for decreasing EG yields during recycling tests [11].

In an attempt to solve the stability challenges of the nickel promoted tungsten carbide catalyst [8] Tai et al. developed a temperature-controlled phase-transfer catalyst system based on tungsten acid (H_2WO_4) in combination with an activated carbon supported Ru catalyst (Ru/AC) [9]. This catalyst system is robust and can sustain the harsh hydrothermal conditions during reaction. In the same way as parts of other tungsten species dissolving and forming H_xWO_3, the acid dissolved in hot water during reaction and acts as a homogeneous catalyst for the C-C bond cleavage and hydrolysis reactions of cellulose. The secondary component, Ru/AC, is a catalyst for the hydrogenation of glycolaldehyde into EG. After reaction the dissolved tungsten precipitates upon cooling and can easily be recovered by filtration. In addition, the catalyst exhibited excellent reusability of more than 20 times in the one-pot conversion of cellulose to EG [9].

2.5. Catalyst support and synthesis methods

2.5.1. Carbon supports

In the conversion of cellulose or lignocellulose to polyols several catalysts have been developed and tested. In addition to the active metals, the support material is of great importance. The support must have the correct properties for the application. In the conversion of cellulose to EG compressed hot water is used as a medium and the catalysts must therefore be resistant to hydrothermal attack [7]. The structural stability is essential and commercially available metal oxide supports often suffer structural and textural deterioration and collapse during reaction [7]. As a catalyst support, carbon has several advantages which make it favorable, such as excellent stability under hydrothermal conditions, high resistance to acid and base attack and being inert toward chelating with chemicals [7]. Other structural properties might also affect the reaction. Zhang et al. reports that their 3D mesoporous carbon supported WC_x catalyst reached very high EG yields without a transition metal, indicating that the support material itself affected the hydrogenation activity of the catalyst [11]. The 3D interconnected mesoporous structure facilitates the dispersion and accessibility of the active component. The transportation of molecules is also facilitated by this structure and enhances the hydrogenation activity for unsaturated intermediates [7].

Among the more successful catalysts for conversion of cellulose, activated carbon has proven an effective support material. Li et al., Liu et al. and Tai et al. all developed activated carbon supported tungsten based catalysts for the conversion of cellulose to polyols with superior reusability [2,9,17]. At the Norwegian University of Science and Technology, NTNU, a lot of work has been done using carbon nanotubes as catalyst support material. With this knowledge the previous study conducted by the author aimed to improve the Ni promoted tungsten oxide catalyst by using CNTs as support material.

As mentioned, both activated carbon and carbon nanotubes have been used as catalyst support. Other carbon supports successfully used in the conversion of cellulose includes mesoporous carbon, MC, [11], carbon nanofibres, CNF, and carbon nanotubes, CNT [7].

Activated carbon has the advantage of large surface area and well developed porosity [16]. However, during reactions with H_2 methanation might occur, which would be a noticeable side reaction at high temperatures [16]. In contrast to the microporous structure of activated carbon, carbon nanotubes/fibres have a mesoporous, open structure. This material property will affect both the preparation method of the catalyst and the performance of the catalyst itself [7]. Zhang et al. reports that mesoporous supports have higher yields than microporous activated carbon with tungsten carbide catalysts [11]. One of the reasons for this difference might be the dispersion of tungsten carbide on the support. On the microporous material, significant sintering took place, while good dispersion was observed on the mesoporous structure.

Due to the mesoporous structure of CNT it has been considered as catalyst support in the conversion of cellulose to polyols. Another reason why CNTs are considered for this application is the future prospect of industrialising the conversion process. For industrial purposes continuous stirred tank reactors, CSTRs, which allow for good mass transport, are used. CNTs have the possibility to grow on fixed substrates, such as different types of metal foils, fixed inside the reactor, making it a structured reactor [18]. It also allows for stirring of the reactants and continuous removal of the products. Another advantage with the CNTs is filtration. As the structure of the CNTs is open, filtration is made much easier when compared to compact powders etc. This lessens the problem of separation of the product from the solid catalyst.

2.5.2. Catalyst synthesis

Based on information from literature, this master thesis involves the use of both CNTs and AC as support for tungsten based catalysts. Obtaining the chosen catalyst involves a series of steps, including loading the support with a tungsten precursor, drying and heat treating it to transform the precursor into the desired compound. Activation of the metal component might also be necessary. In this study the aim of the catalyst synthesis is to obtain tungsten oxide and tungsten carbide catalysts. In the case of WO_3 a uniform coat is desired, while high dispersion of tungsten carbide is preferred.

Several methods are available for loading the precursor onto the support. In this case, a solid support is used and liquid-solid methods are most appropriate. One such liquid-solid method is a deposition technique called impregnation. Impregnation involves contacting a solid with a solution of the components to be deposited on the surface [19]. This method can be executed in many different ways, such as soaking or with an excess of solution; dry or pore volume impregnation; incipient wetness impregnation; deposition by selective reaction with the surface of the support; impregnation by percolation; co-impregnation where two or several active components are introduced in a single step; successive impregnation where two or several active components are introduced sequentially (drying/calcination takes place between the impregnations); and precipitation-deposition [19].

Independent of the impregnation method used, several processes take place during loading. These processes and the resulting product depend on the nature of the liquid and the solid surface as well as the reaction conditions [19]. Texture, functional surface groups, the presence of exchangeable ions, and reactivity are important parameters of the solid material. The nature of the solvent, pH, and the nature and concentrations of the dissolved substances are main parameters affecting the liquid. The processes occur with different rates depending on the reactants involved and include selective adsorption by Coulomb force, van der Waals

forces or H-bonds; ion exchange between the charged surface and the electrolyte; polymensation/depolymerisation of the species attached to the surface; and partial dissolution of the surface of the solid [19].

The most favourable impregnation options with regard to loading the carbon supports with tungsten are either impregnation by soaking, dry impregnation or incipient wetness impregnation. Soaking involves eliminating excess liquid by evaporation or draining and works best if ion/solid interactions are involved [19]. For deposition of species which interact very weakly with the surface, pore volume impregnation is the best method. Here, the volume introduced is the exact volume of the pores in the support. Incipient wetness impregnation is similar to dry impregnation. However, in this case the volume of the solution is empirically determined by finding the volume at which the surface is wetted.

According to literature, incipient wetness impregnation is one of the preferred methods for catalyst synthesis in the conversion of cellulose to polyols [1,2,8]. However, previous work by the author showed that incipient wetness impregnation of CNTs did not give promising results. Two different tungsten precursors (ammonium tungsten oxide pentahydrate and ammonium tungstate) were used, but neither gave the desired result in combination with incipient wetness impregnation. When the CNTs are pretreated with acid, the surface becomes negatively charged [18]. As the precursor becomes an an-ion solution, the charges will repel and make even distribution difficult [18]. To overcome this problem another loading method, sol-gel, has been considered in this study.

The sol-gel method is a gel-formation process involving the formation of gels or solid-like substances which retain the active elements from an initial solution [19]. A more specific sol-gel method is the Pechini method. The Pechini method involves the formation of a 3D polymer resin of a metal complex [20]. The essential feature in the Pechini method is the in situ polymerisation between citric acid, CA, and ethylene glycol, EG, or 1,2-polyethylene glycol, PEG. This polymerisation leads to the formation of a metal citrate complex solution which can be impregnated onto the support material [20]. However, this method might not be suitable for the AC support. CNTs have a mesoporous, open structure, while AC is a microporous material which might mean that the pores are too small for the metal complexes to enter.

Loading the precursor onto the support is only the first step in obtaining the final catalyst. After loading, the support is dried before it is calcined. The calcination is done to transform the precursor into metal oxides. In the Pechini method, calcination initiates pyrolysis of the organic species which results in the desired metal oxide [20]. In this study, calcination results in WO_3 catalyst. For tungsten carbide catalysts, the carbon supported oxide catalyst must be further treated. In both cases, the temperature is of great influence to the final product. Higher temperatures will result in tungsten carbide, while lower temperatures will result in tungsten oxide. Tungsten carbide catalyst can be obtained via a carbothermal hydrogen reduction process [16]. In this process the tungsten oxide is reduced to tungsten carbide under hydrogen flow and high temperatures (approximately 850 °C). After carburization, the catalyst is passivated by controlled exposure to air or N_2 flow at ambient temperature, preventing exothermic reactions when the catalyst is taken out of the reactor and comes into contact with air [19].

Considering the WO_3 catalysts are to be promoted by nickel, two methods are available for the loading of the tungsten and nickel precursors. For incipient wetness impregnation co-

impregnation is an alternative involving the introduction of two or more components in a single step [19]. Both precursors are dissolved in the same solution and impregnated onto the support. However, avoiding segregation of species and obtaining a uniform distribution is extremely difficult and successive impregnation might be a better option. This method involves introducing the two components sequentially, and can therefore be used as the second step in the Pechini method as well [19]. Drying, and sometimes calcination, is performed in between each impregnation step. After final impregnation, the sample is dried and heat treated to obtain the desired catalyst.

2.5.3. Latest research: carbon nanomaterials as catalyst support

Due to the exceptional advantages of a one-step transformation of lignocellulose into polyols, a lot of research has been done on catalysts for this process. Many studies show that nickel promoted tungsten carbide catalysts are highly effective catalysts for this process with high yields of EG [1,2,5,8]. In addition, tungsten oxide has proven to be an alternative to the tungsten species in similar catalysts [17]. Since nickel promoted tungsten based catalysts have been well tried for this process, the focus of research has shifted to the support material used in these catalysts.

At NTNU, research has been made on carbon nano-material in catalysis [21]. Carbon nanotubes, CNTs, and carbon nanofibres, CNFs, have special characteristics which make them attractive as catalyst supports. These characteristics include tubular or fibrous structures with a large number of edges (providing anchoring sites for catalyst precursors); mesoporous structure with large external surfaces; high resistance to strong acids and bases; easy adjustment of surface properties; high mechanical strength; and other unique advantages over the more traditional materials such as high surface area and being heat and electrical crystallite conductors [21].

Carbon, especially activated carbon, has long been used as catalyst support. However, the use is limited due to mass transfer limitations by the microporous structure [21]. CNTs and CNFs on the other hand has exceptional textural properties which make them ideal supports for liquid-phase reactions where less mass-transport limitation is required. In the case of biomass conversion in the liquid phase, CNTs and CNFs are favourable supports as mass transfer of the large molecules would be facilitated by the mesoporous structure. In addition, large and inert surfaces with tuneable functional groups enable good dispersion of metal particles [21].

Another carbon property is the amphoteric surface of the material [21]. This means that the net surface charge depends on the pH of the solution. High pH values, above the isoelectric point, IEP, or the point of zero charge, PZC, deprotonation of the surface makes it negatively charged. Values below the IEP makes the surface positively charged. In deposition method involving a solution functionalization or activation of the surface might be necessary to achieve uniform coating. Controlling the surface chemistry will facilitate electrostatic interactions during catalyst preparation. Low pH values will give a positively charged surface, making it preferential to solutions containing anions which will selectively adsorb onto surface.

3. Experimental

The previous study [14] leading to this work consisted of the making and characterisation of CNT supported tungsten catalysts for the direct catalysis of lignocellulosic material into polyols. Two catalysts were finished (50 % W loading) and fully characterised, while a second pair (12 % W loading) were not completed. These two catalysts have been completed in this study.

The previous catalysts are named based on the precursor used (AT: ammonium tungstate, ATOPH ammonium tungsten oxide pentahydrate) and the metal loading (50 % and 12 % tungsten, 2 % nickel).

Table 1: Catalysts from previous study [14].

Catalyst	Precursor	Ni loading,%	W loading, %
AT50W2Ni	Ammonium tungstate	2	50
ATOPH50W2Ni	Ammonium tungsten oxide pentahydrate	2	50
AT12W2Ni	Ammonium tungstate	2	12
ATOPH12W2Ni	Ammonium tungsten oxide pentahydrate	2	12

In this study both CNT and AC has been used as support for tungsten carbide and tungsten oxide catalysts. Table 2 shows the CNT based catalyst with the preparation method used for the catalyst synthesis and the metal loadings on the individual catalysts. Table 3 displays the same for the AC based catalysts.

Table 2: CNT based catalyst made in this study.

Catalyst	Preparation method	Tungsten loading, %	Ni loading, %
20WC$_x$/CNT	Pechini	20	
20WO$_3$/CNT	Pechini	20	Before Ni addition
2Ni20WO$_3$/CNT	Pechini	20	2
10WC$_x$/CNT	Pechini	10	
30WC$_x$/CNT	Pechini	30	

Table 3: AC based catalysts made in this study.

Catalyst	Preparation method	Tungsten loading, %	Ni loading, %
20WC$_x$/AC-p	Pechini	20	
20WO$_3$/AC-p	Pechini	20	Before Ni addition
2Ni20WO$_3$/AC-p	Pechini	20	2
20WC$_x$/AC-im	Impregnation	20	
20WO$_3$/AC-im	Impregnation	20	Before Ni addition
2Ni20WO$_3$/AC-im	Impregnation	20	2

3.1. Catalyst preparation

In this study tungsten carbide and nickel promoted tungsten oxide catalysts supported on carbon nanotubes and active carbon were prepared. Based on results from a previous study [14] the carbon nanotubes were loaded by the Pechini method, while the active carbon was loaded by both the Pechini method and incipient wetness impregnation.

3.1.1. Carbon support pretreatment

Before impregnation the carbon supports were treated with nitric acid (HNO_3) to remove impurities. In the case of the carbon nanotubes, CNTs, (Chengdu Organic Chemicals Co. Ltd.) acid was used to remove trace metals from the synthesis process and to introduce functional groups to the surface. Typically, 10 g CNTs and 250 mL nitric acid (65 %) were added to a round bottom flask and stirred while the temperature increased to 100 °C. The flask is connected to a water cooled condenser to retain some of the acid vapour. The mixture was left at 100 °C for 1 hour. After cooling to room temperature the CNTs were filtrated and washed (using filter paper, Büchner funnel, filtration flask and vacuum) and returned to the flask for a second treatment cycle. This was repeated a total of three times. At the end of the last cycle the CNTs were washed with large amounts of deionised water to reach a pH close to 5 and dried in an oven at 110 °C overnight. To ensure a fine powder for even distribution of the metal precursor solution the CNTs were grounded using a mortar and pestle.

In a similar manner as the CNTs, the active carbon (Norit Company, Netherlands) was treated with nitric acid to exclude any possible influences by the impurity metals on the commercial carbon support [10]. Typically, 25 g AC was mixed with 125 mL deionised water in a round bottom flask with a magnetic stirrer. The flask was then fixed to a water cooled condenser and a heat bath. 125 mL nitric acid was then added to the flask. Vapour from the flask was lead through a sodium hydroxide and water mixture to absorb the acidic content. The heat bath was set to 80 °C and left at this temperature for 24 hours.

Picture 1: Carbon support pretreatment set-up.

3.1.2. Catalyst synthesis – the Pechini method and incipient wetness impregnation

The previous study [14] concluded that incipient wetness impregnation of carbon nanotubes did not give the desired uniform tungsten oxide coating. In this study the Pechini method, a modified sol-gel route, will be used for the synthesis of tungsten based catalysts on CNT support.

The Pechini method consists of two steps; firstly, the formation of a three-dimensional polymer resin of a metal-complex; secondly, calcination to obtain the metal oxide [20]. The essential feature in the Pechini method is the in situ polymerisation between citric acid, CA, and ethylene glycol, EG, or 1,2-polyethylene glycol, PEG. This polymerisation leads to the formation of a metal citrate complex solution which can be impregnated onto the CNTs. After drying calcination is preformed, initiating pyrolysis of the organic species, resulting in the desired metal oxide [20].

In this study, ammonium metatungstate, AMT, was used as the precursor for tungsten. By regarding AMT as a positively charged precursor with a charge of +8, $[(NH_4)_6H_2(WO_3)_{12}]^{8+}$, the required molar ratio between AMT and CA can be found. CA has a negative charge of 3, resulting in a molar ratio of 3:8:8 for AMT:CA:EG/PEG. However, doubling the amount of CA, and consequently EG/PEG, giving a ratio of 3:16:16, will ensure enough protective compound to form the metal complex.

The Pechini method was used as a catalyst synthesis method with both CNTs and AC as the support. Typically, for 20 % tungsten loading, 3 g carbon support was used as a base. 1.005 g AMT (Merck, microcrystalline) , 0.381 g CA (Kermel, citric acid monohydrate, 99.5 %) and 0.276 g PEG (Sigma-Aldrich, PEGsolution ~50% in H2O) was dissolved in 7 mL (CNT) or 4.5 mL (AC) deionised water (The initially calculated amount of PEG was doubled as a ~50 % H_2O/PEG solution was used). Total dissolution was accomplished using an ultrasonic bath. The solution was then added drop-wise onto the carbon support until the surface was completely wetted. The loaded supports were then dried at 110 °C overnight.

For the active carbon support, incipient wetness impregnation was performed in addition to the Pechini method. In a similar manner as the Pechini method the tungsten precursor is dissolved in water and added drop-wise onto the support. Typically, for 3 g AC and 20 % tungsten loading, 0.1005 g AMT was dissolved in 4.5 mL deionised water. The solution was added onto the AC until the surface of the support was completely wetted. The sample was then dried at 110 °C overnight.

In all cases the tungsten loaded supports were calcined prior to further treatment. Calcination is done to obtain the finished catalysts by transforming the tungsten precursor into tungsten oxide, WO_3. This is done based on the calcination/carburization program described in "Catalytic Performance of Activated Carbon Supported Tungsten Carbide for Hydrazine Decomposition"[16]. All samples are initially calcined at 500 °C in N_2-flow with a heating rate of 5 °C/min. After 3 h at 500 °C WO_3/support was obtained.

Picture 2: Calcination set-up.

For the nickel promoted tungsten oxide catalysts, nickel was loaded onto the WO_3/support using incipient wetness impregnation. Typically, for 2 % nickel loading, 0.4 g nickel nitrate (Nickel(II) nitrate hexahydrate, Fluka) was dissolved in 8.7 mL (CNT) or 5.6 mL (AC) distilled water before the solution was added drop-wise onto the tungsten oxide catalyst. After drying overnight the catalyst was reduced to obtain the active nickel species. This was done using the same process as for tungsten carbide catalyst synthesis. Tungsten carbide catalysts are obtained by further carburising the WO_3/support in H_2 with the following heating ramp: from room temperature to 450 °C in 40 min, then to 850 °C at a rate of 1 °C/min and kept at 850 °C for 1 h. Reduction of the Ni-loaded WO_3/support is performed using the same technique.

The catalysts from the previous study were loaded with nickel and reduced to obtain the finished catalysts.
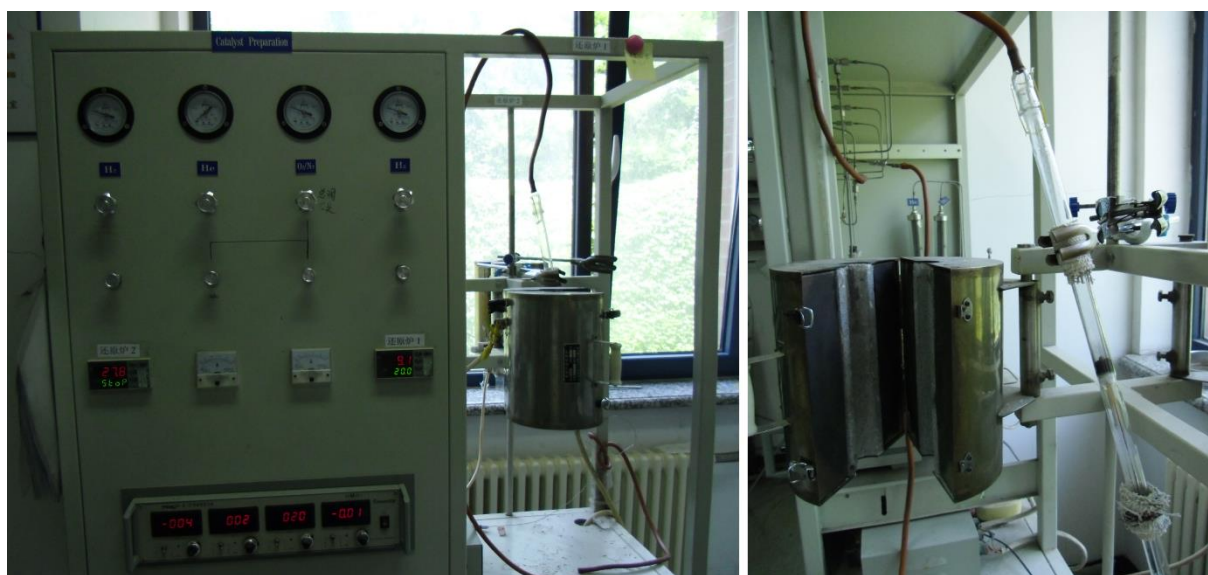
Picture 3: Carburization/reduction set-up.

3.2. Catalyst characterisation

A number of different analysis methods were used to characterise the catalysts and catalyst materials. The main objective of the catalysts synthesis was to manufacture catalysts with high dispersion of tungsten carbide or a uniform layer of tungsten oxide on the support surface. Scanning Transmission Electron Microscope, S(T)EM, analysis was used to image the surface of the catalyst to identify possible uniform layers or particles of metal oxides/carbides, and their size, on the carbon support surface. High dispersion of metal particles and maintaining a large surface area is key issues in catalyst synthesis with both CNT and AC as support. The specific surface area was therefore estimated by BET, while chemisorption was used to give an indication of the metal dispersion and particle size. H_2 chemisorption and TPR-TPO-TPR programs were made to determine the reduction temperature of WC_x. The bulk phase of the catalyst was identified using X-ray diffraction, XRD, while surface WO_3 was detected by Raman spectroscopy. Thermogravimetric analysis, TGA, was used to estimate the actual metal loading on the carbon support and Inductively Coupled Plasma, ICP, analysis was used to support these estimations while including values for the individual metal compounds.

3.2.1. BET analysis

BET analysis was used to determine the specific surface area of the catalysts. Nitrogen adsorption-desorption isotherms were obtained on a MICROMERITICS - ASAP 2010 apparatus at -196 °C. The Micromeritics ASAP 2010 (Accelerated Surface Area and Porosimetry System) applies the gas adsorption theory to provide surface area (BET) and porosity measurement for different types of solid materials [22]. The specific surface area is calculated by the Brunauer–Emmett–Teller (BET) method.

The apparatus consists of two sample preparation ports and one analysis port. For the analysis the weight of the empty sample holder was first noted. Approximately 0.1 g of sample was added to the sample holder and the weight was noted again. Prior to measurements, the samples were degassed. Given that the samples are powders this was done by first subjecting the sample to slow vacuum until it the value was below 500 μm Hg. At this point fast vacuum was initiated and left for one hour. Heat was introduced to the system, first up to 110 °C, and then to 300 °C until the vacuum reached 006 μm Hg. After cooling to room temperature, liquid nitrogen was added to the instrument, the sample holder moved to the analysis port and the analysis program initiated.

3.2.2. Thermogravimetric analysis, TGA

Thermogravimetric analysis, TGA, was used to estimate the actual metal loading on the carbon support by indicating the amount of metallic catalytic residue on the carbon support. The analysis was performed on a Setaram SETSYS 16/18 thermoanalyzer (SETARAM, France) from room temperature up to 1200 ºC at a constant heating rate of 10 ºC/min in air flow.

For analysis the crucibles were filled with approximately 10 mg sample and placed in the instrument. The TGA process measures the sample's mass as a function of temperature. During analysis, the weight (percentage) is plotted against temperature as the sample is heated in a controlled manner.

The data collected was exported to an Excel document. The final mass percentage represents the amount of metallic catalytic residue on the carbon nanotubes. In order to calculate the tungsten loading and compare the value to the intended loadings it was assumed that all tungsten species were oxidised during the analysis and WO_3 is the final compound. Based on this assumption the tungsten loading can be calculated by the following equation:

$$\boldsymbol{Tungsten\ loading}\ (\%) = \boldsymbol{TG\ mass}\ \%\ \boldsymbol{at\ end\ of\ analysis}\ \times \frac{Molar\ mass\ W}{Molar\ mass\ WO_3}$$

Equation 2

3.2.3. Inductively Coupled Plasma, ICP, analysis

In this study the ICP analysis was conducted to obtain an additional estimation of the metal content of the catalysts. The ICP analysis can measure the elemental content of a material in the range of ppt to wt% [23]. Normally, solid samples are dissolved in an acidic solution before introduced to the instrument. Analysis is achieved by ionizing the sample with inductively coupled plasma which can reach very high temperatures. The resulting ions are then detected and quantified with either an emission spectrometer (OES) or a mass spectrometer (MS) [23]. In this case, the ICP was used to obtain values for both tungsten and nickel content.

The ICP analysis was performed on an IRIS Intrepid II XSP instrument (Thermo Electron Corporation). Dissolution of the solid catalysts was obtained using microwave treatment on MARS 240/50 (CEM Corporation) at 800W. First the temperature was increases from 20 ℃ to 120 ℃ at a heating rate of 10 ℃/min. The temperature was left at 120 ℃ for 2 min, and then increased to 200 ℃ at 8 ℃/ min. Finally the temperature was left at 200 ℃ for 20 min.

ICP analysis was performed on both solid catalysts and liquid products from reactions. Due to time constraints it was decided to investigate the solid catalysts made by the Pechini method and the liquid products from the reusability tests. For the solid catalyst analysis approximately 0.005 g catalyst, for tungsten analysis, and 0.02 g catalyst, for nickel analysis, was dissolved in a mixture of 3 mL HCl and 4 mL HNO_3 and microwaved to ensure dissolution. The dissolved samples were then diluted to 100 mL. For the liquid product analysis 1 mL product was diluted to 50 mL and analysed for both nickel and tungsten.

3.2.4. Chemisorption

Chemisorption measurements were done to estimate the metal dispersion and the metal particle size on the surface of the catalyst. Initially this analysis was conducted for all catalysts made. However, the WO_3 catalyst could not be fully characterised by chemisorption as the analysis method is a form of reduction. The metal oxide would be reduced during analysis and the results would not give an accurate indication of the dispersion.

The analysis was performed on a MICROMERITICS AutoChem II 2920 automated Catalyst Characterisation System with a pulse chemisorption mode, using 10 % H_2/Ar as the adsorbate gas. The analysis was carried out at in a temperature range of 50 – 900 ℃.

Typically, 50 mg sample was added to a u-shaped quartz reactor and fitted to the instrument. Initially the sample was pretreated at 150 ℃ for 1 hour to remove adsorbed water prior to the

measurement. However, to eliminate oxide that might have formed during storage of the tungsten carbide catalysts, the samples were reduced in a pure H_2 flow at 400 °C for 30 min followed by purging with Ar flow at 410 °C 30 min. After cooling to 50 °C, the gas flow was switched to 10 % H_2/Ar to start the H_2 chemisorption. Loop gas was injected for each pulse, and pulses were introduced until peaks were equal or after 15 times.

3.2.5. H_2 chemisorption and TPR-TPO-TPR

H_2 chemisorption and TPR-TPO-TPR programs were made to determine the reduction temperature of WC_x. An assumption is made that the reduction temperature might depend on the carbon support used.

The cellulose conversion takes place under high pressure hydrogen. During the reaction WC_x is oxidised by the high pressure water, and at the same time being reduced by the high pressure hydrogen. Due to the interaction between the support and the metal carbide a different might be seen between AC and CNT as the catalyst support.

In the same way as normal chemisorption the analysis was performed on a MICROMERITICS AutoChem II 2920 automated Catalyst Characterisation System. 50 mg sample was added to a u-shaped quartz reactor and fitted to the instrument. For H_2 chemisorption the samples were pretreated at 450 °C for 1 h followed by purging with Ar flow at 120 °C 30 min. The gas flow was switched to 10% H_2/Ar to start the H_2 chemisorption. Loop gas was injected for each pulse, and pulses were introduced until peaks were equal or after 15 times. For the TPR-TPO-TPR analysis a cold trap was used to capture water that forms during oxidation.

3.2.6. Scanning Transmission Electron Microscope, S(T)EM, analysis

S(T)EM imaging can be used to evaluate the morphology of the catalysts. In this study the analysis method was used to evaluate the surface coating of the support.

The S(T)EM analysis was performed by the State key Laboratory of Catalysis at DICP. The TEM analysis was performed on a FEI with the voltage of 120 KV (Tecnai G2 Spirit 120kV). For high resolution SEM, HRSEM, the images were taken on a Hitachi S5500. The beam current and voltage information for each sample is included in the images.

SEM imaging was done on tungsten based catalysts (oxide and carbide) before promotion with nickel. All samples were prepared on Cu grids before analysis.

3.2.7. X-ray diffraction, XRD

The bulk phases of the catalysts can be identified by XRD analysis. Structural properties of catalysts and catalytic model surfaces can be studied by means of interference effects in scattered radiation. The x-rays have sufficient energy to penetrate solid and are well suited to probe their internal structure [24]. In this study, the XRD diffraction patterns will be used to identify the bulk composition of the catalyst. Each peak on the diffraction pattern will allow for identification of a compound it the sample.

For the XRD analysis, powder sample holders were used. The catalysts were grounded to make a fine powder and placed in the sample holders. The samples were compressed to make a smooth surface. The X-ray diffraction was carried out on a PANalytical X'pert diffractometer using nickel-filtered Cu Kα radiation, operated at 40 kV and 40 mA. The instrument is fitted with an X'Celerator RTMS detector and the X-ray diffraction patterns were recorded from 10° to 80°.

3.2.8. Raman

Raman spectroscopy is a surface analysis technique that can determine the chemical structure of a catalyst surface and identify the compounds on the surface [25]. The analysis is performed by measuring molecular vibrations and result in a Raman spectrum. Each compound has distinct bands and is identified based on the resulting bands in the Raman spectrum. According to literature [26] microcrystalline WO_3 is characterised by bands at 807, 715 ad 274 cm^{-1}.

The Raman spectra were collected at room temperature on a LabRam HR800 confocal microprobe Raman instrument (HORIBA Jobin Yvon, France). The laser excitation was at 532 nm with a He-Ne laser, and a laser power of approximately 7 mW.

3.3. Catalysts testing

Catalyst testing was done by catalytic conversion of cellulose. This reaction was carried out using a stainless-steel autoclave (Parr, 100 mL). Typically, cellulose (0.5 g), catalyst (0.2 g) and deionised water (50 mL) were charged into the autoclave. The reactor was initially purged with H_2 to remove air from the system. The hydrogen pressure was then adjusted to 60 bar and the system was stirred at a rate of approximately 1000 rpm. Heat was introduced to the reaction by the following heat ramp: from room temperature to 160℃ in 40 minutes, then to 230 ℃ at a heating rate of 10 ℃/min, finally the temperature is increased to 245 ℃ at 1 ℃/min and kept at this temperature for 2 hours (30 minutes for initial testing). Note that the reactor pressure increases with the increasing temperature, reaching approximately 130 bar at 245 ℃.

After completed reaction gas sample bags were used to collect some of the gas inside the reactor. This gas was then analysed by gas chromatograph (Agilent 6890N, TDX-1 column, TCD detector). The temperature of the column was kept at 110 °C for 2 minutes, then increased to 250 °C at a heating rate of 8 °C/min and kept at this temperature for 10 minutes. Helium was used as the carrier gas.

The liquid product was analysed by external standard method with HPLC system (Agilent 1200, Shodex Sugar SC1011 column and differential refractive index detector (RID)). Water was used as the mobile phase, at a flow rate of 0.6 mL/min. The injection volume was 5.0 μL, the RID opt. temperature 35 °C and the oven temperature 45 °C. This analysis gives an estimation of the product yield. Based on an estimation of the peak areas, the yields of EG, Sorbitol, Mannitol, Erythritol, 1,2-PG, glycerol and 1,2-butanol are found. In this report the total yield will be given as the sum of these compounds, even though several other compounds might exist in small amounts.
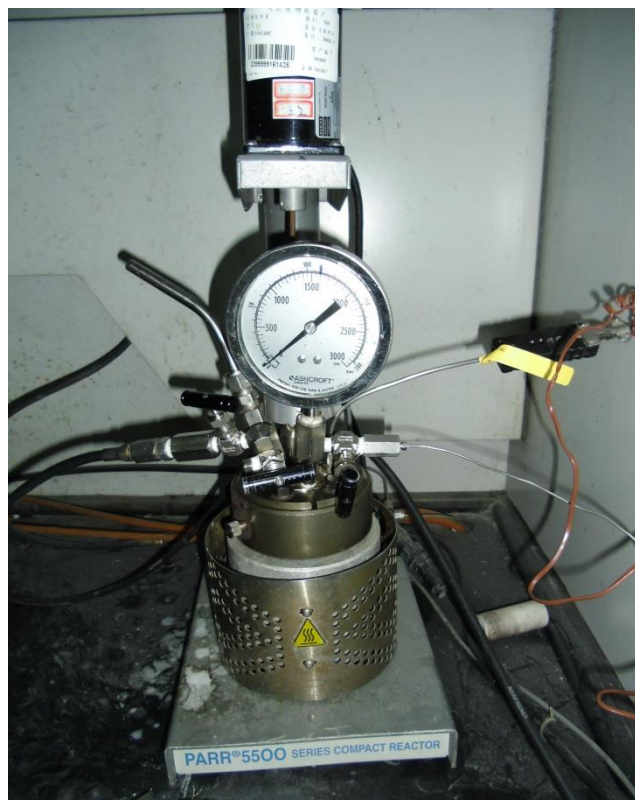
Picture 4: Catalyst testing/reactor set-up.

Recovery of the catalyst was done by filtering the liquid product and recovering the solid material. In the case of incomplete conversion of cellulose the solid material will be both cellulose and catalyst. The reactor was washed with deionised water and all solid particles are recovered. Initially the weight of the filter paper was noted and the filter paper and solid material from the reaction was dried overnight before it was weighed. The mass based conversion can be calculated in the following matter:

$$Conversion = \frac{cellulose\ feed}{cellulose\ at\ end\ of\ reaction} \times 100$$

Equation 3

$$Cellulose\ at\ end\ of\ reaction = solid\ at\ end\ of\ reaction - catalyst\ feed$$

3.3.1. Reusability

The reusability of the catalysts was tested by carrying out a reaction using the catalyst left from the previous reaction. In most cases the amount of catalyst left will be less than the original 0.2 g and the amount of cellulose and water were adjusted accordingly.

3.3.2. Effect of tungsten loading

The effect of changes in tungsten loading on the catalyst was tested by performing identical reactions with catalysts with different tungsten loading. The procedure of the reaction process was the same as described in Section 3.3.

4. Result and discussion

4.1. Characterisation

4.1.1. BET analysis

The BET surface area of the catalysts from the previous study was estimated using the same equipment as the new catalysts. The results are shown in Table 4. In the previous study it was found that the addition of tungsten precursor to the carbon support reduce the surface area of the sample. However, addition of nickel and calcination again increased the surface area, especially in the case of lower tungsten loading (12 %). In the case of 50 % tungsten loading the final surface area remained lower than the initial area of the CNT.

Table 4: BET surface area of catalysts made in previous study.

Sample	CNT support*	AT12W2Ni	ATOPH12W2Ni	AT50W2Ni	ATOPH50W2Ni
BET surface area m²/g	102.6	106.4	107.5	84.6	96.1

* Value from previous study [14].

The BET results from this study show that the surface area of the CNT based catalysts are reduced compared to that of the original CNT support (see Table 5). In the case of the tungsten oxide catalyst the surface area is significantly reduced by more than half the area before the addition of nickel. After addition of nickel and subsequent reduction, the surface area is increased, yet not enough to reach the original area of the CNT support. Tungsten carbide on the other hand gives a catalyst with a larger surface area; still the area is considerably reduced from that of the original support. Reduction of the catalysts, both after addition of nickel and for carbide formation, is conducted at high temperatures, which may result in methanation of the carbon support. During methanation, carbon from the support reacts with hydrogen in the flow and produces methane. Removal of carbon from the support may lead to additional porous structure, thereby increasing the surface area.

Table 5: BET surface area of CNT based catalysts.

Sample	CNT support	20WC$_x$/CNT	20WO$_3$/CNT	2Ni20WO$_3$/CNT
BET surface area m²/g	107.6	82.1	49.2	70.0

In the case of catalysts with AC as the support, the surface areas are much larger than for CNT catalysts. The surface area of AC is originally much larger than that of CNTs. Similarly to that of the CNT catalyst it can be seen that the surface area is reduced compared to the original AC support (see Table 6 and Table 7). In the case of the incipient wetness impregnation method, addition of nickel to the tungsten oxide catalyst increases the surface area. This is however not the case for the catalyst made by the Pechini method. Presence of nickel can accelerate the methanation of the carbon support [10], and the loading method might affect the way in which methanation occur. Methanation will lead to loss of carbon support and might in that case reduce the surface area. However, in the case of incipient wetness impregnation it seems methanation is less pronounced than for the Pechini loaded catalysts.

It is also evident that the incipient wetness impregnation method gives a lager surface area of the finished catalysts compared to the Pechini method. One reason that might explain this is the physical properties of the carbon support. AC is a microporous material and the metal complexes made in with the Pechini method might be too large to enter the pores. Some of the micropores will therefore by blocked by metal particles upon calcination/reduction which reduces the surface area.

Table 6: BET surface area of AC based catalysts made with the Pechini method.

Sample	AC support	20WCx/AC-p	20WO3/AC-p	2Ni20WO3/AC-p
BET surface area m²/g	709.0	521.7	555.4	536.0

Table 7: BET surface area of AC based catalysts made with incipient wetness impregnation.

Sample	AC support	20WCx/AC-im	20WO3/AC-im	2Ni20WO3/AC-im
BET surface area m²/g	709.0	650.1	562.9	604.3

In terms of the CNT based catalysts with different tungsten loading, it first looked like a trend could be seen with regard to the surface area and the tungsten loading. The lowest tungsten loading, not including the pure CNTs, gave the smallest surface area, and the highest loading the largest surface area. However, after thermogravimetric analysis, it was found that the actual tungsten loading was not as originally intended (see Section 4.1.2.) and this trend is not valid. In this case the lowest loading still gives the lowest surface area; however, the highest loading does not give the largest surface area. An additional peculiarity arises with the surface area presented by 30WCx/CNT. This catalyst presents a surface area larger than that of the pure CNTs.

Table 8: BET surface area of CNT based catalysts with different tungsten loading.

Sample	CNT-blank	$20WC_x$/CNT	$10WC_x$/CNT	$30WC_x$/CNT
BET surface area m²/g	106.9	82.1	71.4	116.7

4.1.2. Thermogravimetric analysis, TGA

Thermogravimetric analysis was used to estimate the metal loading of the catalysts. Initially, pure CNTs were analysed to estimate the purity of the support. The initial analysis showed a TG mass reduction of 100 % indicating a pure carbon sample. However, a second sample of pure CNTs from a different pretreated batch showed a metal residue loading of 5.7 %. This might indicate that some CNT support will contain residual trace amounts of metals from the CNT synthesis. A solution to this issue could be harsher pretreatment of the CNTs with larger amount of acid and several treatments.

The metal loadings based on the resulting TG cor. % values are shown in Table 9. The intended loading calculated based on the amount of precursor and support used was 20 % W for the initial catalysts. However, the calculated tungsten loading does not correspond to the intended loading. This might be due to methanation during reduction and carburisation. When carbon is removed the ratio between carbon support and metals change and the metal loading increases.

Table 9: TGA results and calculated metal loading.

Catalyst	TG cor. (%)	TG mass % end	Calculated W loading
CNT support	-100	0	0.00
20WCx/CNT	-55.3	44.7	35.45
20WO3/CNT	-74.2	25.8	20.46
2Ni20WO3/CNT	-73.2	26.8	21.25*
CNT	-94.3	5.7	0
10WCx/CNT	-69.8	30.2	23.95
30WCx/CNT	-62.3	37.7	29.89
20WCx/AC-p	-61.8	38.2	30.29
20WO3/AC-p	-69.2	30.8	24.42
2Ni20WO3/AC-p	-65.3	34.7	27.52*
20WCx/AC-im	-63.4	36.6	29.02
2Ni20WO3/AC-im	-68.1	31.9	25.30*
20WO3/AC-im	-67.5	32.5	25.77

* The W loading is calculated by disregarding the Ni present and assuming W is the only metal in the catalyst.

Figure 12 show the resulting diagram from the TGA for the CNT based catalysts. The plot indicate at what temperature carbon begins to oxidise, at approximately 500 °C, and the point of maximum oxidation, in the range of 660-690 °C. Due to some irregularities during the analysis of 2Ni20WO3/CNT it is difficult to see the effect addition of nickel might have had on the oxidation temperature.
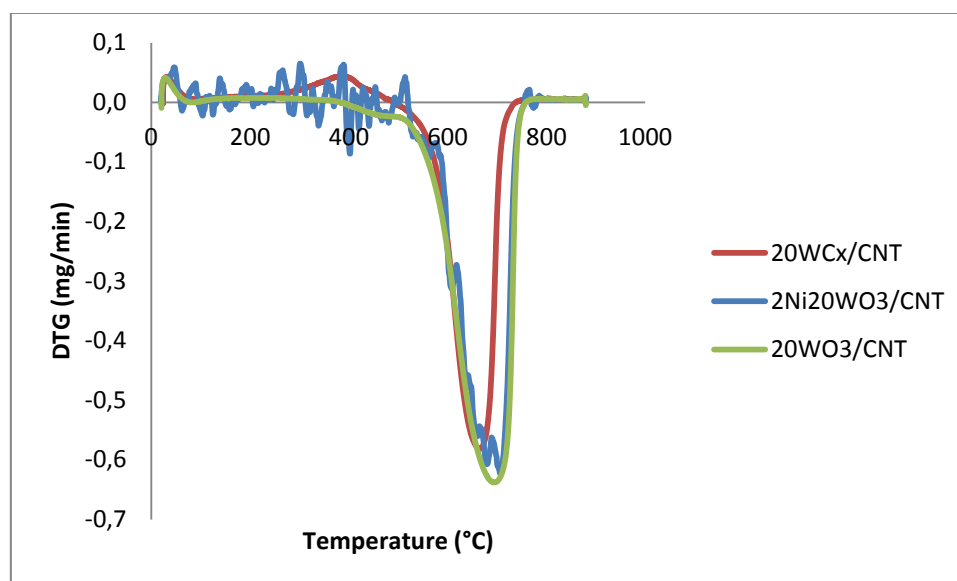
Figure 12: DTG vs. temp. curves for CNT based catalysts made by the Pechini method.

Figure 13 display the mass loss curve for the same CNT catalysts. In this case it is easier to see a possible effect of nickel addition and reduction. Both 20WCx/CNT and 2Ni20WO3/CNT have been reduced as part of the catalyst synthesis; 20WO3/CNT on the other hand has only been calcined. The results indicate that the mass loss of 20WO3/CNT starts at a lower temperature than for the 2Ni20WO3/CNT. This would suggest that addition of nickel and reduction reduces the oxidation temperature. Additionally, a slight initial increase in mass can be noted for 20WCx/CNT. This is also evident in Figure 12. This increase in mass might be due to initial oxidation of WCx on the surface of the catalyst.
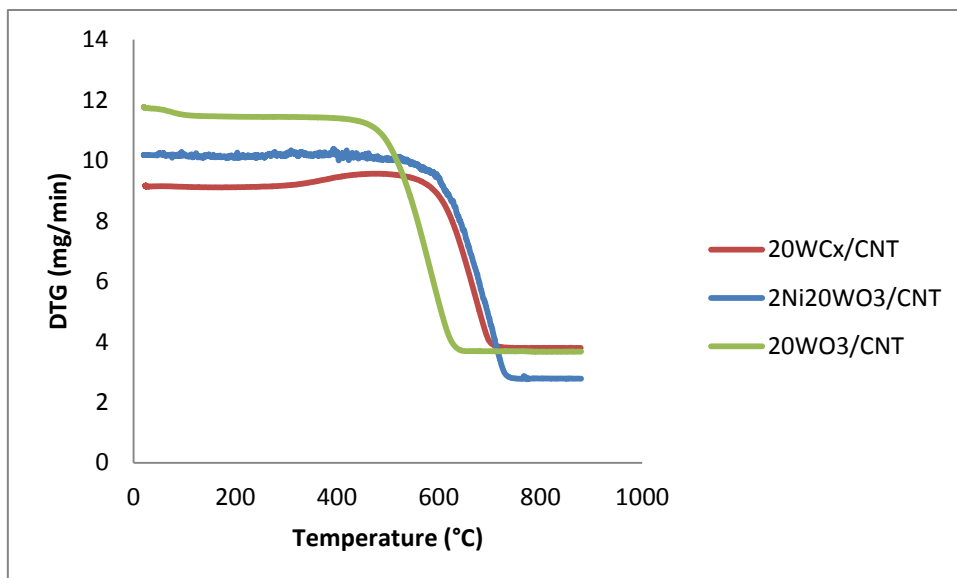
Figure 13: TG cor. mg vs. temp. curves for CNT based catalysts made by the Pechini method.

Figure 14 and Figure 15 show the resulting diagrams from the TGA for the AC based catalysts. When compared to the CNT based catalysts the point of maximum oxidation is somewhat lower, at approximately 600°C. Similarly the temperature at which the carbon begins to oxidise is lower, 420 °C compared to the considerably higher 500 °C. Similarly to the CNT based tungsten carbide catalyst, both 20WCx/AC-p and 20WCx/AC-im display an initial mass increase due to oxidation of WCx.
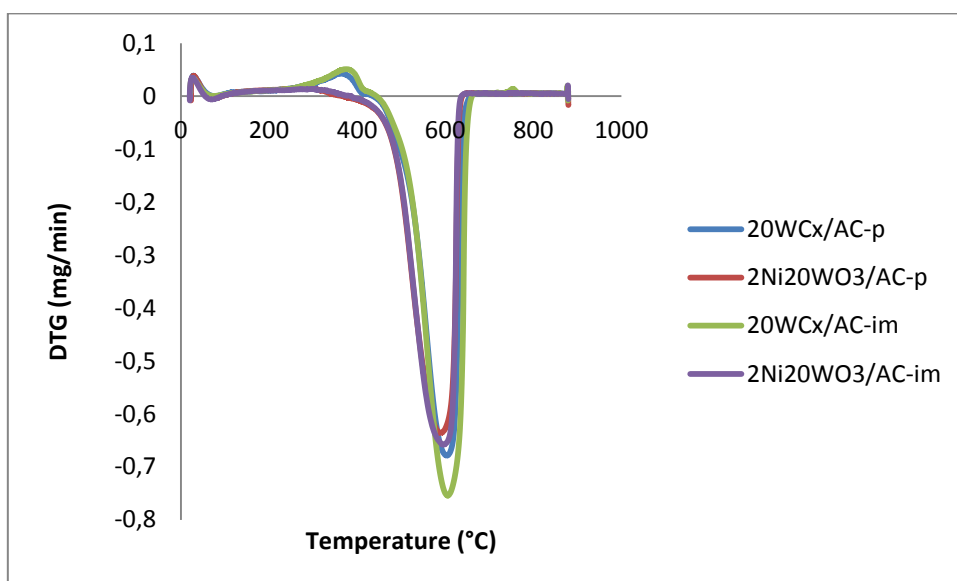
Figure 14: DTG vs. temp. curves for AC based catalysts made by both incipient wetness impregnation and the Pechini method.
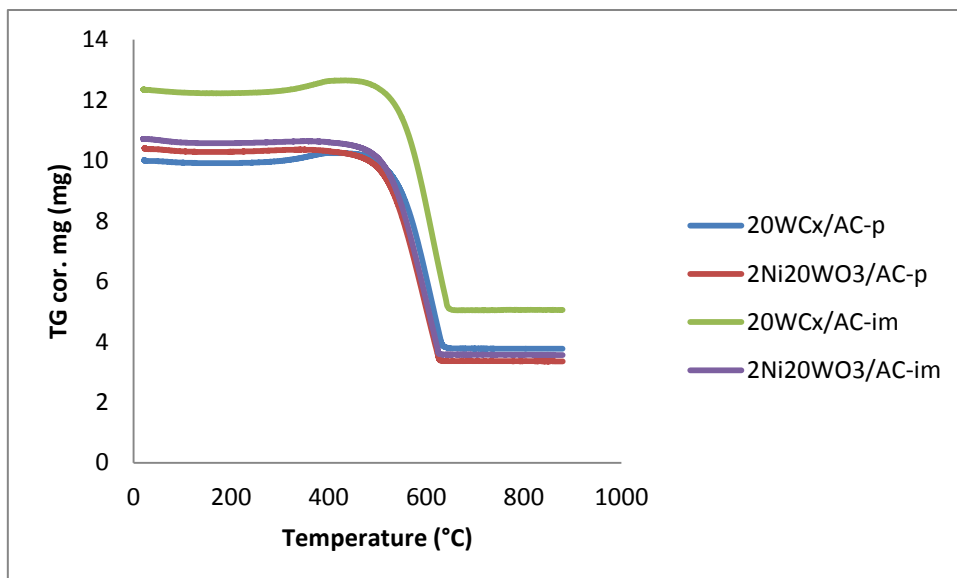
Figure 15: TG cor. mg vs. temp. curves for AC based catalysts made by both incipient wetness impregnation and the Pechini method.

With regard to the AC based catalysts addition of nickel and reduction seem to have nearly no effect on the results of the TGA. Both the carbon oxidation and the mass loss occur at the same temperature independent of nickel addition or not (see Figure 16 and Figure 17).
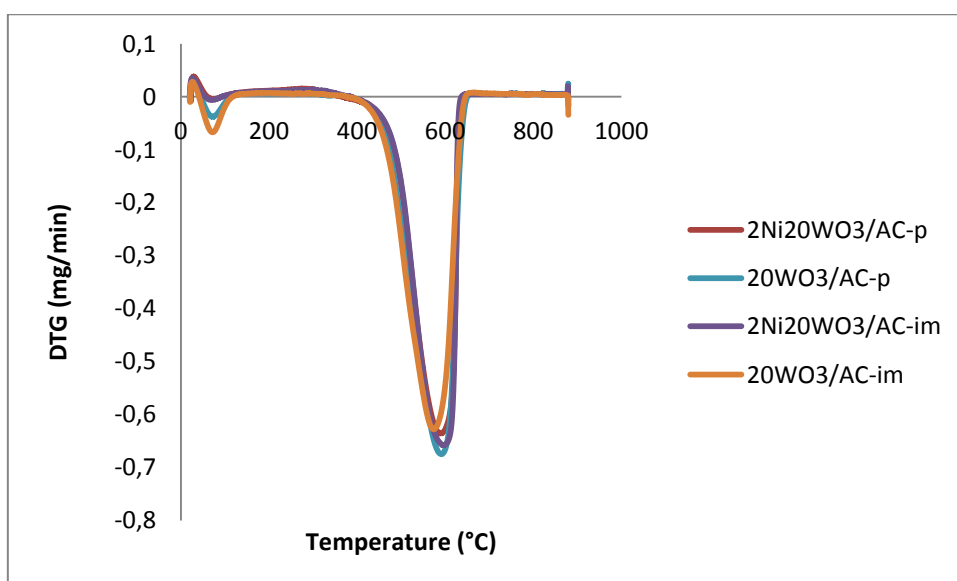
Figure 16: DTG vs. temp. curves for AC based tungsten oxide catalysts; made by both incipient wetness impregnation and the Pechini method, and calcination at 500 °C in N_2-flow.
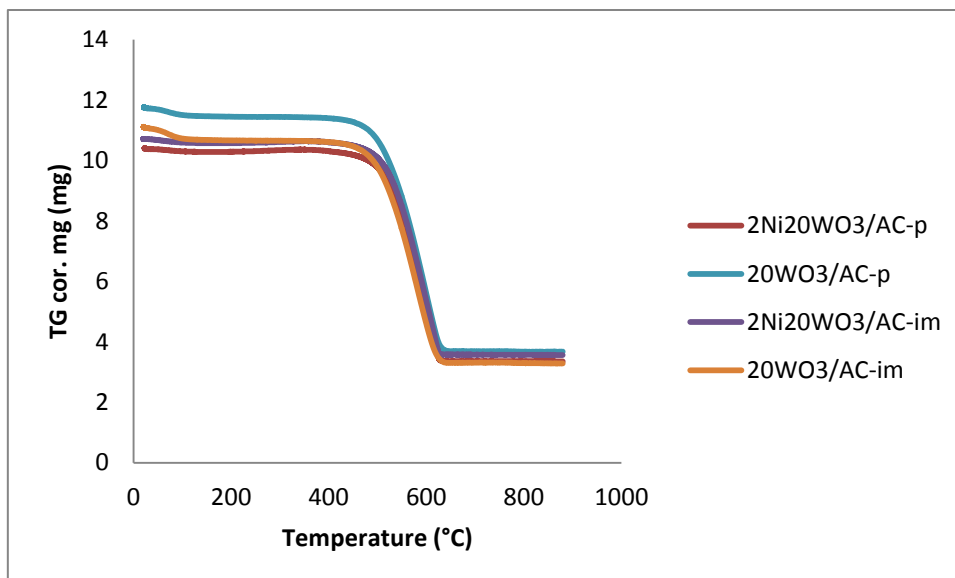
Figure 17: TG cor. mg vs. temp. curves for AC based tungsten oxide catalysts: made by both incipient wetness impregnation and the Pechini method, and calcination at 500 °C in N$_2$-flow.

Figure 18 and Figure 19 show the resulting diagrams from the TGA for the CNT based catalysts with different tungsten loading. A possible trend can be seen in that 20WCx/CNT has a lower oxidation temperature and mass loss occur at a slightly lower temperature, than 10WCx/CNT and 30WCx/CNT. 30WCx/CNT has the highest oxidation temperature and temperature for mass loss. However, the actual metal loading based on the TGA results do not support this trend. A conclusion can therefore not be made regarding the effect of tungsten loading alone. A possible reason for the slight difference in oxidation temperatures might be the particle size. Both particle size and tungsten loading might affect the oxidation of the catalysts. Still, further study is needed to make a conclusion regarding features affecting the oxidation of tungsten carbide catalysts.
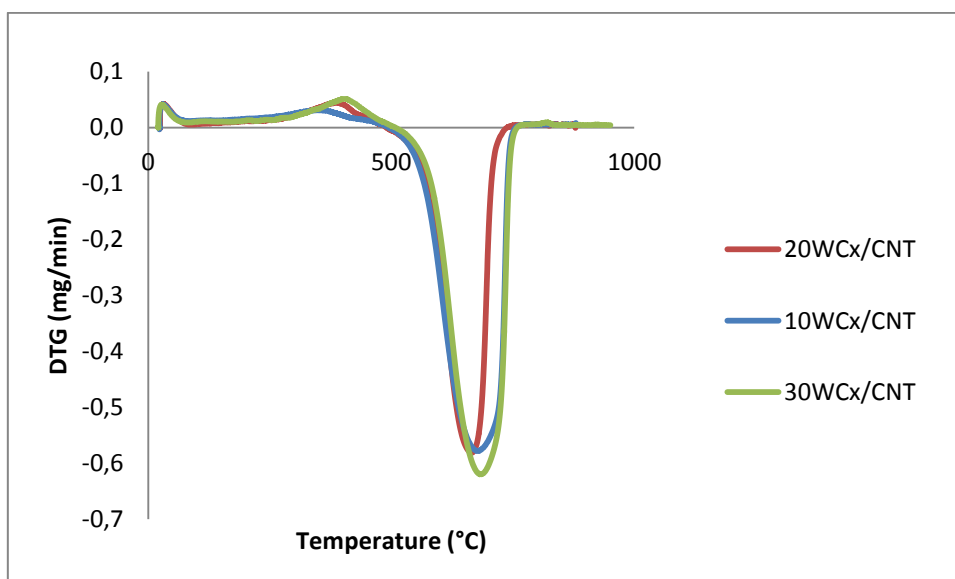
Figure 18: DTG vs. temp. curves for CNT based carbide catalysts with different tungsten loading; made by the Pechini method, calcination at 500 °C in N$_2$-flow and carburisation at 850 °C in H$_2$-flow.
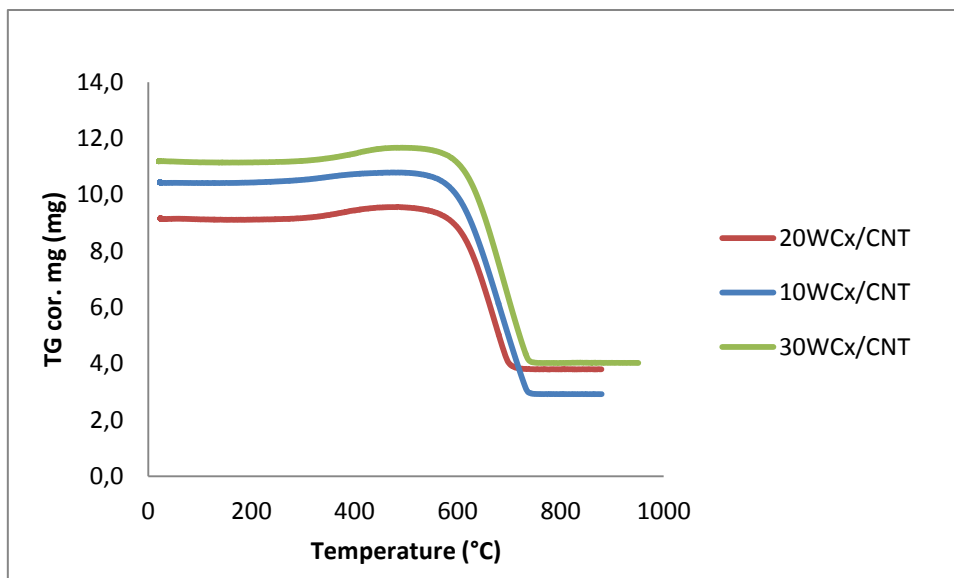
Figure 19: TG cor. mg vs. temp. curves for CNT based carbide catalysts with different tungsten loading; made by the Pechini method, calcination at 500 °C in N$_2$-flow and carburisation at 850 °C in H$_2$-flow.

4.1.3. Inductively Coupled Plasma, ICP, analysis

Table 10 show the results from the ICP analysis. However, due to incomplete dissolution of the catalyst the tungsten analysis cannot be used in this case. The preparation for the nickel analysis on the other hand, gave a more complete dissolution of the sample and can be used to indicate the nickel loading. It was found that 20WCx/CNT contained a small amount of nickel. As no nickel was used in the preparation of the catalyst, this nickel has to come from the CNT support which is contrary to the TGA results where the metal loading of the CNTs were zero. However, the support might not be a uniform batch and some nickel might be present in the amount of CNTs used as catalyst support.

The intended nickel loading of the 2Ni20WO3/CNT catalyst was 2 %. The ICP results indicate a loading of 2.45 %. Still, since the CNT were found to contain a small amount of nickel in the case of 20WCx/CNT, the same can be assumed for 2Ni20WO3/CNT.

In terms of the AC supported catalysts made by the Pechini method it was found that the tungsten carbide catalyst contained virtually no amount of nickel. This indicate that the AC support do not contain any nickel. This is also supported by the results for the 20WO3/AC-p catalyst. This catalyst was intended to contain 2 % nickel and the resulting ICP value is 1.81 % which is in relatively good agreement.

Table 10: Solid catalysts ICP results.

Catalyst	Analyse for	ICP value (ppm)	Metal loading (%)
20WCx/CNT	W	0.6465	1.20
2Ni20WO3/CNT	W	0.115	0.23
20WCx/AC-p	W	0.0975	0.19
P0WO3/AC-p	W	2.628	4.78
20WCx/CNT	Ni	2.223	1.15
2Ni20WO3/CNT	Ni	4.903	2.45
20WCx/AC-p	Ni	0.0196	0.01
2Ni20WO3/AC-p	Ni	3.902	1.81

For the liquid products analysis it was found that the tungsten leaching is quite severe. In the case of the tungsten carbide catalyst, the tungsten leaching is twice as high for the catalysts after reusability tests (2 reactions). The tungsten oxide catalyst shows approximately the same amount of tungsten leaching in both the fresh catalyst and after reusability tests.

In terms of nickel leaching the values are calculated based on the Ni content found in the ICP analysis of the solid catalysts. In the case of tungsten leaching, the carbide catalyst displayed a slightly higher leaching than the oxide catalyst in the first run. However, for nickel leaching the value is slightly higher for the tungsten oxide catalyst. Still, after the reusability test, 20WCx/CNT shows much more severe leaching than 2Ni20WO3/CNT.

Metal leaching is normally most significant in the first run, and keeps as a constant lower value in subsequent runs [27]. However, the results presented here indicate an increase in leaching after the first run. As these results do not match the normal trend, repetition of the analysis might be necessary to obtain accurate results. Still, 20WCx/CNT showed a lower degree of Ni leaching in the first run, indicating better performance in the second run.

Table 11: Liquid product ICP analysis results.

Liquid product from	Analyse for	ICP value (ppm)	Leaching (%)
20WCx/CNT	W	1.479	**9.2**
20WCx/CNT-reusability	W	3.305	**20.7**
2Ni20WO3/CNT	W	1.12	**7.0**
2Ni20WO3/CNT-reusability	W	1.106	**6.9**
20WCx/CNT	Ni	0.028	**3.1***
20WCx/CNT-reusability	Ni	0.1073	**11.7***
2Ni20WO3/CNT	Ni	0.1093	**5.6***
2Ni20WO3/CNT-reusability	Ni	0.129	**6.6***

* The nickel leaching is calculated based on the nickel content determined by the solid ICP analysis if nickel.

4.1.4. Chemisorption

Table 12 shows the metal dispersion and crystallite size of the two catalysts made in the previous study [14]. Both catalysts showed very low dispersion and large crystallite sizes. S(T)EM imaging was also performed and was in agreement with the low dispersion. It was concluded that too high calcination temperature caused carbide formation and sintering of particles.

Table 12: Chemisorption results of catalysts made in previous study [14].

Catalyst	Metal dispersion (%)	Crystallite size^a (nm)
AT50W2Ni	0.57	176.5
ATOPH50W2Ni	0.50	200.7

^{a}6.000 V/A

As the preparation of the catalysts in this study include reduction of the active metal (tungsten and nickel), a test was done as to see if oxidation might have occurred during storage and re-reduction of the sample before chemisorption is necessary. As an example, 20WCx/CNT was

used. Table 13 shows that the re-reduction greatly affects the results. The metal dispersion is significantly increased after reduction and the crystallite size is considerably reduced. Re-reduction before chemisorption analysis was therefore performed on all the samples.

Table 13: Effect of re-reduction before chemisorption analysis.

Catalyst	Metal dispersion (%)	Cubic Crystallite Size (nm)
20WCx/CNT	0.2216	474.6169
20WCx/CNT with reduction	8.0941	12.9921

Table 14 shows the chemisorption results for the tungsten carbide catalysts in this study. It can be seen that the CNT based catalyst and the AC catalyst made with incipient wetness impregnation have larger metal dispersions and smaller crystallite sizes than the AC based catalyst made with the Pechini method.

As previously mentioned the physical properties of the support might affect the synthesis of the catalysts. The microporous structure of the AC does not allow the larger metal complexes in the Pechini method enter the pores, giving a lower dispersion.

It is to be noted that the instrument used for the analysis might not have been suitable for this kind of catalyst and the results should not be taken as factual.

Table 14: Chemisorption results of CNT and AC based catalysts.

Catalyst	Metal dispersion (%)	Cubic Crystallite Size (nm)
20WCx/CNT	8.0941	12.9921
20WCx/AC-p	0.7154	146.9961
20WCx/AC-im	6.4768	16.2363

4.1.5. H2 chemisorption and TPR-TPO-TPR

Figure 20 indicate that the catalyst sample did not display any chemisorption during the analysis. Increasing intensity in the peaks indicate chemisorption of hydrogen. However, in this case the peaks are of approximately the same intensity throughout the analysis, signifying no chemisorption. It is expected that the surface oxidation layer might affect the chemisorption properties of the catalyst. However, pretreatment was conducted to remove the oxidation layer and should not affect the analysis. In addition, the hydrogen might be weakly adsorbed on the surface, and when the sample is purged with helium as part of the program, the weakly adsorbed hydrogen might be removed from the surface.

Figure 20: H$_2$ chemisorption diagram of 20WCx/CNT (made by the Pechini method, calcination at 500 °C in N$_2$-flow and carburisation at 850 °C in H$_2$-flow).

Table 15: H$_2$ chemisorption raw data for 20WCx/CNT.

Peak number	Temperature at maximum (°C)	Quantity Adsorbed (cm3/g STP)	Cumulative Quantity (cm3/g STP)
1	449.2	0.15525	0.15525
2	449.3	0.08393	0.23918
3	449.2	0.06088	0.30006
4	449.2	0.05247	0.35253
5	449.4	0.02350	0.37603
6	449.2	0.00941	0.38545
7	449.3	0.00000	0.38545

With TPR analysis it is assumed that an oxide layer exists on the surface of the catalyst. Due to this oxide layer hydrogen is consumed during TPR and this consumption is proven by peaks in the TPR diagram. However, Figure 21 only indicates a weak peak at approximately 300 °C. This peak indicates the reduction of a WO$_3$ layer on the surface of the catalyst. In addition, the baseline is not very stable.

Figure 21: 1st TPR diagram for 20WCx/CNT (made by the Pechini method, calcination at 500 °C in N₂-flow and carburisation at 850 °C in H₂-flow).

The TPO analysis is a re-oxidation of the reduced catalyst. However, Figure 22 shows no peak for the oxidation of the sample. The TPO analysis was conducted in the temperature range of room temperature to 120 °C. This temperature might be too low for oxidation of this catalyst to occur. The negative peak indicated in the TPO diagram cannot be easily explained, and the TPO analysis should be conducted again to see if this is a property of the catalyst or, most likely, just a fault with this analysis run.
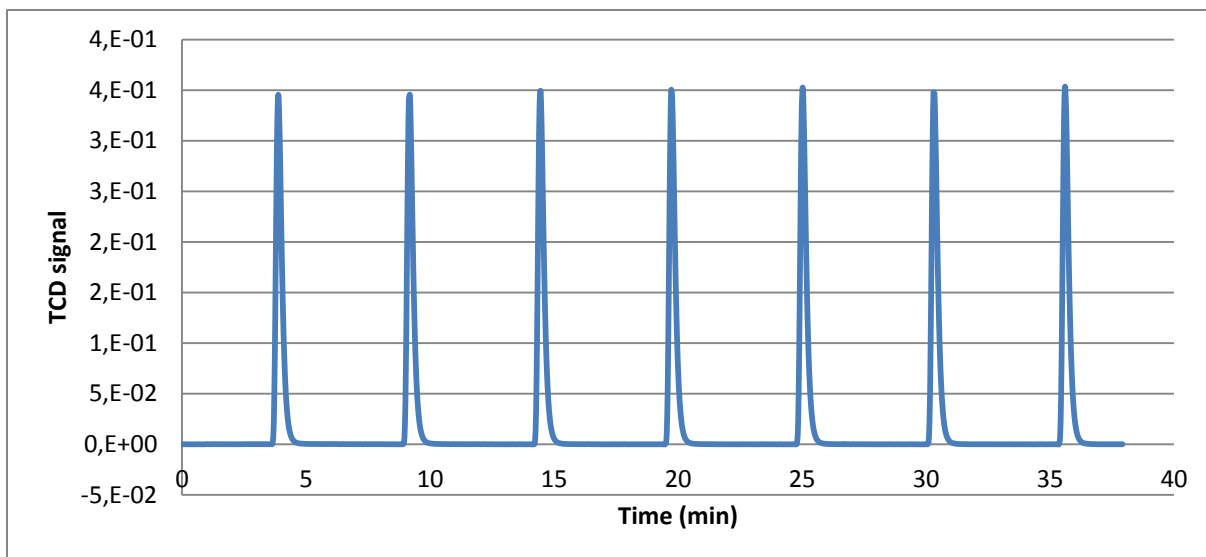

Figure 22: TCD signal vs. time TPO diagram for 20WCx/CNT (made by the Pechini method, calcination at 500 °C in N₂-flow and carburisation at 850 °C in H₂-flow).

TPO
TCD signal vs. temperature
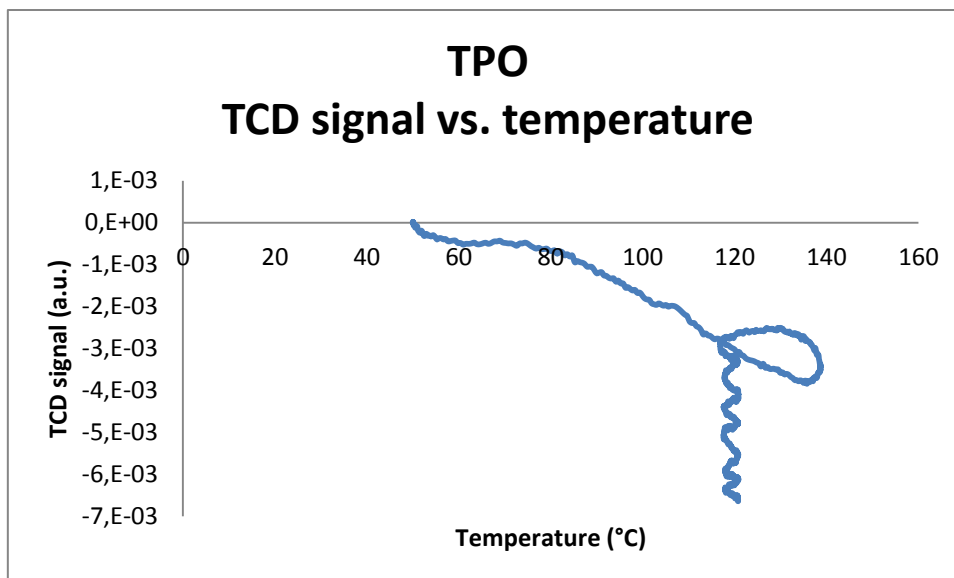
Figure 23: TCD signal vs. temperature TPO diagram for 20WCx/CNT (made by the Pechini method, calcination at 500 °C in N$_2$-flow and carburisation at 850 °C in H$_2$-flow).

In the second TPR run, it is evident that no oxidation layer is present on the catalyst surface. Seeing as no oxidation occurred in the TPO this appears correct.
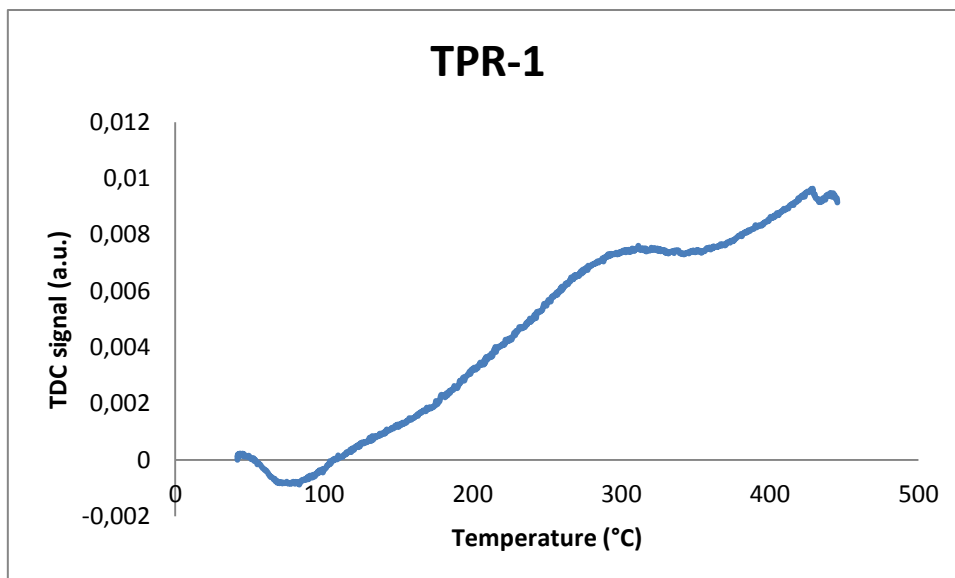

TPR-2
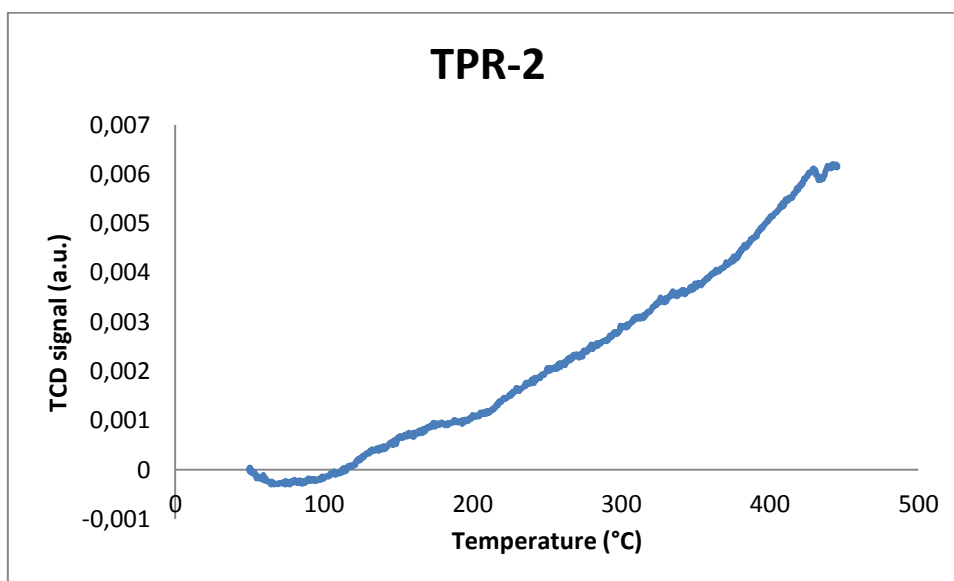
Figure 24: 2nd TPR diagram for 20WCx/CNT (made by the Pechini method, calcination at 500 °C in N$_2$-flow and carburisation at 850 °C in H$_2$-flow).

4.1.6. Scanning Transmission Electron Microscope, S(T)EM

The SEM imaging was done to evaluate the surface coverage of tungsten on the carbon supports. The previous study [14] concluded that the incipient wetness impregnation method in combination with too high calcination temperatures did not give a uniform layer of tungsten oxide on the CNT support. In this study both tungsten oxide and tungsten carbide catalysts were made and the impregnation method was substituted with the Pechini method in the case of CNTs as support.

Figure 25 shows S(T)EM images of pure CNTs and tungsten loaded CNTs from the previous study.
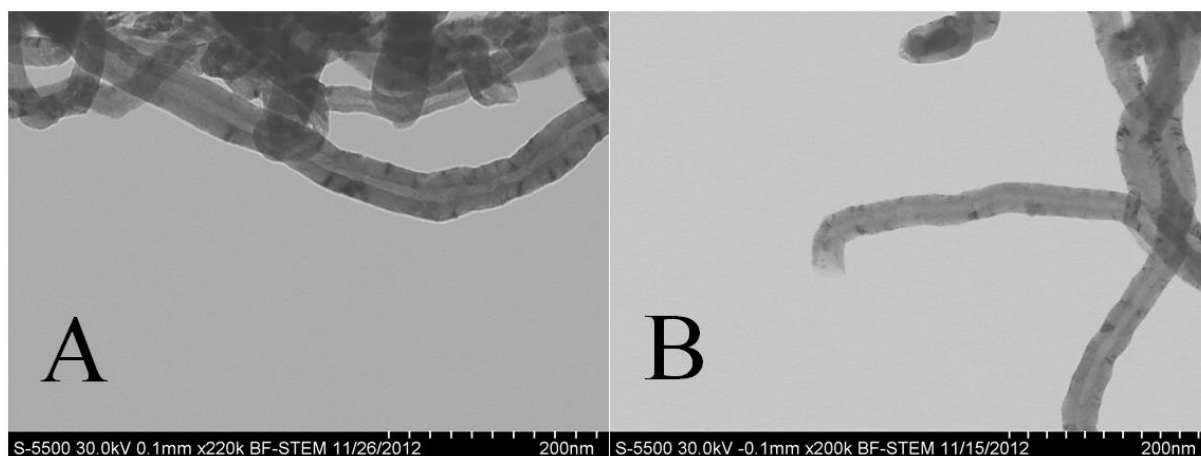
Figure 25: S(T)EM images: (A) CNTs and (B) W/CNT [14].

Figure 26 and Figure 27 show the SEM images of the CNT based catalysts obtained in this study. Similarly to that of the previous study, no uniform layer of either tungsten carbide or tungsten oxide is found on the surface. However, the images of the tungsten carbide catalyst indicate some metal particles on the CNT surface. The metal particle size seems in agreement with that found in the chemisorption analysis (~13 nm). As a uniform layer is not found, a lower dispersion is to be expected. This is also supported by the chemisorption results. The SEM images of the tungsten oxide catalyst show hardly any obvious particles on the CNT surface. One explanation might be a too low contrast between the WO_3 and the CNT support, making it impossible to distinguish an oxide layer or particles on the surface. This evaluation cannot be supported by chemisorption analysis as it could not be performed on the oxide catalysts.
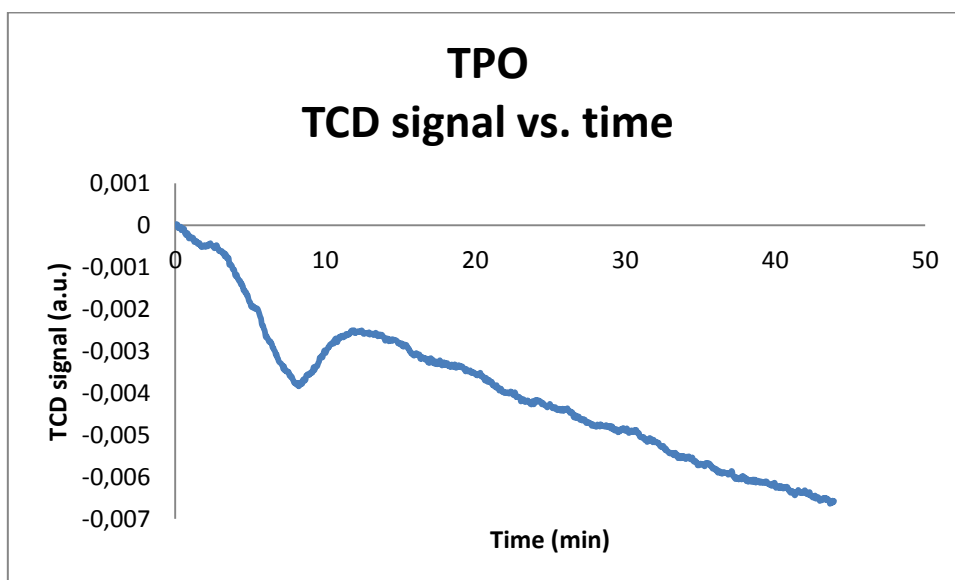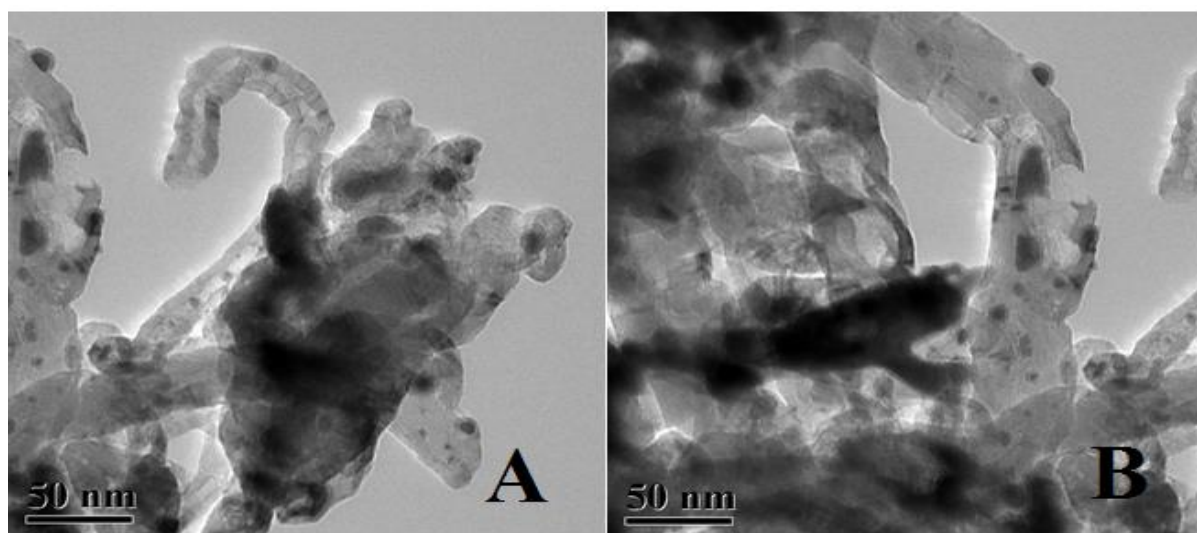

Figure 26: SEM images of 20WCx/CNT (made by the Pechini method, calcination at 500 °C in N_2-flow and carburisation at 850 °C in H_2-flow)..
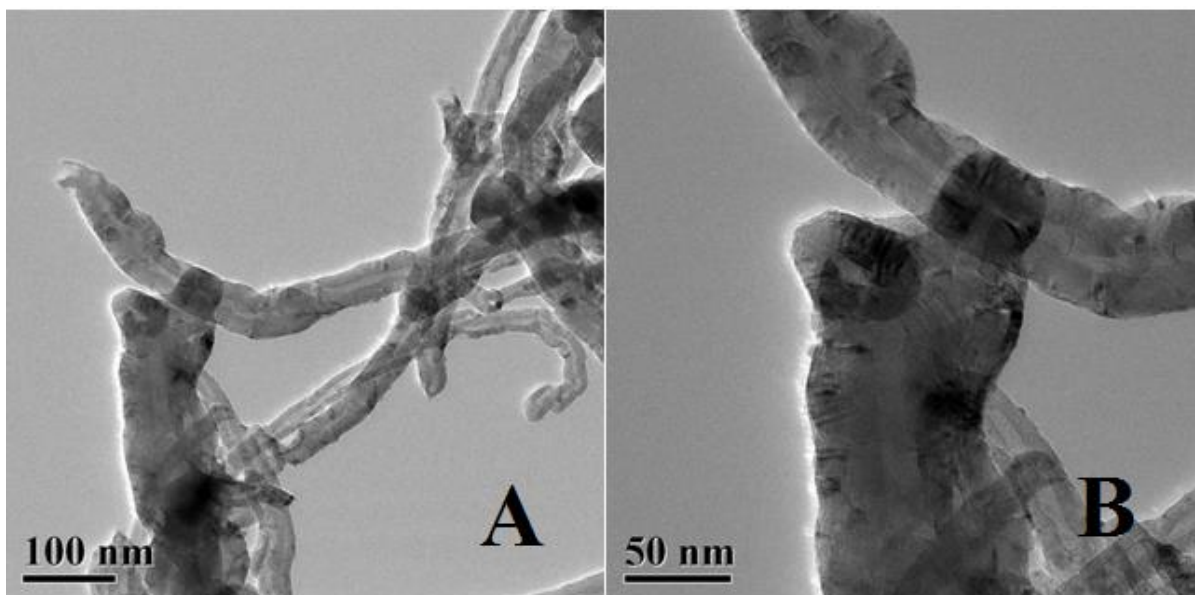
**Figure 27: SEM images of 20WO3/CNT (made by the Pechini method and calcination at 500 °C in N$_2$-flow).**

Based on Figure 28 the metal dispersion on 20WCx/AC-p is not very good. Figure 28 A (arrow) indicates aggregation of the particles, supporting the very low dispersion and large particle size found with chemisorption analysis.
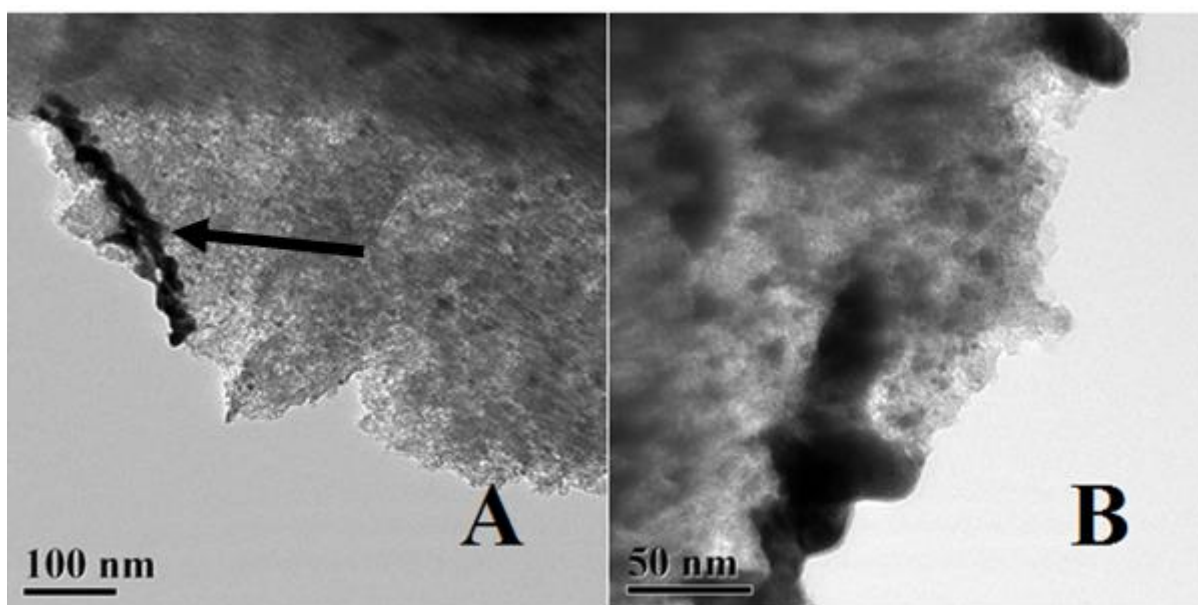
Figure 28: SEM images of 20WCx/AC-p (made by the Pechini method, calcination at 500 °C in N$_2$-flow and carburisation at 850 °C in H$_2$-flow).

Similarly to 20WO3/CNT, 20WO3/AC-p no oxide layer can be seen on the carbon surface. Again, the contrast between AC and WO3 might be too low to distinguish a layer from the carbon support.
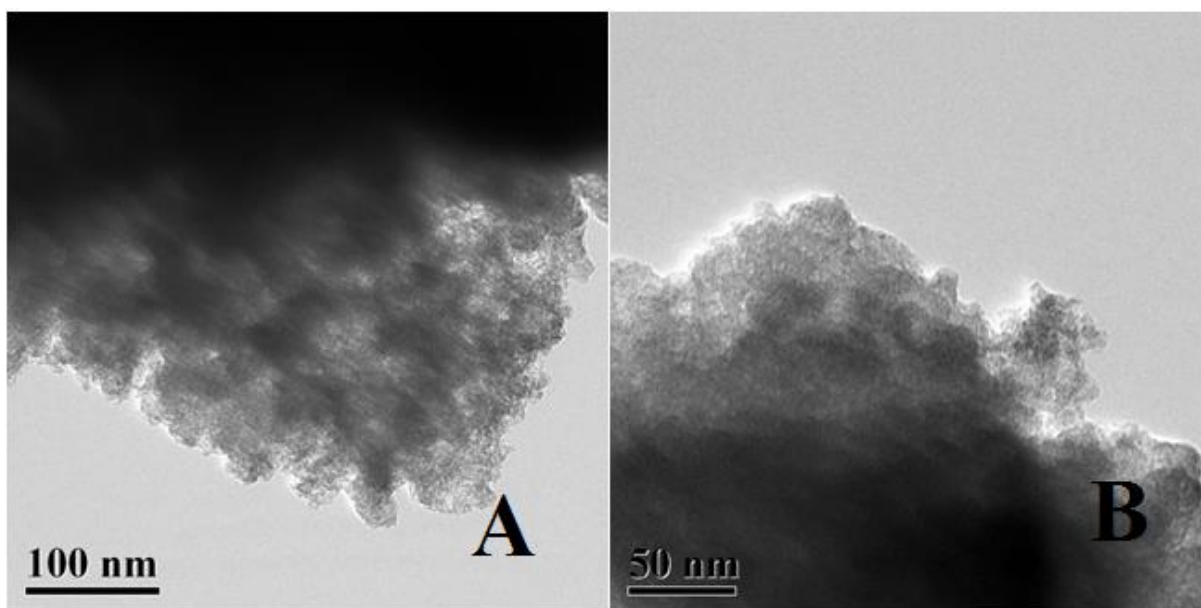
Figure 29: SEM images of 20WO3/AC-p (made by the Pechini method and calcination at 500 °C in N$_2$-flow).

Compared to 20WCx/AC-p, 20WCx/AC-im displays a much better dispersion and smaller particle size. Tungsten carbide particles are clearly visible in Figure 30. The catalyst also displays a type of core-shell structure (see Figure 30 B arrow). The apparent shell might be carbon covering WCx particles which could reduce the activity of the catalyst.
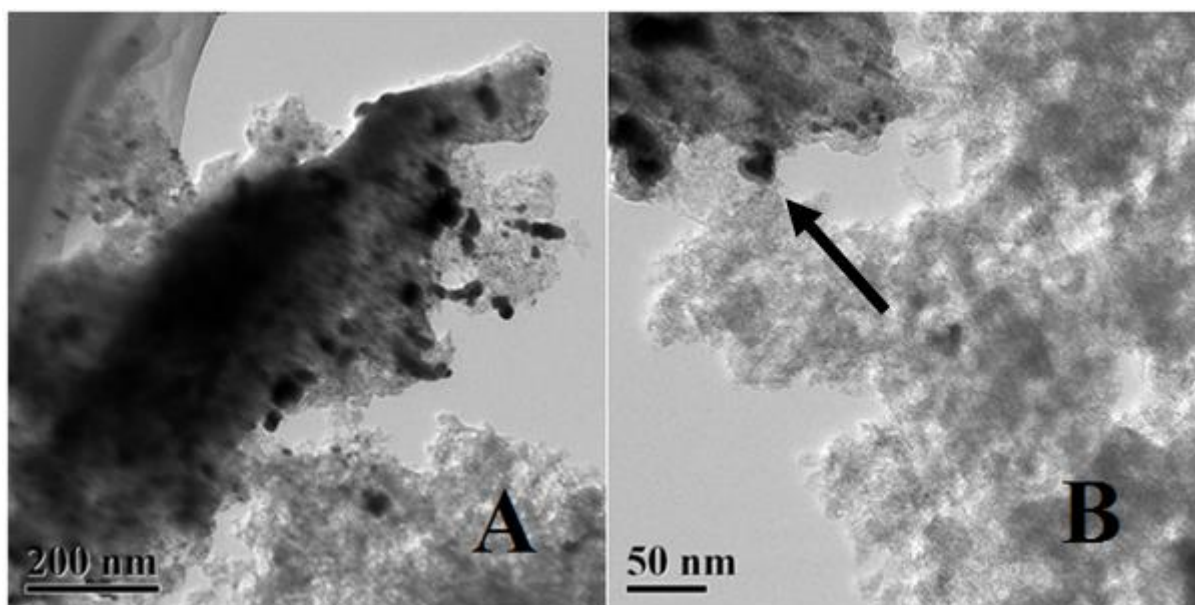
Figure 30: SEM images of 20WCx/AC-im (made by incipient wetness impregnation, calcination at 500 °C in N$_2$-flow and carburisation at 850 °C in H$_2$-flow).

In terms of 20WO3/AC-im, no apparent oxide layer can be distinguished from the AC support.
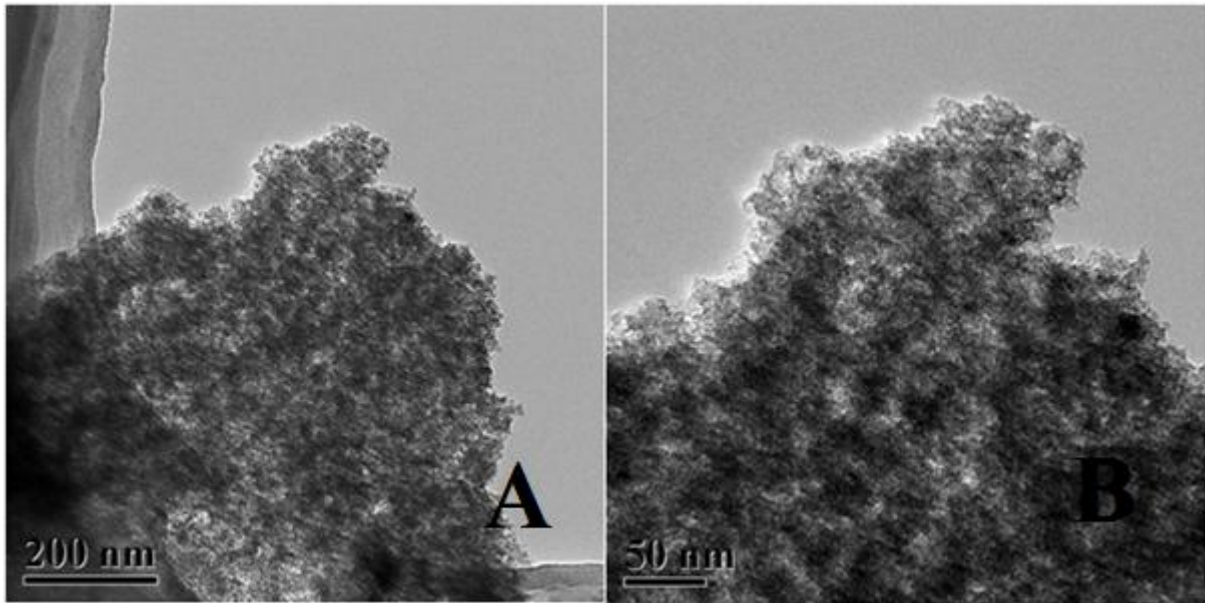
Figure 31: SEM images of 20WO3/AC-im (made by incipient wetness impregnation and calcination at 500 °C in N$_2$-flow).

4.1.7. X-ray diffraction, XRD

X-ray diffraction pattern for the pretreated carbon nanotubes show a distinct peak indicating carbon (see Figure 32). As previously mentioned the pretreatment of the CNTs did not manage to remove all trace metals from the CNT synthesis. Some nickel is therefore apparent in the XRD pattern in the form of nickel carbide.
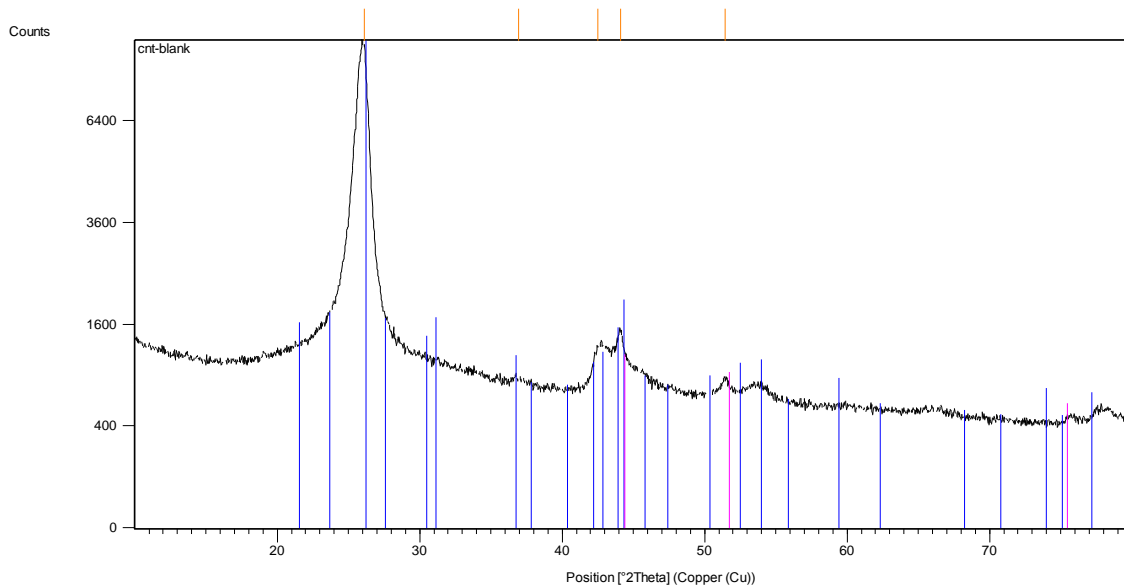
	Compound Name	Ref. Code	Chemical Formula
(blue)	Carbon	00-046-0945	C
(red)	Nickel Carbide	00-014-0020	Ni C

Figure 32: XRD pattern of pretreated CNTs.

The XRD pattern for 20WCx/CNT shows distinct peaks represent tungsten carbide. In addition, an obvious peak of carbon is clearly visible.
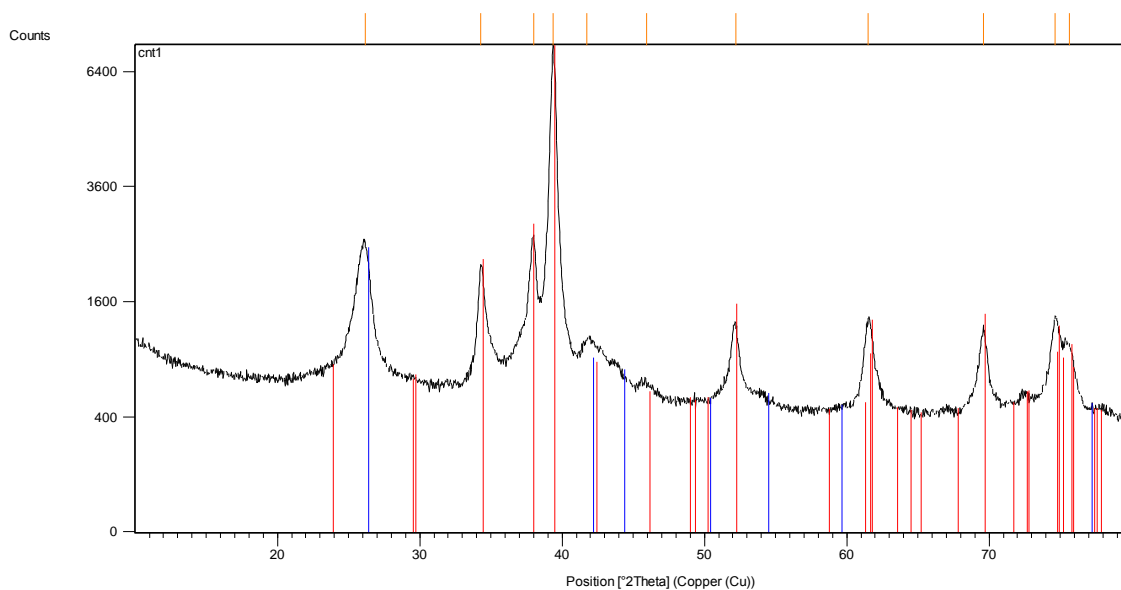
|	Compound Name	Ref. Code	Chemical Formula
(red)	Tungsten Carbide	01-089-2371	W2C
(blue)	Carbon	00-041-1487	C

Figure 33: XRD pattern for 20WCx/CNT (made by the Pechini method, calcination at 500 °C in N$_2$-flow and carburisation at 850 °C in H$_2$-flow).

The tungsten oxide catalyst also gives a distinct peak for the carbon support in the XRD pattern. In the previous study XRD results indicated that tungsten carbide had been formed during calcination, indicating that a too high temperature had been used. In this study the formation of tungsten carbide was avoided, even during reduction of nickel. The results indicate that the WO$_3$ might have formed as a monolayer on the surface of the CNTs. With monolayers there are hardly any peaks in XRD patterns as the XRD analysis is bulk analysis. Monolayer dispersion is common for WO$_3$. The assumption of monolayer WO$_3$ cannot be confirmed by either chemisorption or SEM imaging. The XRD pattern also indicates nickel as part of the bulk composition.
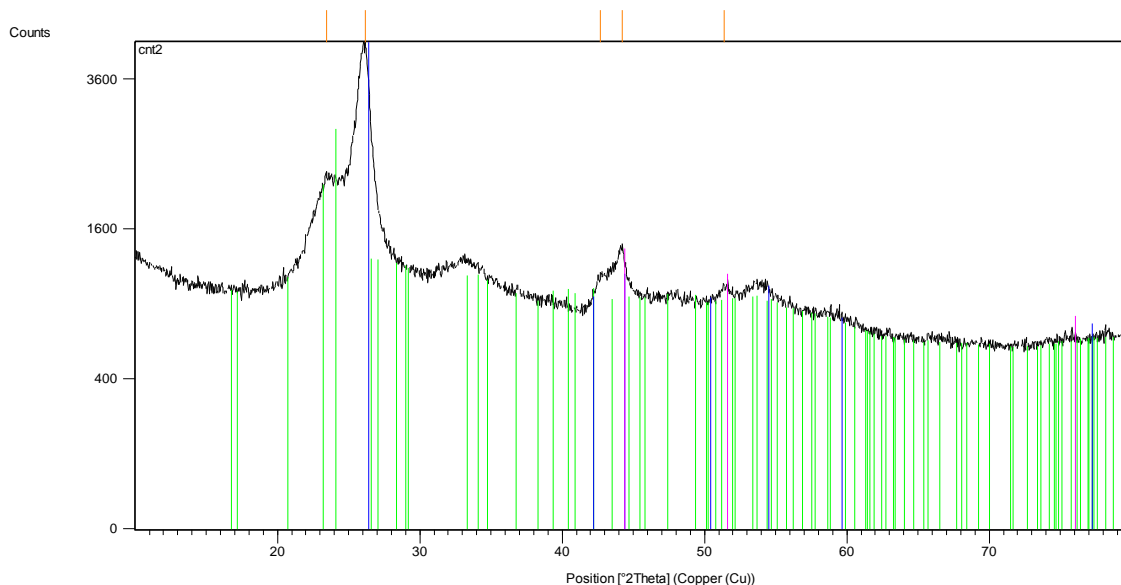
	Compound Name	Ref. Code	Chemical Formula
(green)	Tungsten Oxide	01-088-0545	WO3
(blue)	Carbon	00-041-1487	C
(magenta)	Nickel	00-001-1258	Ni

Figure 34: XRD pattern for 2Ni20WO3/CNT (made by the Pechini method, calcination at 500 °C in N$_2$-flow and reduction at 850 °C in H$_2$-flow).

Figure 35 displays both the XRD patterns before and after addition of nickel and reduction. It can be seen that the pattern does not change significantly with this process. The peaks indicating the presence of nickel is visible in the tungsten oxide catalyst before the promotion of nickel. This is to be excepted as the CNT support might contain some nickel. However, the peaks are a bit more pronounced in the final nickel promoted catalyst.
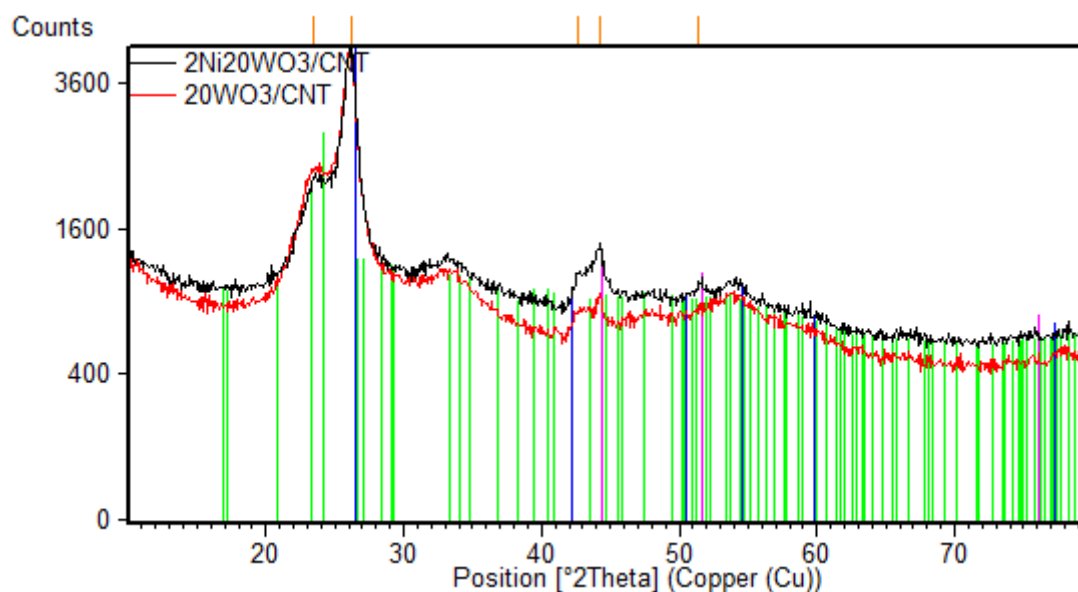
Figure 35: XRD patterns for 2Ni20WO3/CNT and 20WO3/CNT.

In terms of the AC based catalysts a similarity can be seen between the CNT and AC based tungsten carbide catalysts. The same distinct peaks representing tungsten carbide are clearly

45

visible. For the AC supported catalysts the carbon support is noticeable, especially in one very sharp peak. However, the initial broadening and uneven baseline might also indicate amorphous carbon. The first peak visible in Figure 36 could not be identified by the XRD analysis using carbon, tungsten, nickel and oxygen as possible compounds. This peak might indicate an impurity in the AC support. Further work can be carried out by conducting an XRD analysis on the pure AC support to find out what this impurity might be.
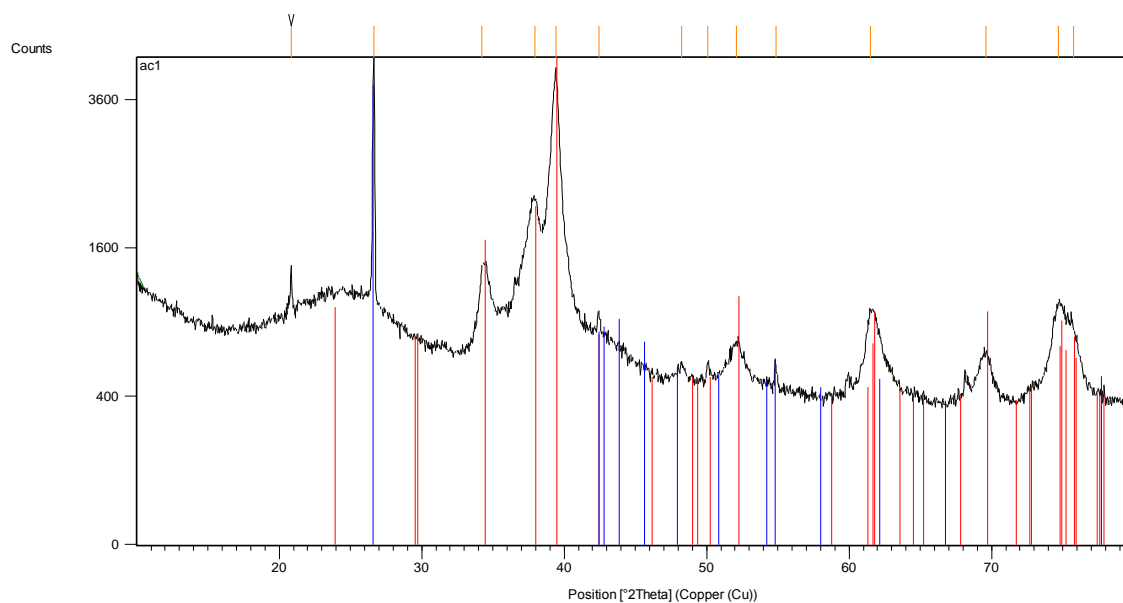
	Compound Name	Ref. Code	Chemical Formula
(red)	Tungsten Carbide	01-089-2371	W2C
(blue)	Carbon	00-026-1077	C

Figure 36: XRD pattern for 20WCx/AC-p (made by the Pechini method, calcination at 500 °C in N$_2$-flow and carburisation at 850 °C in H$_2$-flow).

The tungsten oxide catalyst show very distinct peaks for tungsten oxide (see Figure 37). Similarly to the CNT based tungsten oxide catalyst, formation of tungsten carbide was avoided during synthesis. However, in this case strong peaks are visible for WO$_3$, which might indicate a less pronounced monolayer compared to the CNT supported WO$_3$ catalyst. The presence of nickel is apparent in the XRD results, even though distinct peaks for this compound are harder to distinguish.
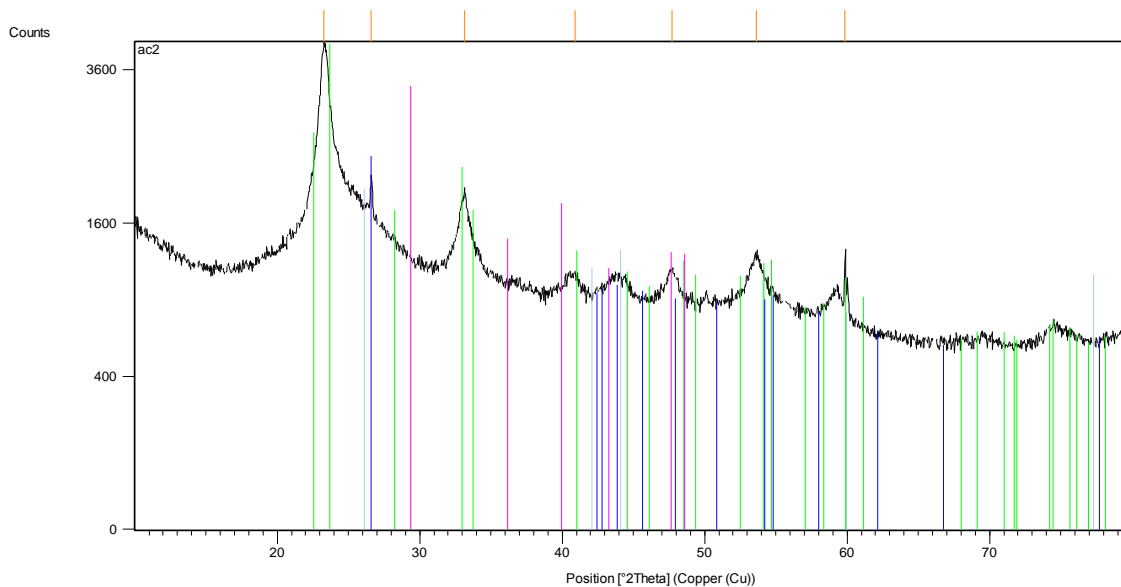
	Compound Name	Ref. Code	Chemical Formula
🟩	Tungsten Oxide	01-089-8053	WO3
🟥	Nickel Carbide	00-045-0979	Ni Cx
🟦	Carbon	00-026-1077	C

Figure 37: XRD pattern for 2Ni20WO3/AC-p (made by the Pechini method, calcination at 500 °C in N$_2$-flow and reduction at 850 °C in H$_2$-flow).

Comparing the XRD patterns before and after addition of nickel and reduction, show little alteration, except for the presence of nickel (see Figure 38).
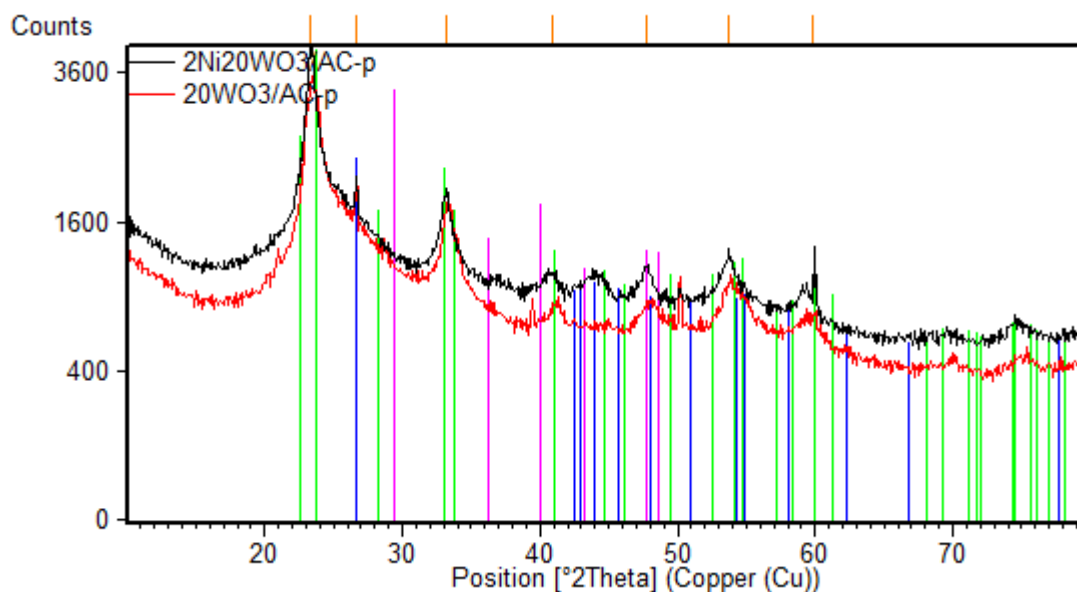
Figure 38: XRD patterns for 2Ni20WO3/AC-p and 20WO3/AC-p.

The tungsten carbide catalyst made by incipient wetness impregnation displays a very similar XRD pattern as the tungsten carbide catalyst made by the Pechini method. The same distinct peaks are visible for both tungsten carbide and carbon. The amorphous region is also evident in the XRD pattern for 20WCx/AC-im and the impurity peak is clearly visible.
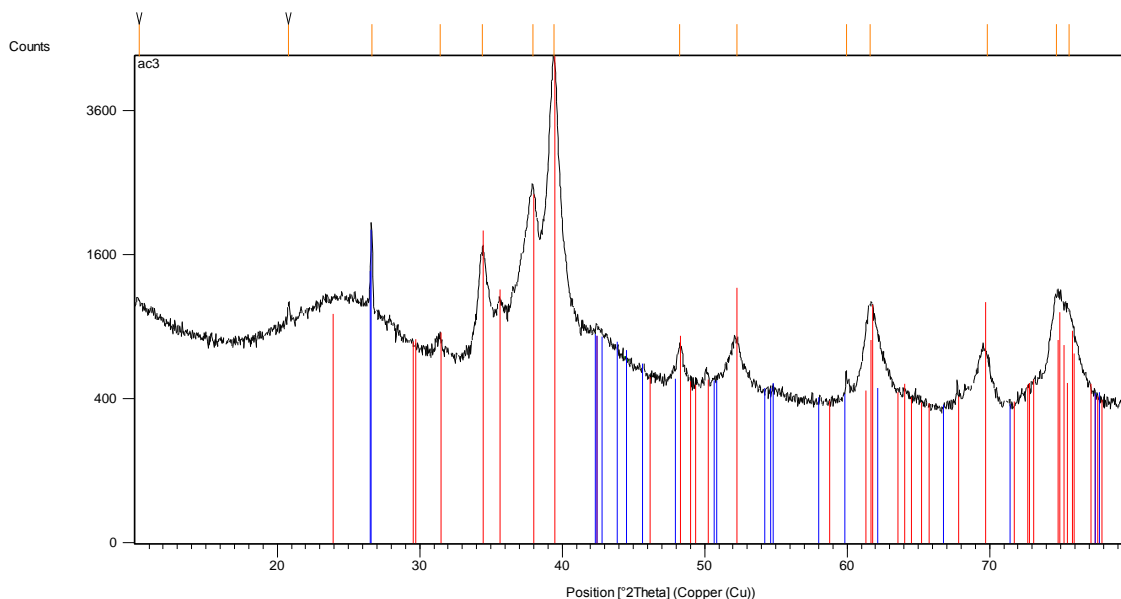
	Compound Name	Ref. Code	Chemical Formula
🟥	Tungsten Carbide	01-073-2182	W2C
🟦	Carbon	00-026-1077	C

Figure 39: XRD pattern for 20WCx/AC-im (made by incipient wetness impregnation, calcination at 500 °C in N$_2$-flow and carburisation at 850 °C in H$_2$-flow).

Similarly for the tungsten oxide catalyst, the AC catalyst made by incipient wetness impregnation display the same distinct tungsten oxide peaks and less distinguishable nickel peaks as the catalyst made by the Pechini method. Figure 41 also show little alteration in the XRD patterns before and after addition of nickel and reduction.
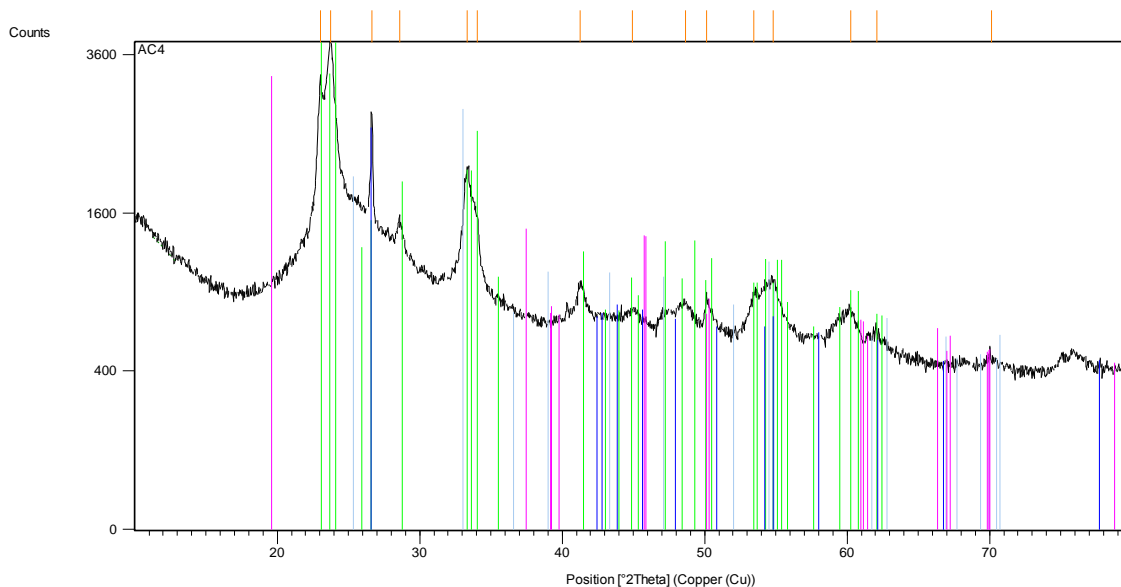
	Compound Name	Ref. Code	Chemical Formula
🟩	Tungsten Oxide	00-020-1324	WO3
🟥	Nickel Oxide	01-089-8397	Ni O2
🟦	Carbon	00-026-1077	C

Figure 40: XRD pattern for 2Ni20WO3/AC-im (made by incipient wetness impregnation, calcination at 500 °C in N$_2$-flow and redutcion at 850 °C in H$_2$-flow).

48
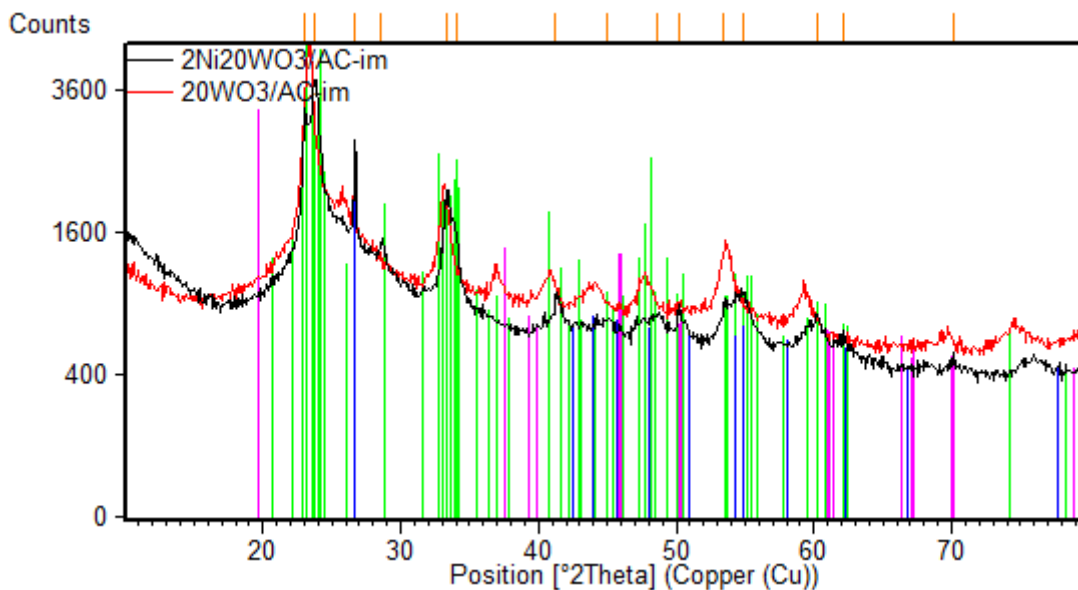
Figure 41: XRD pattern for 2Ni20WO3/AC-im and 20WO3/AC-im.

Placing the XRD patterns for all the AC based catalysts against each other gives a clear indication of what compound the most distinct peaks represent. The carbon peak is evident in all plots, while the tungsten carbide peaks are clearly visible for 20WCx/AC-p and 20WCx/AC-im. 20WO$_3$/AC-p and 20WO$_3$/AC-im have XRD patterns where tungsten oxide is the most distinguishable peaks.
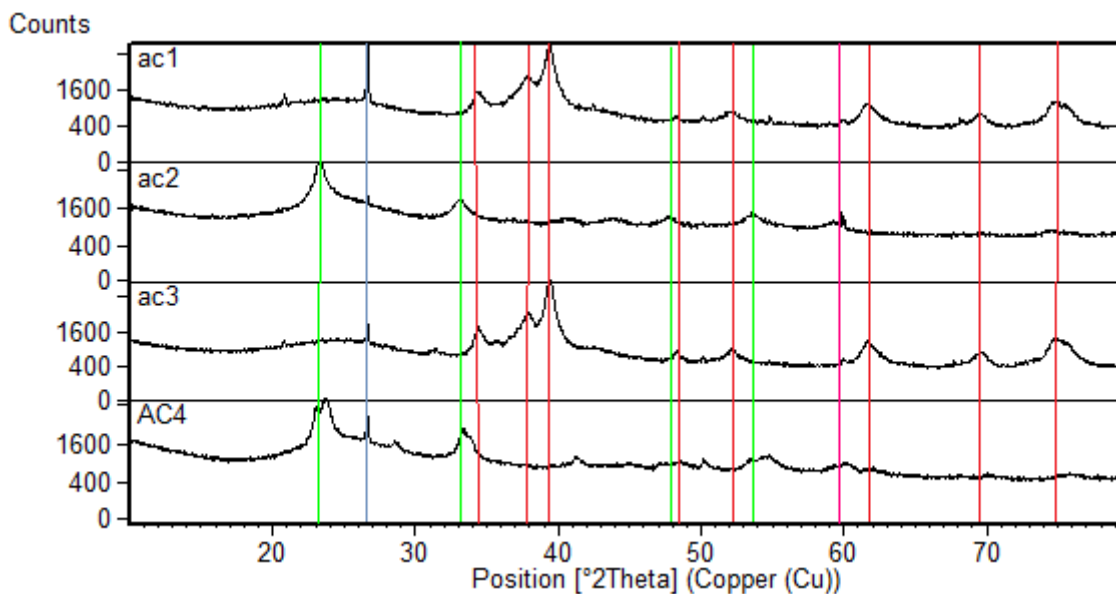
Compound Name
Tungsten Carbide
Tungsten Oxide
Carbon
Nickel

Figure 42: XRD pattern for AC based catalysts.

The tungsten carbide catalyst with CNTs as support was also analysed after reusability tests. The leftover catalyst from the reusability reaction was analysed in the same way as the fresh catalyst. Figure 43 display both the XRD pattern for the fresh catalyst and the catalyst after reusability tests. It can be seen that the catalyst has changed somewhat during the reactions.

However, the distinct tungsten carbide peaks are still clearly visible. A few additional peaks have occurred in the XRD pattern for the reusability catalyst, still, Figure 44 show that the peaks represent the same compounds as present in the fresh catalyst. The WO_3 is more visible in the catalyst after reusability tests. This might be because oxidation of tungsten carbide could have occurred during reaction. Nickel is also more pronounced in the pattern, which could be the result of sintering of Ni particles during reaction.
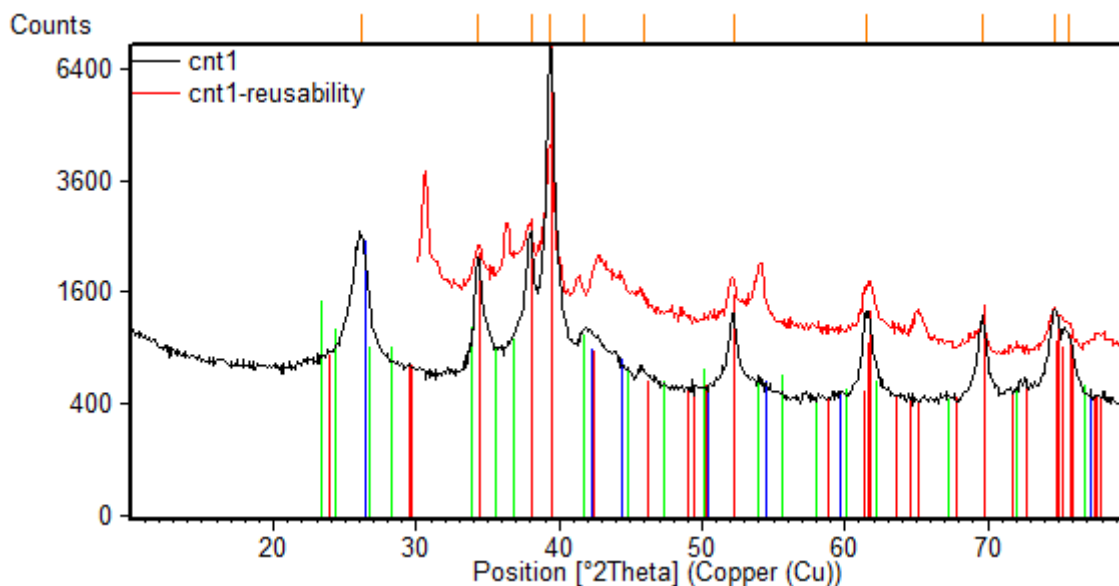
Figure 43: XRD pattern for 20WCx/CNT and 20WCx/CNT-reusability.
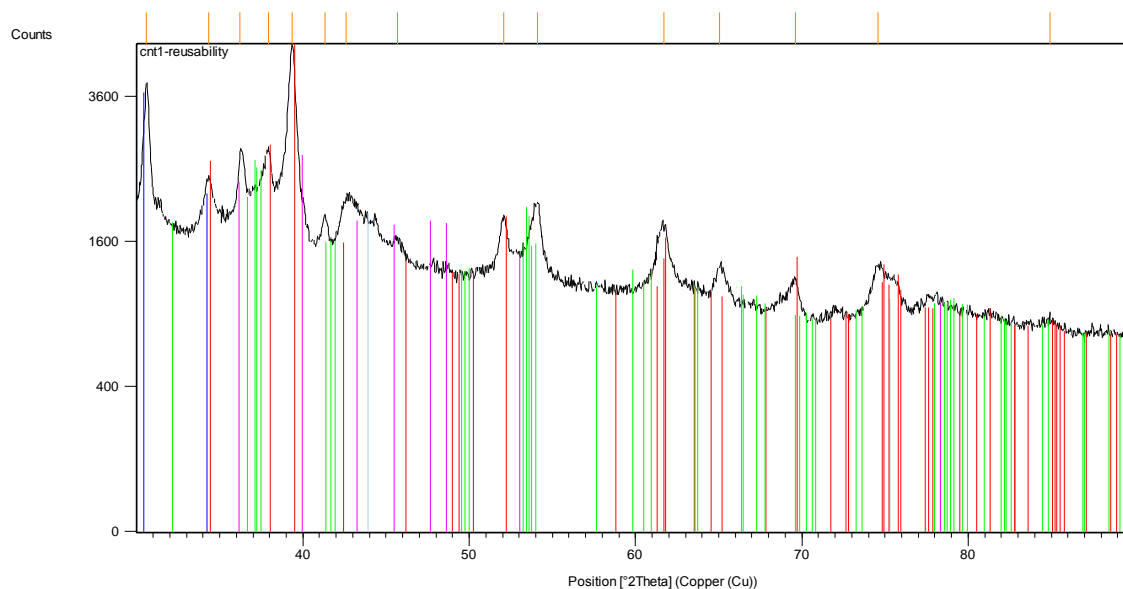
	Compound Name	Ref. Code	Chemical Formula
	Tungsten Carbide	01-089-2371	W2C
	Tungsten Oxide	01-071-0614	WO2
	Carbon	00-050-0926	C
	Nickel/Nickel Carbide	01-088-2326/00-045-0979	Ni/Ni Cx

Figure 44: XRD pattern for 20WCx/CNT-reusability.

The catalyst made to test the effect of tungsten loading on CNTs were also analysed by XRD. As seen in Figure 45 and Figure 46 the carbide catalyst show the same distinct peaks for tungsten carbide, carbon and nickel.
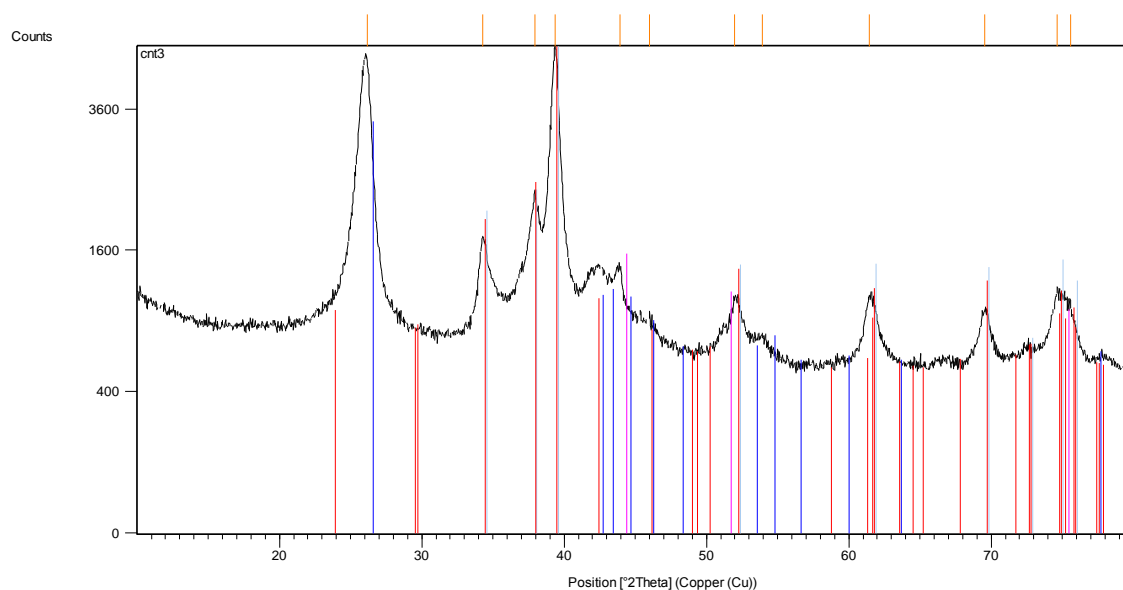
	Compound Name	Ref. Code	Chemical Formula
	Tungsten Carbide	01-089-2371	W2C
	Carbon	00-026-1076	C
	Nickel Carbide	00-014-0020	Ni C

Figure 45: XRD pattern for 10WCx/CNT (made by the Pechini method, calcination at 500 °C in N₂-flow and carburisation at 850 °C in H₂-flow).
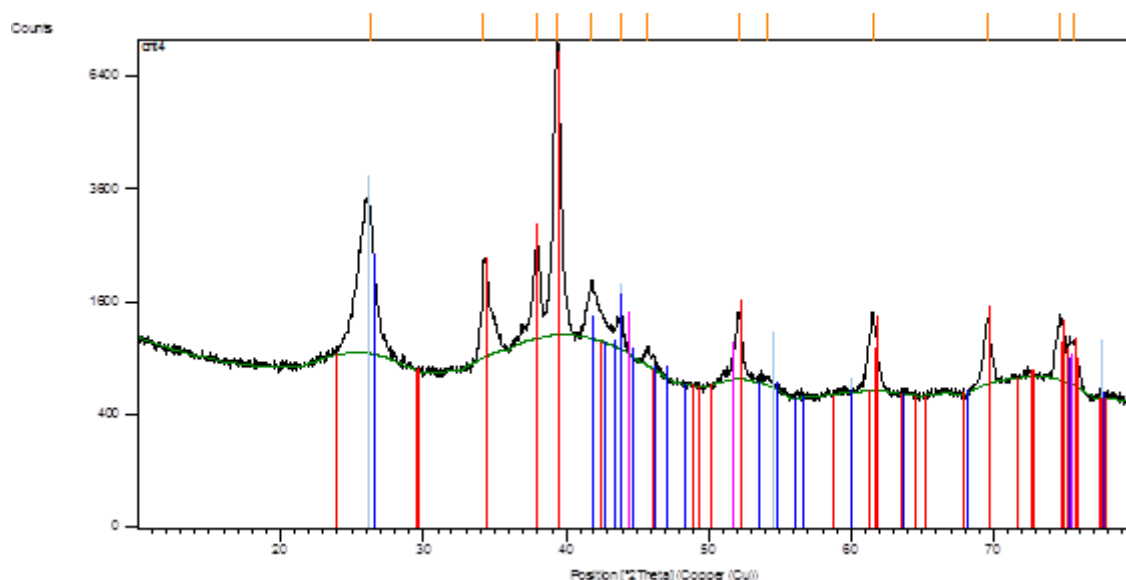
	Compound Name	Ref. Code	Chemical Formula
	Tungsten Carbide	01-089-2371	W2C
	Carbon	00-026-1076	C
	Nickel Carbide	00-014-0020	Ni C

Figure 46: XRD pattern for 30WCx/CNT (made by the Pechini method, calcination at 500 °C in N₂-flow and carburisation at 850 °C in H₂-flow).

Comparing all catalysts used to test the effect of tungsten loading on CNTs allows for evaluation of the distinct peaks and which compounds they represent (see Figure 47). It is evident that the first peak in the XRD patterns represents carbon. The peak representing nickel is also visible, yet not as distinguishable as the tungsten carbide peaks.

	Compound Name
	Tungsten Carbide
	Carbon
	Nickel
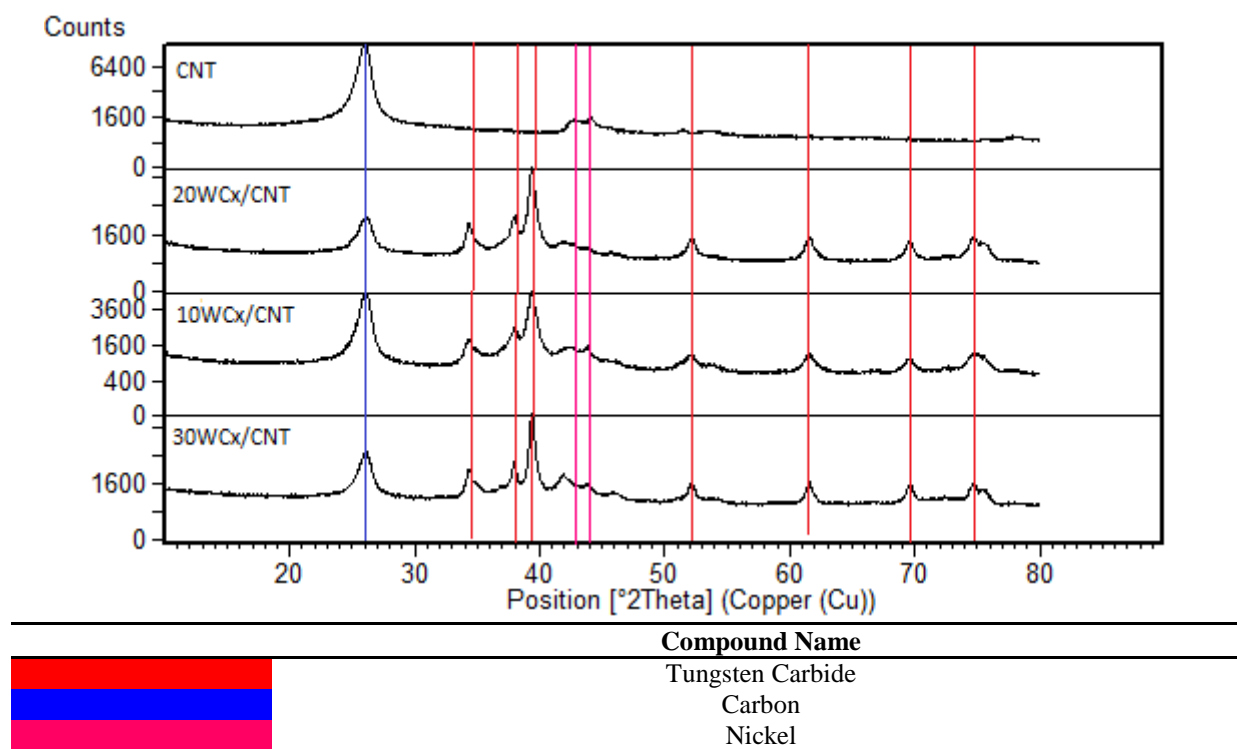
Figure 47: XRD pattern for catalysts used to test the effect of tungsten loading on CNTs.

4.1.8. Raman

A sample of pure WO_3 (Aldrich, Tungsten(VI)oxide, ≥99.5%) was used to get a Raman spectra for comparison. Two peaks were clearly visible in the 500 to 1000 range. The peaks at 715 and 807 perfectly match the literature values [26] of microcrystalline WO_3.
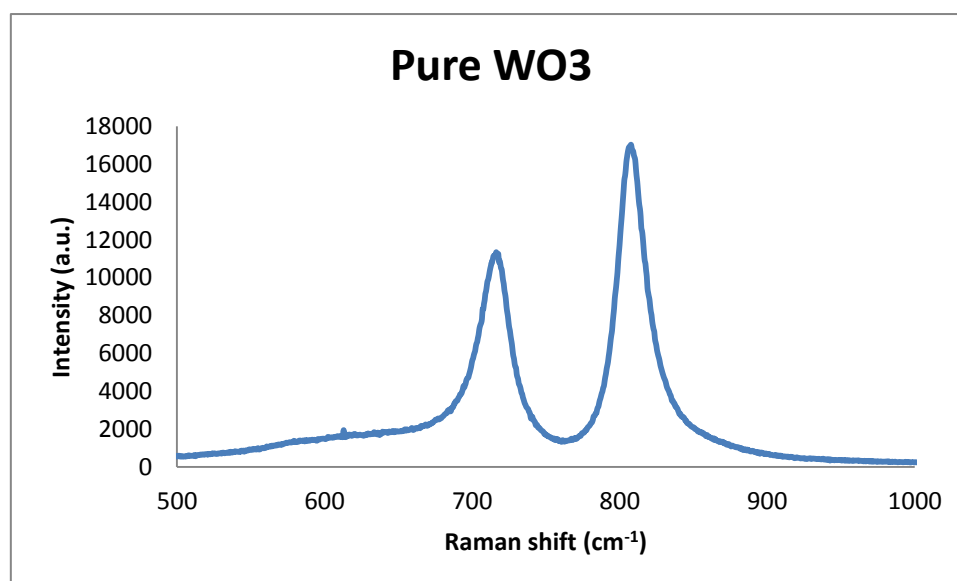
Figure 48: Raman spectra for pure WO_3.

The Raman spectroscopy for 20WCx/CNT indicates that some WO_3 is present on the catalyst surface. Two small peaks can be seen at the Raman shift of 715 and 807 cm^{-1} (see Figure 49). The presence of tungsten oxide on the surface might be due to oxidation of WCx during storage. In addition, a stronger peak is visible at 880 cm^{-1}. Further analysis must be made to determine which compound this peak represents.
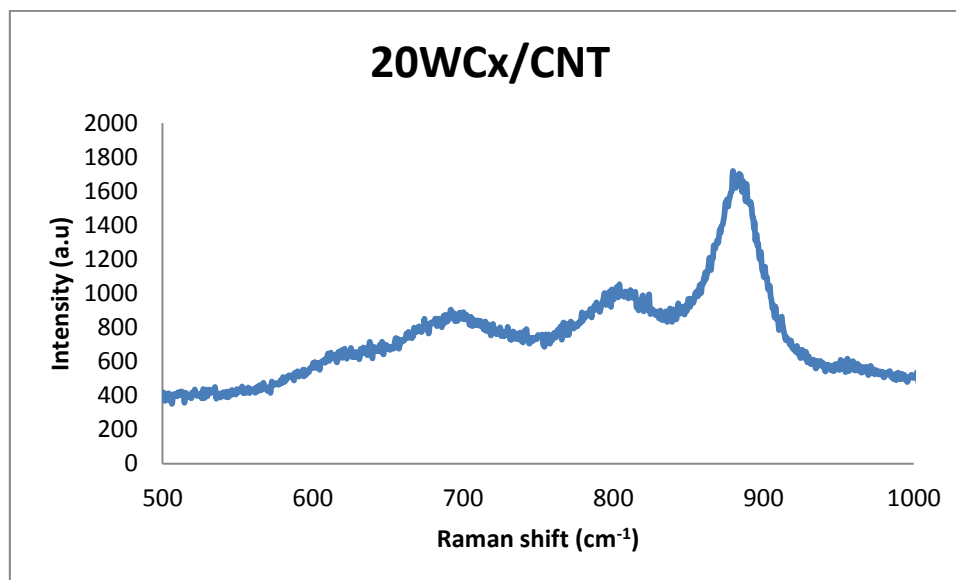
Figure 49: Raman spectra for 20WCx/CNT (made by the Pechini method, calcination at 500 °C in N$_2$-flow and carburisation at 850 °C in H$_2$-flow).

In terms of 2Ni20WO3/CNT, clearly visible peaks of WO_3 are expected as the catalyst is a tungsten oxide catalyst. However, Figure 50 does not indicate any clear peaks. The TGA results indicate a metal loading of 26.8 % and XRD show a strong presence of WO_3. However, contrary to the XRD results, the Raman does not support the assumption of a WO_3 monolayer on the surface.
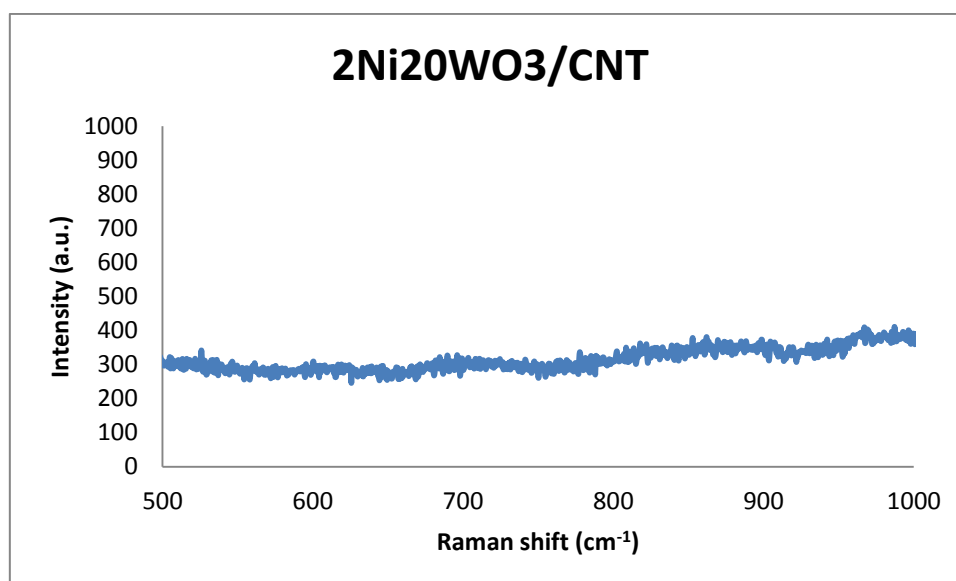
Figure 50: Raman spectra for 2Ni20WO3/CNT(made by the Pechini method, calcination at 500 °C in N$_2$-flow and reduction at 850 °C in H$_2$-flow).

Contrary to 20WCx/CNT, the Raman spectra for 30WCx/CNT indicate very little presence of WO_3 on the surface of the catalysts. However, the Raman analysis was conducted soon after the synthesis of 30WCx/CNT, while 20WCx/CNT had been stored for a period of time. Oxidation of the tungsten carbide on the surface of the catalyst might therefore be more severe in the case of 20WCx/CNT.
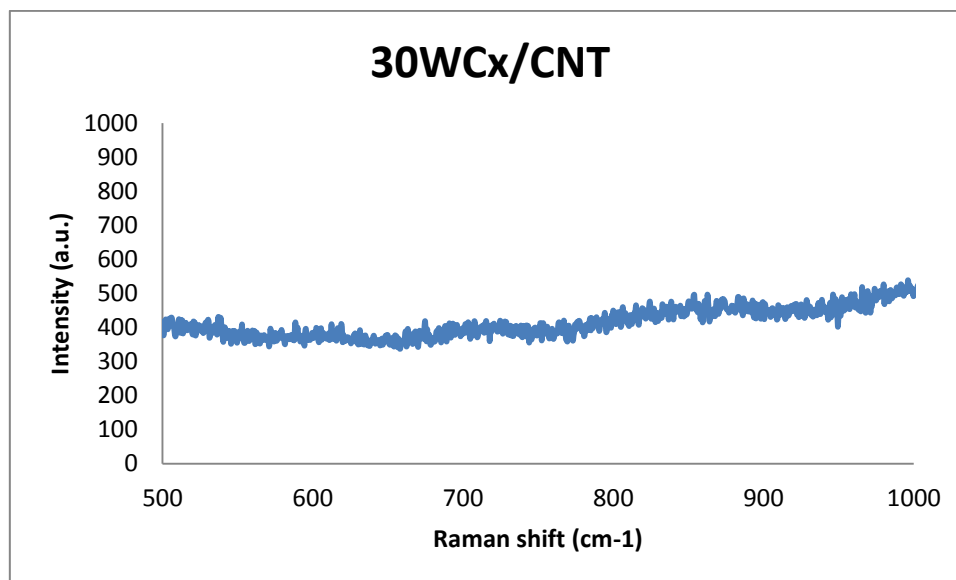
Figure 51: Raman spectra for 30WCx/CNT (made by the Pechini method, calcination at 500 °C in N$_2$-flow and carburisation at 850 °C in H$_2$-flow).

Similarly to the first CNT based tungsten carbide catalyst 20WCx/AC-p show a clear presence of WO_3 on the surface of the catalyst. In the same way, this catalyst had been stored for a period of time before analysis and oxidation of tungsten carbide might have occurred on the surface.
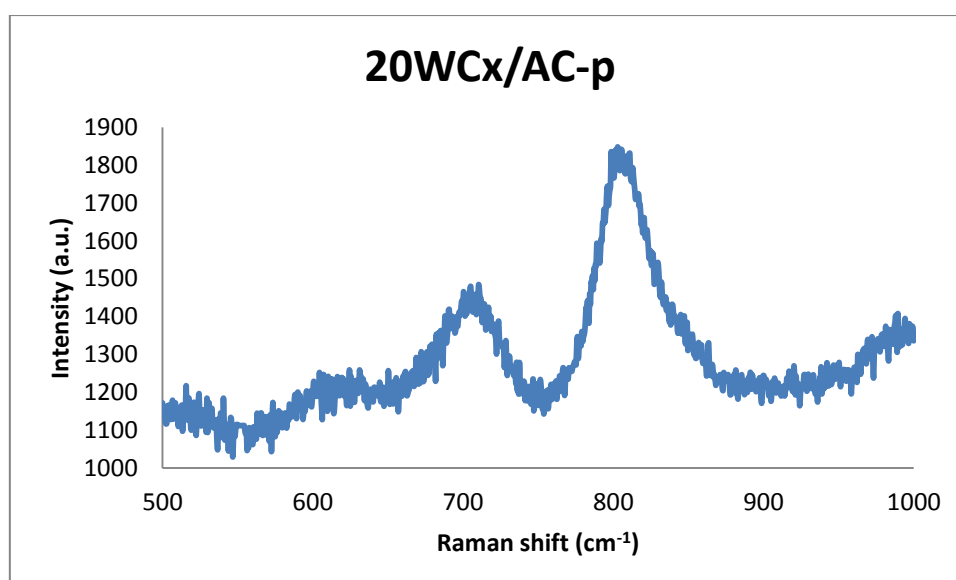
Figure 52: Raman spectra for 20WCx/AC-p (made by the Pechini method, calcination at 500 °C in N$_2$-flow and carburisation at 850 °C in H$_2$-flow).

The Raman spectra for 2Ni20WO3/AC-p display a strong peak at 807 cm^{-1}, however the peak at 715 cm^{-1} is much weaker. Still, it is evident that WO_3 is present on the catalyst surface. In addition, a peak is visible at approximately 880 cm^{-1}, similarly to 20WCx/CNT.
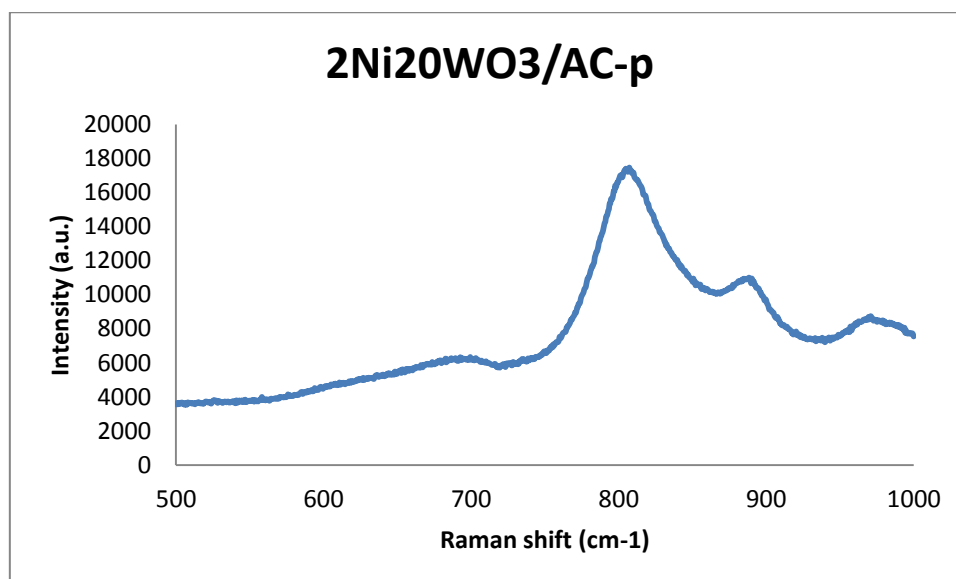
Figure 53: Raman spectra for 2Ni20WO3/AC-p (made by the Pechini method, calcination at 500 °C in N$_2$-flow and reduction at 850 °C in H$_2$-flow).

In the same way as 20WCx/CNT and 20WCx/AC-p, 20WCx/AC-im displays a clear presence of WO_3 on the surface most likely due to oxidation during storage.
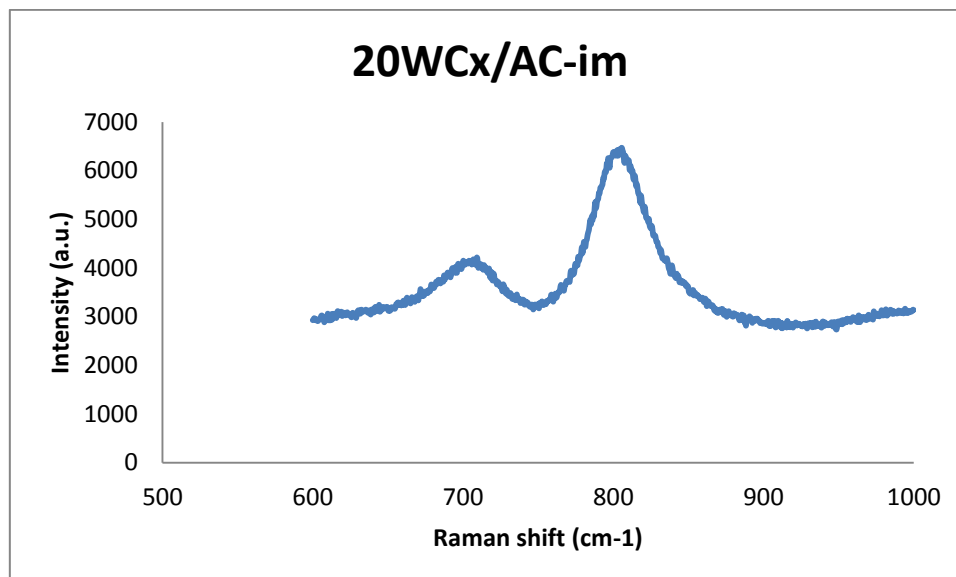
Figure 54: Raman spectra for 20WCx/AC-im (made by incipient wetness impregnation, calcination at 500 °C in N$_2$-flow and carburisation at 850 °C in H$_2$-flow).

Correspondingly to 2Ni20WO3/AC-p, 2Ni20WO3/AC-im shows a stronger peak at 807 cm^{-1} than at 715 cm^{-1}. The peak at approximately 880 cm^{-1} is also clearly visible.
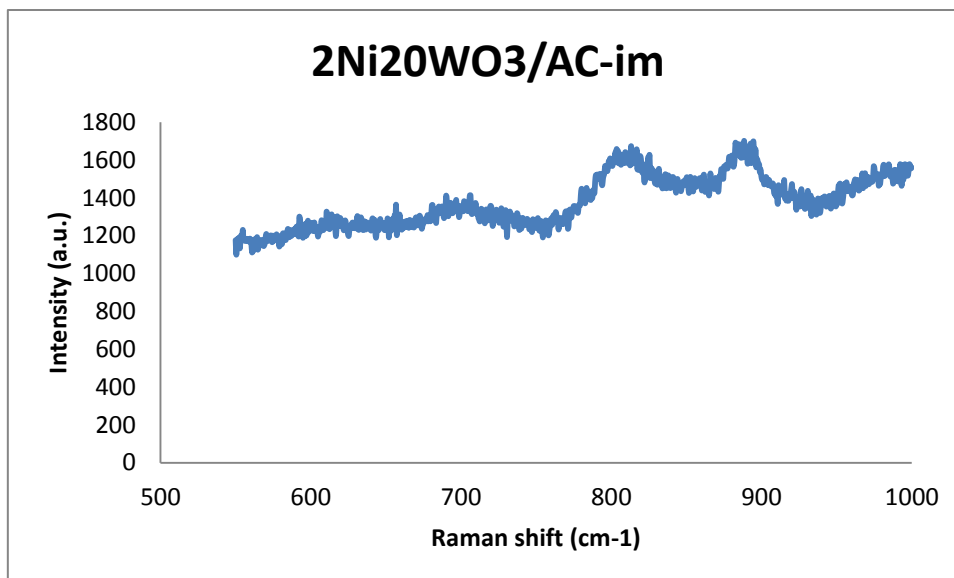
Figure 55: Raman spectra for 2Ni20WO3/AC-im (made by incipient wetness impregnation, calcination at 500 °C in N$_2$-flow and reduction at 850 °C in H$_2$-flow).

In general, the Raman results were not as expected and repetition of analysis might be necessary to avoid experimental error.

4.2. Catalyst testing

Initially one catalyst was used to evaluate the reaction time for the catalyst testing reactions. Catalyst AT50W2Ni was tested at both 30 minutes and 2 hours. It was found that the yield was significantly higher for the 2 hour reaction, and this time was therefore used for all succeeding reactions.

Table 16: Product yields for the AT50W2Ni at 30 minutes and 2 hours reaction time.

Catalyst	EG	Sorbitol	Mannitol	Erythritol	1,2-PG	Total yield
AT50W2Ni 30 minutes	21.8	6.0	1.1	1.2	3.8	35.9
AT50W2Ni 2 hours	51.6	7.6	2.0	2.4	9.1	80.1

4.2.1. Mass based conversion

It was found that the cellulose conversion was complete in nearly all reactions. The catalysts created in the previous study [14] were evaluated in the same fashion as the catalysts made in this study. It was found that the cellulose conversion was complete for all catalysts from the previous study (see Table 17). With regard to the catalysts made in this study 20WCx/CNT display a lower conversion than the rest of the catalyst, however, considering that all other reactions obtained a 100 percent conversion it is unlikely that this is due to properties of the catalyst and might be the result of incorrect measurement or a mistake during the experimental work (see Table 18). Due to the method of measuring the conversion, the values are subject to an error of ± 10 % [27].

Table 17: Mass based conversion of catalyst from previous study.

Catalyst	Conversion
AT50	100
ATOPH50	100
AT12	100
ATOPH12	100

Table 18: Mass based conversion of catalyst made in this study.

Catalyst	Conversion
20WCx/CNT	71
2Ni20WO3/CNT	100
20WCx/AC-p	100
2Ni20WO3/AC-p	100
20WCx/AC-im	100
2Ni20WO3/AC-im	100

Table 19 shows the mass based conversion for the catalysts used for reusability tests. It can be seen that the cellulose conversion was complete for both the tungsten carbide and the tungsten oxide catalyst in the reusability reactions.

Table 19: Mass based conversion of reusability catalysts

Catalyst	Conversion
20WCx/CNT reusability	100
2Ni20WO3/CNT reusability	100

The reactions carried to test the effect of different tungsten loadings on the CNT support gave varying values for the conversion. The CNTs with zero percent loading had a mass based conversion of 100 %. During acid pretreatment of the CNTs acidic sites are introduced to the surface. The acidic sites have catalytic properties for the conversion of cellulose [27]. However, no target products are produced in significant amounts.

The varying values for the conversion in the other cases are not conclusive, and might as previously mentioned be the result of incorrect measurement or a mistake during the experimental work.

Table 20: Mass based conversion of CNT supported catalysts with different tungsten carbide loading

Catalyst	Conversion
CNT	100
20WCx/CNT	71
10WCx/CNT	100
30WCx/CNT	98

4.2.2. Liquid product yield

Table 21 shows the product yields for the catalysts evaluated in this study. The catalysts made in the previous study have been tested in the reactor in this study. However, those results will not be further evaluated as the preparation of the catalysts was not executed in the same manner and location.

Table 21: Liquid product yields

Catalyst	EG	Sorbitol	Mannitol	Erythritol	1,2-PG	Total yield
AT50W2Ni II	51.6	7.6	2.0	2.4	9.1	80.1
ATOPH50W2Ni I	49.0	4.9	1.4	1.7	7.4	76.5
AT12W2Ni	13.1	4.7	0.5	0.8	9.6	32.8
ATOPH12W2Ni	24.9	18.8	3.5	2.6	8.4	67.0
20WCx/CNT	53.8	7.0	3.0	3.0	8.7	85.0
2Ni20WO3/CNT	51.1	1.6	0	1.0	8.4	65.5
20WCx/AC-p	34.5	1.5	0.7	0.9	13.3	50.9
2Ni20WO3/AC-p	63.8	1.8	1.1	1.5	8.1	79.0
20WCx/AC-im	32.0	1.6	0	1.1	15.8	56.1
2Ni20WO3/AC-im	57.6	2.4	11.4	1.7	7.0	82.7
20WCx/CNT-reusability	21.1	4.2	1.3	0.6	12.7	44.7
2Ni20WO3/CNT-reusability	11.9	0	5.7	0.4	2.4	21.2
CNT	2.0	0.5	1.5	0.2	0.9	5.1
10WCx/CNT	31.7	15.9	4.0	3.9	11.2	79.5
30WCx/CNT	25.1	18.6	4.0	3.4	10.1	75.3
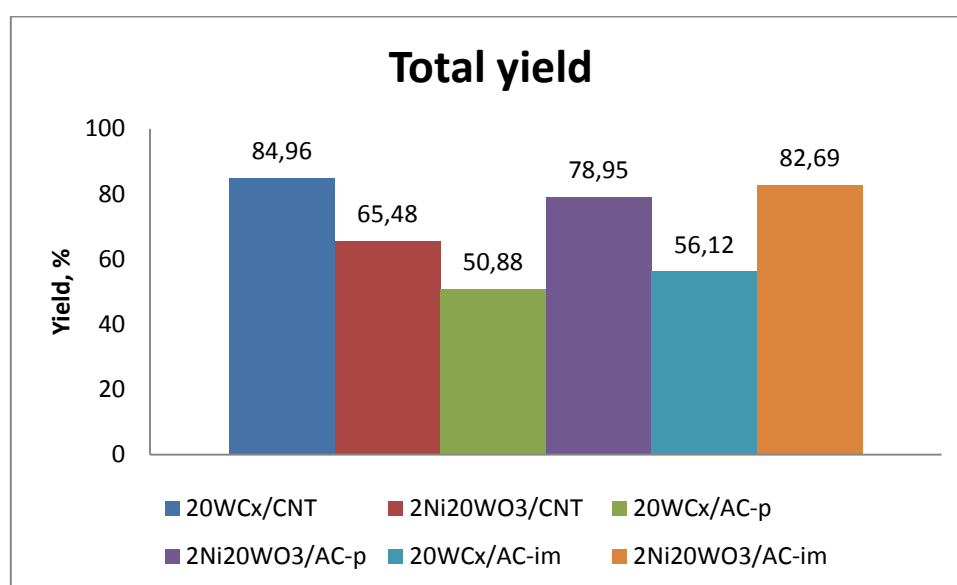
Figure 56: Total yields for tungsten carbide and tungsten oxide catalysts.

The results show that 20WCx/CNT has the highest total yield (85 %) and the second highest EG yield (53.8 %). The corresponding tungsten carbide catalysts supported on AC, 20WCx/AC-p and 20WCx/AC-im, both show remarkably lower EG yields (34.5 % and 32.0 % respectively). On the other hand, the tungsten carbide AC catalysts display a higher 1,2-PG yield, when compared to the CNT based catalyst.
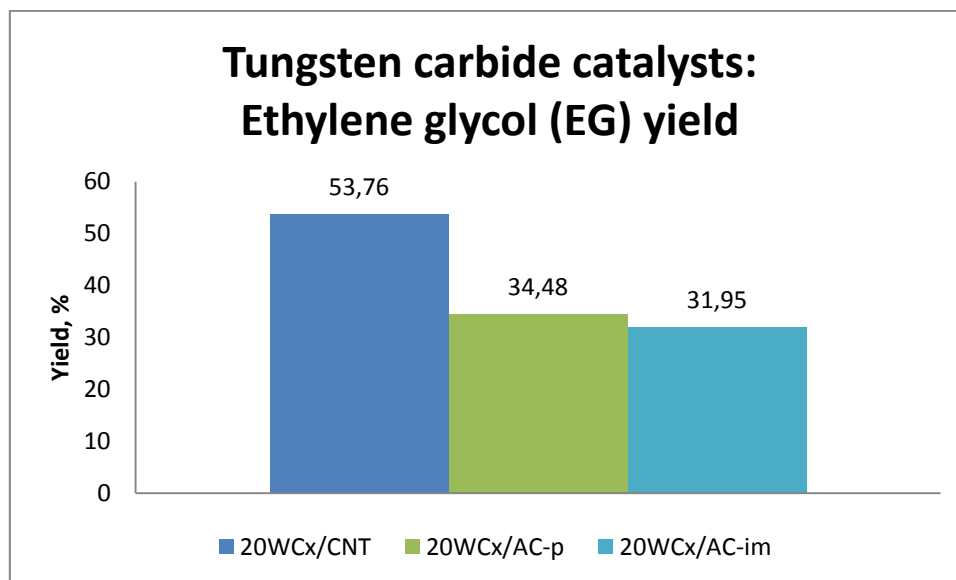
Figure 57: EG yields for tungsten carbide catalysts..

Better performance with regard to the EG yield for the CNT based catalyst may be because the CNT support contains a small amount of nickel. The ICP results showed a nickel content of 1.15 % for 20WCx/CNT, while 20WCx/AC-p had a nickel content close to zero. The chemisorption results also indicate that 20WCx/CNT has much greater dispersion and lower crystallite size than 20WCx/AC-p. This could be a contributing factor towards the better product yield. However, the chemisorption results are quite different for the two AC supported tungsten carbide catalysts, 20WCx/AC-p and 20WCx/AC-im, and difference in product yield is so small that it the dispersion seems to be of no great significance to the yield.

With regard to the 1,2-PG yields, the AC based tungsten carbide catalysts give a higher value than the CNT catalyst. In this case, 20WCx/AC-im, with the lower EG yield, gives a higher yield than 20WCx/AC-p. The tungsten oxide catalysts on the other hand, show a different trend. In this case the CNT based catalyst give the highest 1,2-PG yield, if only slightly higher than 2Ni20WO3/AC-p.
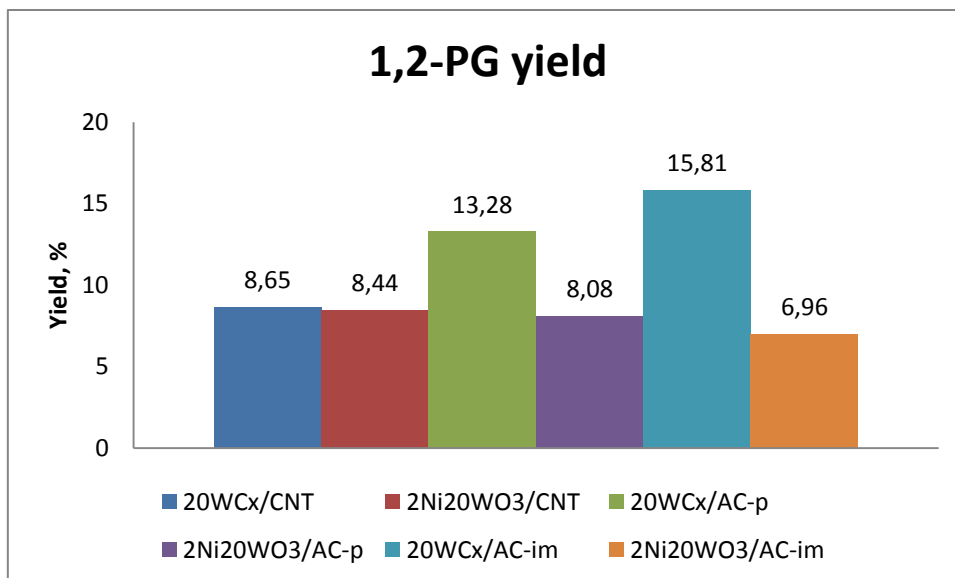
Figure 58: 1,2-PG yields for tungsten carbide and tungsten oxide catalysts.

The tungsten oxide catalysts have generally very high EG yields. This is to be expected due to the promotion of nickel. However, in this case the AC based catalysts have higher yields than the CNT based catalyst. 2Ni20WO3/AC-p made by the Pechini method has the highest EG yield (63.8 %) out of all the catalysts tested in this study. Even with this remarkably high EG yield, 2Ni20WO3/AC-im has a higher total product yield. This is due to the very high yield of mannitol. Mannitol is produced from hydrogenation of glucose, which is catalysed by nickel. The high yield of mannitol might be the result of better nickel dispersion on the catalyst.
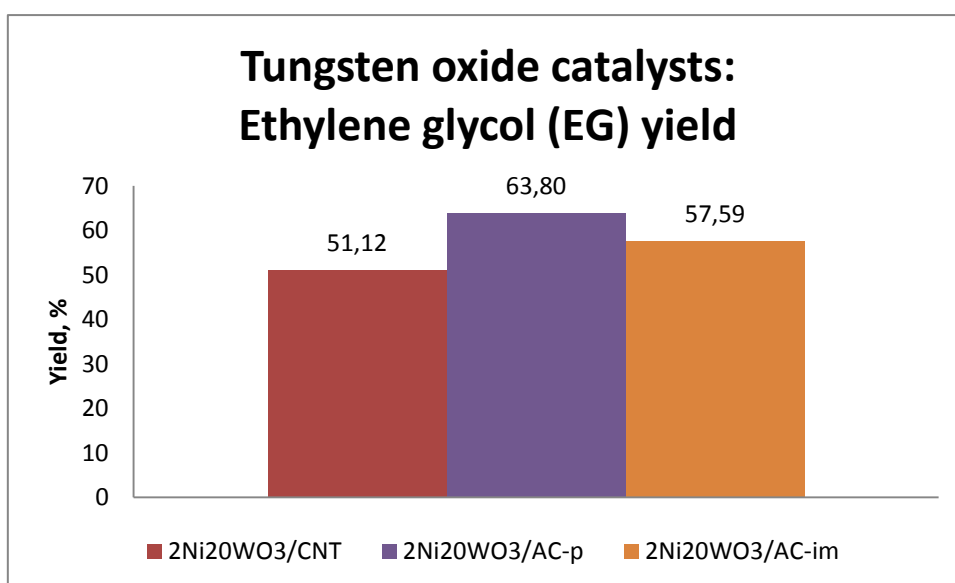
Figure 59: EG yields for tungsten oxide catalysts.

The results obtained with 20WCx/CNT are exceptionally good considering the catalyst has not been intentionally promoted by nickel. Although some nickel has been proven to be present in the CNT support, the results are interesting and reusability tests were performed on both the tungsten carbide and the tungsten oxide catalysts supported on CNTs.

In terms of the EG yield is can be seen that it is significantly reduced in the second run for both 20WCx/CNT and 2Ni20WO3/CNT. Considering that the initial EG yields are

approximately the same for both catalyst, the reusability of 20WCx/CNT is slightly better than 2Ni20WO3/CNT with a higher EG yield in the second run. These results correspond with the ICP results indicating slightly more severe nickel leaching in the first run for the tungsten oxide catalyst, and thereby a better performance on the carbide catalyst in the second run.

In terms of other product yields, 20WCx/CNT gave a higher 1,2-PG yield in the second run (from 8.65 % to 12.69 %). 1,2-PG is favoured by basicity, while EG is favoured by acidity [27]. After reaction, some of the acidic sites present from the CNT pretreatment might be lost, making the catalyst more active for 1,2-PG. However, the 1,2-PG yield was reduced in the second run with the use 2Ni20WO3/CNT. Instead the catalyst showed an increase in the yield of mannitol (from 0 % to 5.65 %). Mannitol formation is promoted by nickel, and might therefore give a higher yield with 2Ni20WO3/CNT, while in the case of 20WCx/CNT it was reduced in the second run.
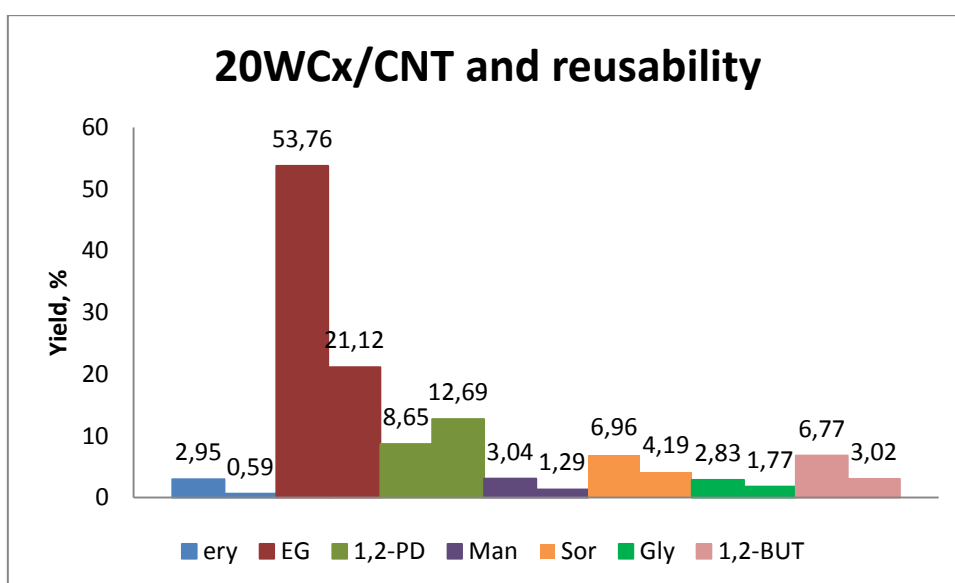
Figure 60: Product yields for both fresh 20WCx/CNT and 20WCx/CNT after reusability tests.
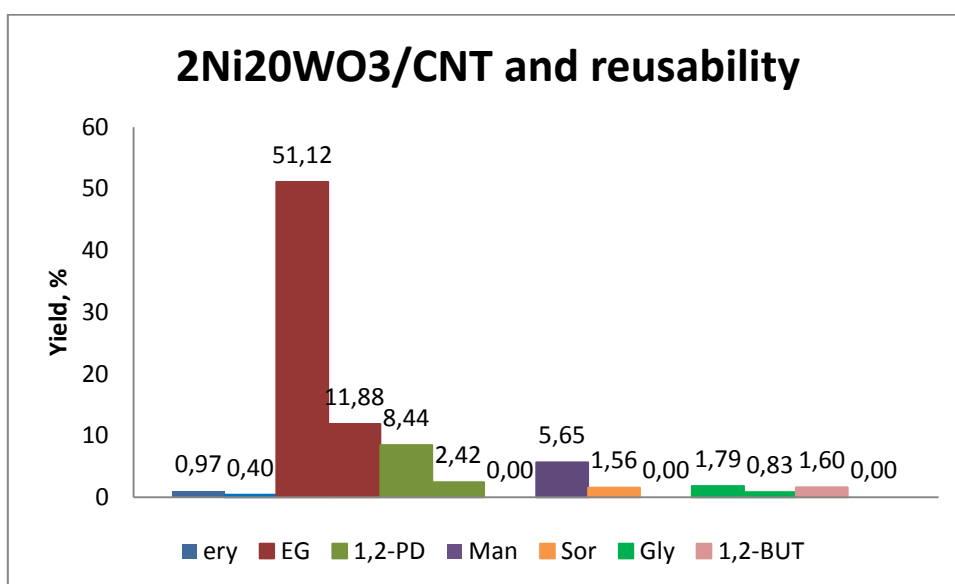
Figure 61: Product yields for both fresh 2Ni20WO3/CNT and 2Ni20WO3/CNT after reusability tests.

The effect of tungsten loading on the product yield was also investigated. Figure 62 shows the metal and tungsten loading obtained from the TG analysis. The pure CNTs were proven to contain some metal, most likely in the form of nickel from the CNT synthesis, and the catalysts did not have the loading as initially intended. However, it can be seen that both the total product yield and the EG yield is highest for the catalyst with the highest loading. Still, this trend is not upheld by the other catalysts. 10WCx/CNT displays lower tungsten loading according to the TGA results, yet both the total and EG yield is higher than those obtained by 30WCx/CNT. A possible explanation to why there is no trend between the tungsten loading and product yields might be the effect of metal dispersion. If the metal dispersions of the independent catalysts are very different, this effect might be more pronounced than the metal loading.
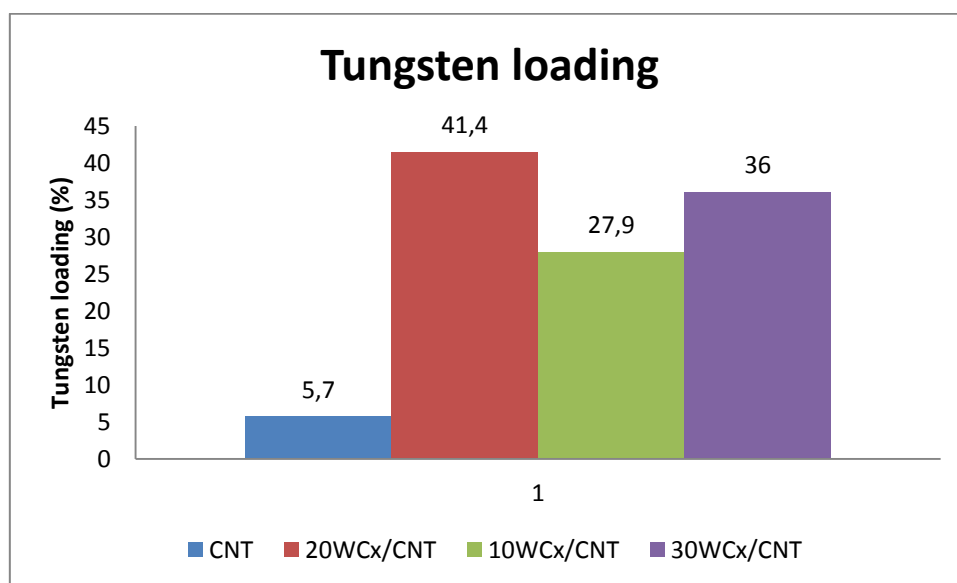
Figure 62: Tungsten (other metal in the case of CNT) loading obtained from TGA.
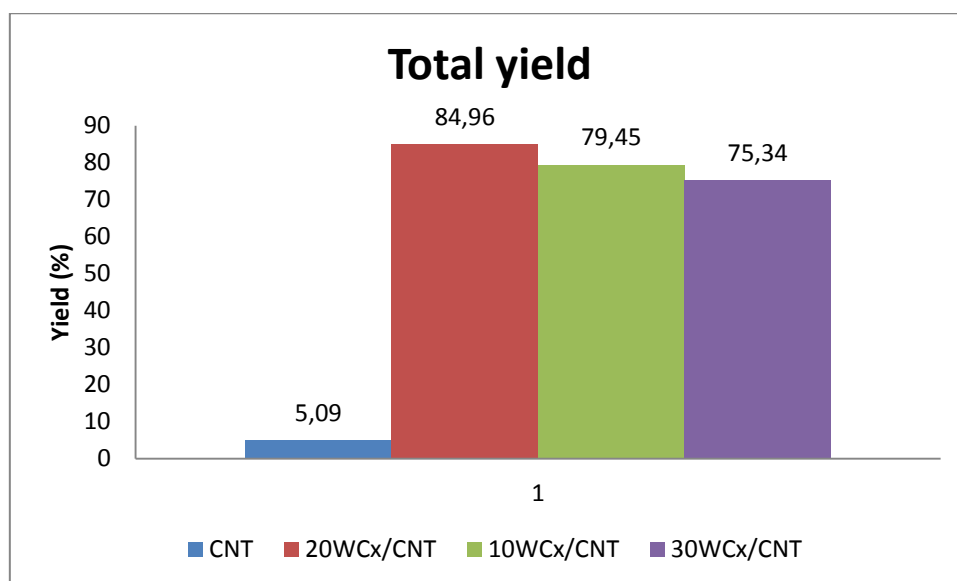
Figure 63: Product yields for tungsten carbide catalyst supported on CNTs used to test the effect of tungsten loading.
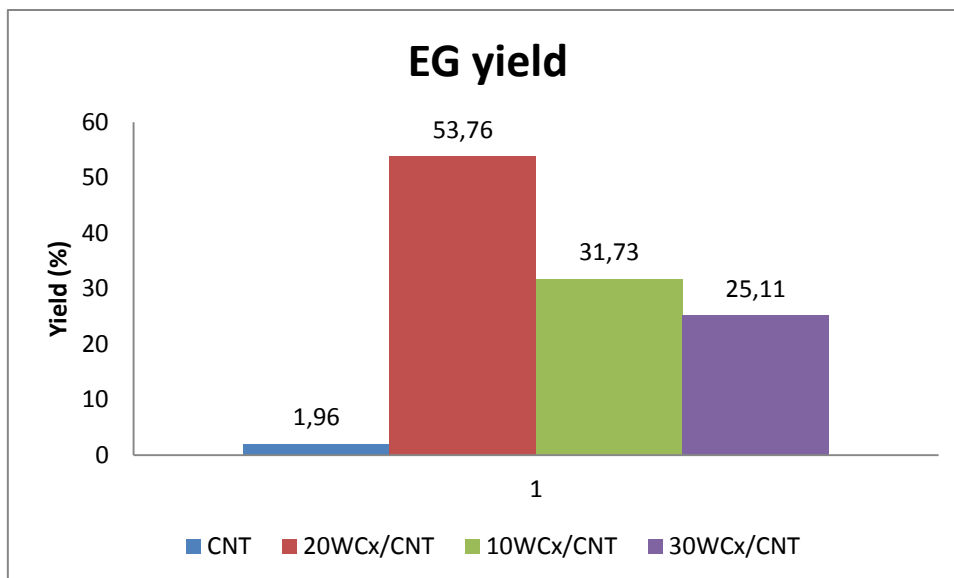
Figure 64: EG yields for tungsten carbide catalyst supported on CNTs used to test the effect of tungsten loading.

4.2.3. Gas product yield

Due to some technical difficulties not all samples were analysed. No results are available for 2Ni20WO3/CNT, 20WCx/AC-p and 2Ni20WO3/AC-p, however, all other samples show total gas yields below 2.5 %. It is not to be expected that other samples would exceed this value.

Table 22 show the yields of carbon containing gas products in addition to the total yield of carbon containing gases. As expected, only very small amounts of cellulose has been converted to gases and is of little effect to the liquid product yields.

Table 22: Gas product yields

Catalyst	mol % (carbon)				Total yield (%)
	CO	CH_4	CO_2	C_2H_6	
AT50W2Ni	0.00	0.54	0.33	0.13	1.01
ATOPH50W2Ni	0.00	0.60	0.36	0.00	0.96
AT12W2Ni	0.00	0.50	0.81	0.00	1.31
AT12W2Ni	0.00	0.78	0.31	0.00	1.09
20WCx/CNT	0.00	0.27	0.29	0.23	0.79
20WCx/CNT-reusability	0.12	0.27	0.94	0.25	1.59
2Ni20WO3/CNT	n.d.				
2Ni20WO3/CNT-reusability	0.07	0.30	2.15	0.00	2.53
10WCx/CNT	0.00	0.37	0.42	0.00	0.78
30WCx/CNT	0.00	0.49	0.46	0.00	0.95
20WCx/AC-p	n.d.				
2Ni20WO3/AC-p	n.d.				
20WCx/AC-im	0.05	0.40	0.59	1.33	2.36
2Ni20WO3/AC-im	0.00	0.72	0.53	0.09	1.33

5. Conclusion

Tungsten carbide and nickel promoted tungsten oxide catalysts were prepared by incipient wetness impregnation and the Pechini method using carbon nanotubes and activated carbon as support. The catalysts were characterised and evaluated for the catalytic conversion of cellulose towards polyols, especially EG. A previous study by the author concluded that incipient wetness impregnation does not result in a uniform coating when carbon nanotubes are used as support. Incipient wetness impregnation on activated carbon on the other hand gave higher dispersion and smaller particle size than the Pechini method. In all cases involving tungsten oxide, the contrast between the carbon support and WO_3 might be too low to distinguish a coated layer in the S(T)EM analysis. For CNTs, the Pechini method resulted in low, but even distribution of small sized tungsten carbide particles on the surface. Due to the difference in structural properties between CNTs and AC, the Pechini method might be more suitable for the CNTs, while incipient wetness impregnation gives better results with AC.

Among the catalysts evaluated, 20WCx/CNT had the best catalytic activity, giving a total yield of 85 % and the second highest EG yield of 53.8 %. This is exceptionally good results considering no promotion of nickel has intentionally been made. The highest EG yield (63.8 %) was obtained with the 2Ni20WO3/AC-p catalyst. However, reusability testes showed significant reduction in the EG yields after the first run for both catalysts. Tungsten leaching was found to be an issue for both AC and CNT based catalysts. In reusability tests of CNT catalysts, nickel leaching was found to increase in the second run. The carbide catalyst displayed the lowest leaching in in the first run, indicating better performance in the second run. EG is an important chemical in industry and cellulose conversion is a promising alternative to the petroleum based methods currently in use. Using CNTs as support for tungsten carbide catalysts in this process looks promising with regard to EG yields. Further investigations can be made into increasing the yield by nickel promotion. However, the problem of yield loss during reusability reactions must be overcome.

References

[1] M.-Y. W. A.-Q. J. N. P. J.-F. W. X.-D. a. Z. T. Zheng, «Transition Metal–Tungsten Bimetallic Catalysts for the Conversion of Cellulose into Ethylene Glycol,» ChemSusChem: 3(1): pp. 63–66, 2012.

[2] C. Z. M. W. A. a. Z. T. Li, «One-pot catalytic hydrocracking of raw woody biomass into chemicals over supported carbide catalysts: simultaneous conversion of cellulose, hemicellulose and lignin,» Energy & Environmental Science: 5(1): pp. 6383–6390, 2012.

[3] A. P. V. J. L. a. S. N. Vyas, «A review on FAME production processes,» Fuel: 89(1): pp. 1-9, 2012.

[4] J. a. Z. W. He, «Techno-economic evaluation of thermo-chemical biomass-to-ethanol,» Applied Energy: 88(4): pp. 1224–1232, 2011.

[5] Z. J. S. P. M. a. L. C. Xiao, «Conversion of highly concentrated cellulose to 1,2-propanediol and ethylene glycol over highly efficient CuCr catalysts,» Green Chemistry 15: pp. 891-895, 2013.

[6] A. a. D. P. Fukuoka, «Catalytic Conversion of Cellulose into Sugar Alcohols,» Angewandte Chemie-International Edition, 45(31): pp. 5161-5163, 2006.

[7] A. a. Z. T. Wang, «One-Pot Conversion of Cellulose to Ethylene Glycol with Multifunctional Tungsten-Based Catalysts,» Accounts of Chemical Research, 2012.

[8] N. Z. T. Z. M. W. A. W. H. W. X. a. C. J. G. Ji, «Direct Catalytic Conversion of Cellulose into Ethylene Glycol using Nickel-Promoted Tungsten Carbide Catalysts,» Angewandte Chemie: International Edition 47(1): pp. 8510 –8513, 2008.

[9] Z. Z. J. W. A. Z. M. a. Z. T. Tai, «Temperature-controlled phase-transfer catalysis for ethylene glycol production from cellulose,» Chemical Communications: 48(1): pp. 7052–7054, 2012.

[10] N. Z. T. Z. M. W. A. W. H. W. X. S. Y. S. A. L. a. C. J. Ji, «Catalytic conversion of cellulose into ethylene glycol over supported carbide catalysts,» Catalysis Today: 147: pp. 77–85, 2009.

[11] Y. W. A. a. Z. T. Zhang, «A new 3D mesoporous carbon replicated from commercial silica as a catalyst support for direct conversion of cellulose into ethylene glycol,» Chemical Communication: 46(1): pp. 862–864, 2010.

[12] C. W. S. a. L. H. Luo, «Cellulose Conversion into Polyols Catalyzed by Reversibly Formed Acids and Supported Ruthenium Clusters in Hot Water,» Angewewandte Chemie: 119: pp. 7780–7783, 2007.

[13] Y. L. C. a. L. H. Liu, «Tungsten Trioxide Promoted Selective Conversion of Cellulose into Propylene Glycol and Ethylene Glycol on a Ruthenium Catalyst,» Angewandte Chemie: International Edition 51: pp. 3249 –3253, 2012.

[14] C. Bjørgen, «Direct catalysis of lignocellulosic material into polyols using a CNT supported tungsten catalyst,» NTNU specialization project, 2012.

[15] C. T. F. L. Z. F. Z. W. Z. a. L. C. Liang, «Preparation and Adsorption Properties for Thiophene of Nanostructured W2C on Ultrahigh-Surface-Area Carbon Materials,» Chem. Mater.: 15 (25): pp 4846–4853, 2003.

[16] J. Z. M. W. X. W. A. C. R. L. T. a. Z. T. Sun, «Catalytic Performance of Activated Carbon Supported Tungsten Carbide for Hydrazine Decomposition,» Catal. Lett.: 123: pp. 150–155, 2008.

[17] Y. L. C. a. L. H. Liu, «Tungsten Trioxide Promoted Selective Conversion of Cellulose into Propylene Glycol and Ethylene Glycol on a Ruthenium Catalyst,» Angewandte Chemie International Edition 51(1): pp. 3249 –3253, 2012.

[18] D. Chen, *Master Thesis meeting,* Dalian, China, 2013.

[19] J. B. J. H. a. D. B. Haber, «Manual of Methods and Procedures for Catalyst Characterization,» Pure & Applied Chemistry: 67(1): pp. 1257-1306, 1995.

[20] T. B.-E. S. Y. Y. C. D. H. A. a. R. M. Zhao, «Synthesis of Supported Catalysts by Impregnation and Calcination of Low-Temperature Polymerizable Metal-Complexes,» Topics in Catalysis: 54:1163–1174, 2011.

[21] J. H. A. a. C. D. Zhu, «Carbon Nanomaterials in Catalysis: Proton Affinity, Chemical and Electronic Properties, and their Catalytic Consequences,» ChemCatChem: 5: pp. 378-401, 2013.

[22] Nanotube Research Group, University of Oklahoma, «Micromeritics ASAP 2010 (BET surface area measurements),» 2010. [Internett]. Available: http://www.ou.edu/engineering/nanotube/bet.htm. [Funnet 28th June 2013].

[23] Evans Analytical Group LLC , «Inductively Coupled Plasma Spectroscopy (ICP-OES/MS), ICP Analysis,» 2013. [Internett]. Available: http://www.eaglabs.com/mc/inductively-coupled-plasma-spectroscopy.html. [Funnet 28th June 2013].

[24] J. W. Niemantsverdriet, «Chapter 6. Diffraction and EXAFS,» i *Spectroscopy in Catalysis: An Introduction*, Wiley-VCH, 2000, pp. 137-143.

[25] Evans Analytical Group LLC, «Raman Spectroscopy, Raman Analysis,» 2013. [Internett]. Available: http://www.eaglabs.com/mc/raman-spectroscopy.html. [Funnet 14th June 2013].

[26] M. G. R. K. a. K. H. Scheithauer, «Genesis and Structure of WOx/ZrO2 Solid Acid Catalysts,» Langmuir 14: pp. 3019-3029, 1998.

[27] A. Wang, *Master thesis meeting,* Dalian, China, 2013.

[28] S. A. P. L. B. V. L. P. B. a. F. J. L. G. Echeandia, «Synergy effect in the HDO of phenol over Ni–W catalysts supported on active carbon: Effect of tungsten precursors,» Applied Catalysis B: Environmental 101: pp. 1–12 , 2010.

[29] J. a. D. J. Serrano-Ruiz, «Catalytic routes for the conversion of biomass into liquid hydrocarbon transportation fuels,» Energy & Environmental Science: 4(1): pp. 83-99, 2011.

[30] Z. J. S. P. M. a. L. C. Xiao, «Conversion of highly concentrated cellulose to 1,2-propanediol and ethylene glycol over highly efficient CuCr catalysts,» Green Chemistry: 15: pp. 891-895, 2013.

Appendices

APPENDIX A: BET – Surface area reports

20WCx/CNT:

BET Surface Area:	82.1134	±	0.2282 m²/g
Slope:	0.052520	±	0.000146
Y-Intercept:	0.000494	±	0.000020
C:	107.295715		
VM:	18.862764		cm³/g STP
Correlation Coefficient:	9.999768e-01		

20WO3/CNT:

BET Surface Area:	49.1961	±	0.1036 m²/g
Slope:	0.087590	±	0.000185
Y-Intercept:	0.000897	±	0.000026
C:	98.654089		
VM:	11.301130		cm³/g STP
Correlation Coefficient:	9.999867e-01		

2Ni20WO3/CNT:

ET Surface Area:	69.9727	±	0.1660 m²/g
Slope:	0.061749	±	0.000146
Y-Intercept:	0.000464	±	0.000020
C:	134.203771		
VM:	16.073847		cm³/g STP
Correlation Coefficient:	9.999832e-01		

10WCx/CNT:

BET Surface Area:	71.3715	±	0.2032 m²/g
Slope:	0.060895	±	0.000172
Y-Intercept:	0.000099	±	0.000024
C:	617.371387		
VM:	16.395179		cm³/g STP
Correlation Coefficient:	9.999761e-01		

30WCx/CNT:

BET Surface Area:	116.6764	±	0.3686 m²/g
Slope:	0.036932	±	0.000117
Y-Intercept:	0.000378	±	0.000016
C:	98.607675		
VM:	26.802445		cm³/g STP
Correlation Coefficient:	9.999700e-01		

20WCx/AC-p:

BET Surface Area:	521.6659	±	6.5588 m²/g
Slope:	0.008375	±	0.000104
Y-Intercept:	-0.000030	±	0.000014
C:	-276.614644		
VM:	119.835072		cm³/g STP
Correlation Coefficient:	9.995384e-01		

20WO3/AC-p:

BET Surface Area:	555.3984	±	7.2886 m²/g
Slope:	0.007890	±	0.000102
Y-Intercept:	-0.000052	±	0.000014
C:	-151.744563		
VM:	127.583960		cm³/g STP
Correlation Coefficient:	9.995001e-01		

2Ni20WO3/AC-p:

BET Surface Area:	535.9552	±	7.6066 m²/g
Slope:	0.008178	±	0.000114
Y-Intercept:	-0.000055	±	0.000016
C:	-147.021439		
VM:	123.117544		cm³/g STP
Correlation Coefficient:	9.994157e-01		

20WCx/AC-im:

BET Surface Area:	650.0541	±	7.7789 m²/g
Slope:	0.006715	±	0.000079
Y-Intercept:	-0.000018	±	0.000011
C:	-373.739672		
VM:	149.327902		cm³/g STP
Correlation Coefficient:	9.995811e-01		

20WO3/AC-im:

BET Surface Area:	562.8740	±	7.5179 m²/g
Slope:	0.007785	±	0.000102
Y-Intercept:	-0.000051	±	0.000014
C:	-152.703833		
VM:	129.301248		cm³/g STP
Correlation Coefficient:	9.994822e-01		

2Ni20WO3/AC-im:

BET Surface Area:	604.2840	±	8.1479 m²/g
Slope:	0.007247	±	0.000096
Y-Intercept:	-0.000043	±	0.000013
C:	-166.284101		
VM:	138.813781		cm³/g STP
Correlation Coefficient:	9.994717e-01		

APPENDIX B: ICP – detailed table

Liquid product	Analyse for	ICP value (ppm)	g/mL	g in sample (dilution)	g in liquid product (50 mL)	Leaching (%)
20WCx/CNT	W	1.479	1.48E-06	7.40E-05	3.70E-03	**9.2**
20WCx/CNT reusability	W	3.305	3.31E-06	1.65E-04	8.26E-03	**20.7**
2Ni20WO3/CNT	W	1.12	1.12E-06	5.60E-05	2.80E-03	**7.0**
2Ni20WO3/CNT reusability	W	1.106	1.11E-06	5.53E-05	2.77E-03	**6.9**
20WCx/CNT	Ni	0.028	2.80E-08	1.40E-06	7.00E-05	**3.1***
20WCx/CNT reusability	Ni	0.1073	1.07E-07	5.37E-06	2.68E-04	**11.7***
2Ni20WO3/CNT	Ni	0.1093	1.09E-07	5.47E-06	2.73E-04	**5.6***
2Ni20WO3/CNT reusability	Ni	0.129	1.29E-07	6.45E-06	3.23E-04	**6.6***

* The nickel leaching is calculated based on the nickel content determined by the solid ICP analysis if nickel.

APPENDIX C: Chemisorption – raw data

Sample	Metal dispersion (%)	Cubic Crystallite Size (nm)
20WCx/CNT	0.2216	474.6169
20WCx/CNT with reduction	8.0941	12.9921
20WO3/CNT	1.3015	80.7957
2Ni20WO3/CNT	0.6268	166.6972
20WCx/AC-p	0.7154	146.9961
20WO3/AC-p	27.3017	3.8517
2Ni20WO3/AC-p		
20WCx/AC-im	6.4768	16.2363
20WO3/AC-im	2.2769	46.1852
2Ni20WO3/AC-im	n.d.	n.d.

APPENDIX D: Raman – additional Raman spectra

D03-100s

20WO3/CNT

D03-60s

30WCx/CNT

120s

20WCx/AC-im

D
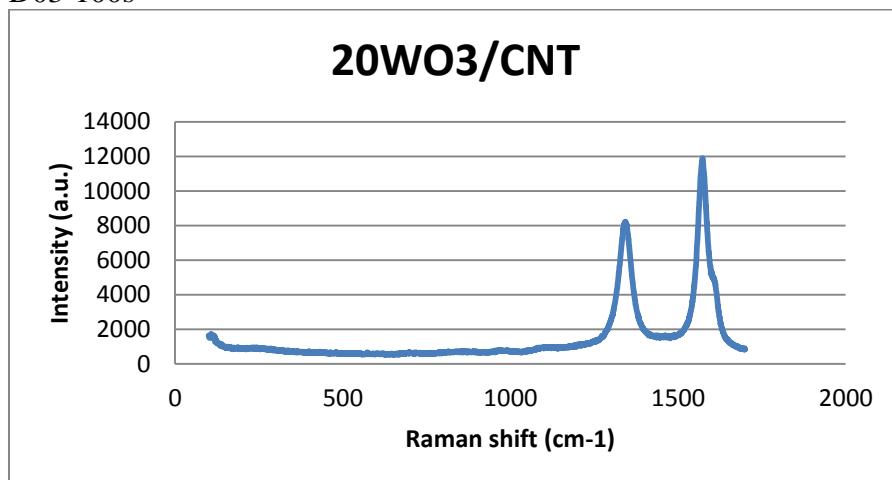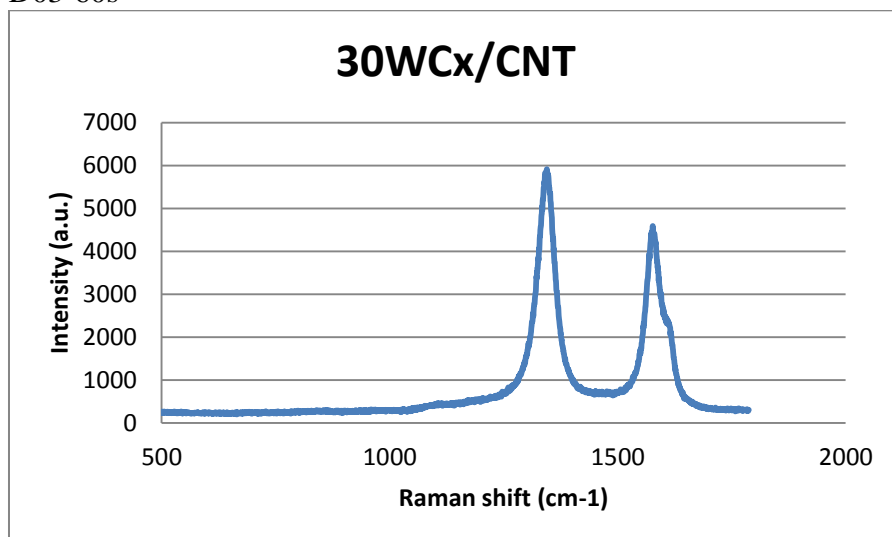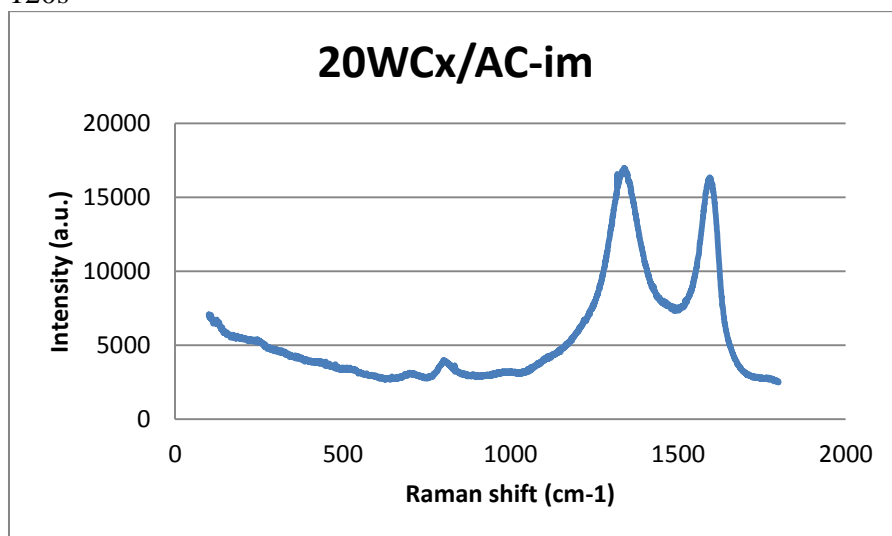
APPENDIX E: Mass based conversion – calculation details

Sample	Catalyst	Cellulose	Total	Filter paper	Sample + filter paper	Sample	Cellulose left	Conversion
Test	0,2013	0,5005	0,7018	0,0853	0,2755	0,1902	-0,0111	102
AT50W2NiI	0,2008	0,5008	0,7016	0,0969	0,4736	0,3767	0,1759	65
AT50W2NiII	0,2	0,4993	0,6993	0,0827	0,2556	0,1729	-0,0271	105
ATOPH50W2NiI	0,2	0,5002	0,7002	0,0858	0,2523	0,1665	-0,0335	107
AT12W2Ni	0,2001	0,4999	0,7	0,0844		-0,0844	-0,2845	157
ATOPH12W2Ni	0,2015	0,5022	0,7037	0,107	0,2398	0,1328	-0,0687	114
#1CNT	0,2002	0,5024	0,7026	0,01817	0,3658	0,34763	0,14743	71
#1AC	0,204	0,5012	0,7052	0,1875	0,383	0,1955	-0,0085	102
#3AC	0,2031	0,5016	0,7047	0,1828	0,3773	0,1945	-0,0086	102
#2CNT	0,2013	0,5037	0,705	0,1857	0,369	0,1833	-0,018	104
#2AC	0,2031	0,5001	0,7032	0,189	0,2586	0,0696	-0,1335	127
#4AC	0,2014	0,506	0,7074	0,1845	0,368	0,1835	-0,0179	104
#1CNT reusability	0,1598	0,3799	0,5397	0,1826	0,3239	0,1413	-0,0185	105
#2CNT reusability	0,176	0,4417	0,6177	0,1879	0,3457	0,1578	-0,0182	104
#3CNT	0,202	0,5027	0,7047	0,183	0,3825	0,1995	-0,0025	100
#4CNT	0,1995	0,5004	0,6999	0,184	0,3959	0,2119	0,0124	98
CNT-blank	0,2006	0,5003	0,7009	0,1825	0,373	0,1905	-0,0101	102

APPENDIX F: Liquid product yield – raw data

AT50W2Ni I (30 min)

	Peak area	Yield
ery	13198,6	1,187874
EG	**109019,4**	**21,80388**
1,2-PG	**18925,5**	**3,7851**
Man	11400,7	1,14007
Sor	59911,4	5,99114
Gly	8650,1	1,73002
1,2-BUT	1290,5	0,3
		35,896184

AT50W2Ni II (2 hours)

	Peak area	Yield
ery	18651,4	1,678626
EG	**258020,5**	**51,6041**
1,2-PG	**45710,8**	**9,14216**
Man	14309,9	1,43099
Sor	49118,7	4,91187
Gly	12073	2,4146
1,2-BUT	44354,6	8,9
		80,053266

ATOPH50W2Ni I (2 hours)

	Peak area	Yield
ery	26676,3	2,400867
EG	**244757,7**	**48,95154**
1,2-PG	**37113,3**	**7,42266**
Man	20163,5	2,01635
Sor	75826,1	7,58261
Gly	11826	2,3652
1,2-BUT	29027,9	5,8
		76,544807

AT12W2Ni (2 hours)

	Peak area	Yield
ery	8786,7	0,790803
EG	**65705,3**	**13,14106**
1,2-PG	**48208,8**	**9,64176**
Man	4543,2	0,45432
Sor	47055,7	4,70557
Gly	8561,9	1,71238
1,2-BUT	11747,7	2,3
		32,795433

20WCx/CNT

	Peak area	Yield
ery	32737,9	2,95
EG	**268801,8**	**53,76**
1,2-PG	**43274,9**	**8,65**
Man	30366,2	3,04
Sor	69592,9	6,96
Gly	14128,6	2,83
1,2-BUT	33867,5	6,77
		84,96

2Ni20WO3/CNT

	Peak area	Yield
ery	10762,6	0,97
EG	**255605,4**	**51,12**
1,2-PG	**42192,7**	**8,44**
Man	0	0,00
Sor	15568,9	1,56
Gly	8960	1,79
1,2-BUT	8014,8	1,60
		65,48

20WCx/CNT-reusability

	Peak area	Yield
ery	6547,9	0,59
EG	**105610,8**	**21,12**
1,2-PG	**63425,4**	**12,69**
Man	12891,1	1,29
Sor	41907,3	4,19
Gly	8831,8	1,77
1,2-BUT	15107,4	3,02
		44,66

2Ni20WO3/CNT-reusability

	Peak area	Yield
ery	4392	0,40
EG	**59377,7**	**11,88**
1,2-PG	**12078,8**	**2,42**
Man	56540,6	5,65
Sor	0	0,00
Gly	4135,9	0,83
1,2-BUT	0	0,00
		21,17

F

20WCx/AC-p

	Peak area	Yield
ery	10141,6	0,91
EG	**172421,9**	**34,48**
1,2-PG	**66384,2**	**13,28**
Man	6780	0,68
Sor	15244,3	1,52
Gly	0	0,00
1,2-BUT	0,0	0,00
		50,88

2Ni20WO3/AC-p

	Peak area	Yield
ery	16169,2	1,46
EG	**318984,9**	**63,80**
1,2-PG	**40379,4**	**8,08**
Man	11058,7	1,11
Sor	17959	1,80
Gly	7738,6	1,55
1,2-BUT	5885,6	1,18
		78,95

20WCx/AC-im

	Peak area	Yield
ery	11830,6	1,06
EG	**159771,3**	**31,95**
1,2-PG	**79056,9**	**15,81**
Man	0	0,00
Sor	15762,2	1,58
Gly	20650	4,13
1,2-BUT	7911,6	1,58
		56,12

2Ni20WO3/AC-im

	Peak area	Yield
ery	18805,9	1,69
EG	**287938,6**	**57,59**
1,2-PG	**34808,9**	**6,96**
Man	114265	11,43
Sor	23480,7	2,35
Gly	8645,2	1,73
1,2-BUT	4745,2	0,95
		82,69

F

CNT

	Peak area	Yield
ery	1996,5	0,18
EG	**9780,4**	**1,96**
1,2-PG	**4691,8**	**0,94**
Man	15026,1	1,50
Sor	5091,1	0,51
Gly	0	0,00
1,2-BUT	0,0	0,00
		5,09

10WCx/CNT

	Peak area	Yield
ery	43195,5	3,89
EG	**158637,7**	**31,73**
1,2-PG	**56053,1**	**11,21**
Man	40398,7	4,04
Sor	158947,2	15,89
Gly	44442,8	8,89
1,2-BUT	19001,6	3,80
		79,45

30WCx/CNT

	Peak area	Yield
ery	38266	3,44
EG	**125543,5**	**25,11**
1,2-PG	**50577,4**	**10,12**
Man	40431,5	4,04
Sor	185712,7	18,57
Gly	50109,9	10,02
1,2-BUT	20163,2	4,03
		75,34

F

APPENDIX G: Gas product yield – raw data

| Catalyst | Peak Area | | | | mol % (carbon) | | | | Total yield (%) |
	CO	CH4	CO2	C2H6	CO	CH4	CO2	C2H6	
AT50W2Ni	0.00	38.70	32.10	6.60	0.00	0.54	0.33	0.13	1.01
ATOPH50W2Ni	0.00	42.70	34.50	0.00	0.00	0.60	0.36	0.00	0.96
AT12W2Ni	0.00	35.90	77.80	0.00	0.00	0.50	0.81	0.00	1.31
AT12W2Ni	0.00	55.30	30.00	0.00	0.00	0.78	0.31	0.00	1.09
20WCx/CNT	0.00	19.20	28.10	11.40	0.00	0.27	0.29	0.23	0.79
20WCx/CNT-reusability	10.80	19.20	91.10	12.70	0.12	0.27	0.94	0.25	1.59
2Ni20WO3/CNT					0.00	0.00	0.00	0.00	0.00
2Ni20WO3/CNT-reusability	6.40	21.50	207.80	0.00	0.07	0.30	2.15	0.00	2.53
10WCx/CNT	0.00	26.00	40.30	0.00	0.00	0.37	0.42	0.00	0.78
30WCx/CNT	0.00	35.00	44.60	0.00	0.00	0.49	0.46	0.00	0.95
20WCx/AC-p					0.00	0.00	0.00	0.00	0.00
2Ni20WO3/AC-p					0.00	0.00	0.00	0.00	0.00
20WCx/AC-im	4.90	28.30	56.60	66.30	0.05	0.40	0.59	1.33	2.36
2Ni20WO3/AC-im	0.00	51.00	50.80	4.30	0.00	0.72	0.53	0.09	1.33

APPENDIX H: Additional analysis not included in report: NH_3-TPD

NH_3-chemisorption

Peak number	Temperature at maximum (C)	Quantity adsorbed (cm³/g STP)	Cumulative quantity (cm³/g STP)
1	99,8	2,95624	2,95624
2	99,6	0,40474	3,36098
3	99,5	0,30687	3,66785
4	99,5	0,07034	3,73819
5	99,5	0	3,73819

Total amount of NH3 adsorption: 1,2295 cm³/g
NH_3-TPD

Peak number	Temperature at maximum (°C)	Quantity (cm³/g STP)	Peak height
1	659,9	10,49023	0,01219
2	783,6	29,95599	0,04351

Risk assessment

Black and white scan

Unit: Kjemisk prosessteknologi
Participants in the identification process (including their function): Cecilie Bjørgen (master student), Professor A. Wang (supervisor).

Date: 28.01.2013

Cecilie Bjørgen   *A. Wang*

Short description of the main activity/main process: Catalyst preparation and the conversion of cellulose under high pressure hydrogen conditions.

Activity/process	Responsible person	Laws, regulations etc.	Existing documentation	Existing safety measures	Comment
Use of toxic and flammable gases (H2)	A. Wang and C. Li		Safety data sheet*	Room detector, local detector, leak testing, gloves, goggles, lab coat.	No open flames in lab
Assembling/use of non toxic and inert gases: CO2/N2/Ar/He	A. Wang and C. Li		Safety data sheet*	Leak testing, gloves, goggles, lab coat.	
Use of acetone for cleaning procedures	A. Wang and C. Li		Safety data sheet*	Gloves, lab coat, goggles.	
Use of CNT	A. Wang and C. Li		Safety data sheet*	Gloves, lab coat, goggles, dust mask.	Unknown long term health effects
Use of liquid nitrogen for BET	A. Wang and C. Li		Safety data sheet*	Lab coat, goggles, special gloves	

* Printed safety data sheets are not available in the lab area at DICP. The relevant data sheets are available on Ecoonline.

Unit: Kjemisk prosessteknologi

Line manager: Øyvind Gregersen

Participants in the risk assessment (including their function): Cecilie Bjørgen (master student), Professor A. Wang (supervisor).

Date: 28.01.2013

Cecilie Bjørgen   *A. Wang*

Activity from the identification process form	Potential undesirable incident/strain	Likelihood: Likelihood (1-5)	Consequence: Human (A-E)	Environment (A-E)	Economy/ material (A-E)	Risk value	Comments/status Suggested measures
Use of toxic and flammable gases (H2)	Leaks, fire, explosion	2	B			2B	Leak testing with noble gases and room and local detectors
Assembling/use of non toxic and inert gases: CO2/N2/Ar/He	Leaks	2	B			2B	Use of gloves, lab coat, goggles.
Use of acetone for cleaning procedures	spill, fire	3	A			2B	Use of gloves, lab coat, goggles.
Use of CNT	Spill	3	A			2B	Use of gloves, lab coat, goggles, dust mask.
Use of liquid nitrogen for BET	spill	3	B			2B	Lab coat, goggles, special gloves.

Likelihood, e.g.:
1. *Minimal*
2. *Low*
3. *Medium*
4. *High*
5. *Very high*

Consequence, e.g.:
A. *Safe*
B. *Relatively safe*
C. *Dangerous*
D. *Critical*
E. *Very critical*

Risk value (each one to be estimated separately):
Human = Likelihood x Human Consequence
Environmental = Likelihood x Environmental consequence
Financial/material = Likelihood x Consequence for Economy/materiel

Potential undesirable incident/strain

Identify possible incidents and conditions that may lead to situations that pose a hazard to people, the environment and any materiel/equipment involved.

ii

NTNU		Prepared by	Number	Date
⊙		HSE section	HMSRV2603E	04.02.2011
HSE/KS	Risk assessment	Approved by	Replaces	
		The Rector	2 out of 2	01.12.2006
			Page	

Criteria for the assessment of likelihood and consequence in relation to fieldwork

Each activity is assessed according to a worst-case scenario. Likelihood and consequence are to be assessed separately for each potential undesirable incident. Before starting on the quantification, the participants should agree what they understand by the assessment criteria:

Likelihood

Minimal 1	Low 2	Medium 3	High 4	Very high 5
Once every 50 years or less	Once every 10 years or less	Once a year or less	Once a month or less	Once a week

Consequence

Grading	Human	Environment	Financial/material
E Very critical	May produce fatality/ies	Very prolonged, non-reversible damage	Shutdown of work >1 year.
D Critical	Permanent injury, may produce serious serious health damage/sickness	Prolonged damage. Long recovery time.	Shutdown of work 0.5-1 year.
C Dangerous	Serious personal injury	Minor damage. Long recovery time	Shutdown of work < 1 month
B Relatively safe	Injury that requires medical treatment	Minor damage. Short recovery time	Shutdown of work < 1week
A Safe	Injury that requires first aid	Insignificant damage. Short recovery time	Shutdown of work < 1day

The unit makes its own decision as to whether opting to fill in or not consequences for economy/materiel, for example if the unit is going to use particularly valuable equipment. It is up to the individual unit to choose the assessment criteria for this column.

Risk = Likelihood x Consequence

Please calculate the risk value for "Human", "Environment" and, if chosen, "Economy/materiel", separately.

About the column "Comments/status, suggested preventative and corrective measures":

Measures can impact on both likelihood and consequences. Prioritise measures that can prevent the incident from occurring; in other words, likelihood-reducing measures are to be prioritised above greater emergency preparedness, i.e. consequence-reducing measures.

iii

Colour scan

Hazardous activity identification process

Unit: Kjemisk prosessteknologi   **Date: 28.01.2013**

Participants in the identification process (including their function): Cecilie Bjørgen (master student), Professor A. Wang (supervisor).

Cecilie Bjørgen   *A. Wang*

Short description of the main activity/main process: Catalyst preparation and the conversion of cellulose under high pressure hydrogen conditions.

Activity/process	Responsible person	Laws, regulations etc.	Existing documentation	Existing safety measures	Comment
Use of toxic and flammable gases (H2)	A. Wang and C. Li		Safety data sheet*	Room detector, local detector, leak testing, gloves, goggles, lab coat.	No open flames in lab
Assembling/use of non toxic and inert gases: CO2/N2/Ar/He	A. Wang and C. Li		Safety data sheet*	Leak testing, gloves, goggles, lab coat.	
Use of acetone for cleaning procedures	A. Wang and C. Li		Safety data sheet*	Gloves, lab coat, goggles.	
Use of CNT	A. Wang and C. Li		Safety data sheet*	Gloves, lab coat, goggles, dust mask.	Unknown long term health effects
Use of liquid nitrogen for BET	A. Wang and C. Li		Safety data sheet*	Lab coat, goggles, special gloves	

* Printed safety data sheets are not available in the lab area at DICP. The relevant data sheets are available on Ecoonline.

Unit: Kjemisk prosessteknologi
Line manager: Øyvind Gregersen
Participants in the risk assessment (including their function): Cecilie Bjørgen (master student), Professor A. Wang (supervisor).

Cecilie Bjørgen   *A. Wang*

Date: 28.01.2013

Activity from the identification process form	Potential undesirable incident/strain	Likelihood: Likelihood (1-5)	Consequence: Human (A-E)	Consequence: Environment (A-E)	Consequence: Economy/material (A-E)	Risk value	Comments/status Suggested measures
Use of toxic and flammable gases (H2)	Leaks, fire, explosion	2	B			2B	Leak testing with noble gases and room and local detectors
Assembling/use of non toxic and inert gases: CO2/N2/Ar/He	Leaks	2	B			2B	Use of gloves, lab coat, goggles.
Use of acetone for cleaning procedures	spill, fire	3	A			2B	Use of gloves, lab coat, goggles.
Use of CNT	Spill	3	A			2B	Use of gloves, lab coat, goggles, dust mask.
Use of liquid nitrogen for BET	spill	3	B			2B	Lab coat, goggles, special gloves.

Likelihood, e.g.:
1. Minimal.
2. Low
3. Medium
4. High
5. Very high

Consequence, e.g.:
A. Safe
B. Relatively safe
C. Dangerous
D. Critical
E. Very critical

Risk value (each one to be estimated separately):
Human = Likelihood x Human Consequence
Environmental = Likelihood x Environmental consequence
Financial/material = Likelihood x Consequence for Economy/materiel

Potential undesirable incident/strain
Identify possible incidents and conditions that may lead to situations that pose a hazard to people, the environment and any materiel/equipment involved.

v

Risk assessment

Criteria for the assessment of likelihood and consequence in relation to fieldwork

Each activity is assessed according to a worst-case scenario. Likelihood and consequence are to be assessed separately for each potential undesirable incident. Before starting on the quantification, the participants should agree what they understand by the assessment criteria:

Likelihood

Minimal 1	Low 2	Medium 3	High 4	Very high 5
Once every 50 years or less	Once every 10 years or less	Once a year or less	Once a month or less	Once a week

Consequence

Grading	Human	Environment	Financial/material
E Very critical	May produce fatality/ies	Very prolonged, non-reversible damage	Shutdown of work >1 year.
D Critical	Permanent injury, may produce serious serious health damage/sickness	Prolonged damage. Long recovery time.	Shutdown of work 0.5-1 year.
C Dangerous	Serious personal injury	Minor damage. Long recovery time	Shutdown of work < 1 month
B Relatively safe	Injury that requires medical treatment	Minor damage. Short recovery time	Shutdown of work < 1week
A Safe	Injury that requires first aid	Insignificant damage. Short recovery time	Shutdown of work < 1day

The unit makes its own decision as to whether opting to fill in or not consequences for economy/materiel, for example if the unit is going to use particularly valuable equipment. It is up to the individual unit to choose the assessment criteria for this column.

Risk = Likelihood x Consequence

Please calculate the risk value for "Human", "Environment" and, if chosen, "Economy/materiel", separately.

About the column "Comments/status, suggested preventative and corrective measures":

Measures can impact on both likelihood and consequences. Prioritise measures that can prevent the incident from occurring; in other words, likelihood-reducing measures are to be prioritised above greater emergency preparedness, i.e. consequence-reducing measures.